ABSTRACT

Title of Document: PIEZOELECTRICALLY-DRIVEN THERMOACOUSTIC REFRIGERATOR

Daniel George Chinn, Master of Science, 2010

Directed By: Professor Amr Baz, Mechanical Engineering

Thermoacoustic refrigeration is an emerging refrigeration technology which does not require any moving parts or harmful refrigerants in its operation. This technology uses acoustic waves to pump heat across a temperature gradient. The vast majority of thermoacoustic refrigerators to date have used electromagnetic loudspeakers to generate the acoustic input. In this thesis, the design, construction, operation, and modeling of a piezoelectrically-driven thermoacoustic refrigerator are detailed. This refrigerator demonstrates the effectiveness of piezoelectric actuation in moving 0.3 W of heat across an 18 degree C temperature difference with an input power of 7.6 W. The performance characteristics of this class of thermoacoustic-piezoelectric refrigerators are modeled by using DeltaEC software and the predictions are experimentally validated. The obtained results confirm the validity of the developed model. Furthermore, the potential of piezoelectric actuation as effective means for driving thermoacoustic refrigerators is demonstrated as compared to the conventional electromagnetic loudspeakers which are heavy and require high actuation energy. The developed theoretical and experimental tools can serve as invaluable means for the design and testing of other piezoelectrically-driven thermoacoustic refrigerator configurations.

Piezoelectrically-driven Thermoacoustic Refrigerator

By

Daniel George Chinn

Thesis submitted to the Faculty of the Graduate School of the
University of Maryland, College Park, in partial fulfillment
of the requirements for the degree of
[Masters of Science]
[2010]

Advisory Committee:
Professor Amr Baz, Chair
Professor Balakumar Balachandran
Professor Nikhil Chopra

Acknowledgements

This work is funded by King Saud University (Visiting Professor Program). Special thanks are due to Professor Osama Aldraihem for serving as a co-advisor with Professor Amr Baz and all his technical inputs throughout the study. Thanks are also due to my colleague Mostafa Nouh for his help throughout this study. Finally, I would like to thank my wife for keeping me sane.

Table of Contents

List of Symbols

A	Cross sectional area
B	Coil inductance
c	Speed of sound
c_p	Constant pressure specific heat
c_v	Constant volume specific heat
E	Energy
f	Frequency
f_k	Spatial average of h_k
f_v	Spatial average of h_v
$\dot{H}$	Power flux
h	Enthalpy
h_k	Function dependant on geometry and thermal penetration depth
h_v	Function dependant on geometry and viscous penetration depth
i	First spatial orthogonal basis vector
I	Current
j	Complex number
j	Second spatial orthogonal basis vector
k	Third spatial orthogonal basis vector
k	Thermal conductivity
LDV	Laser doppler vibrometer
l	Length of coil
m	Mass
p	Pressure
P	Pressure across speaker
Q	Heat flux
R	Gas constant
R_e	Electrical resistance
R_m	Mechanical resistance
s	Entropy
T	Temperature
T_{s1}	Electro-mechanical cross correlation term
T_{s2}	Electro-mechanical cross correlation term
t	Time
U	Volumetric flow
u	Magnitude of velocity in the **i d**irection
V	Volume
V_s	Voltage across speaker
V_{rms}	Root mean squared voltage

v	Magnitude of velocity in the **j d**irection
$\mathbf{v}$	Velocity
W	Work
w	Magnitude of velocity in the **k** direction
x	Spatial dimension in the **i d**irection
y	Spatial dimension in the **j d**irection
Z_m	Mechanical impedance
z	Spatial dimension in the **k d**irection

Greek Symbols

γ	Ratio of specific heats
δ	Infinitesimal quantity
δ_k	Thermal penetration depth
δ_v	Viscous penetration depth
ε	Internal energy
λ	Acoustic wavelength
μ	Dynamic viscosity
ρ	Density
σ	Prandtl number
σ'	Fluid stress tensor
ξ	Displacement from mean position
ω	Angular frequency

Operators

∇	Gradient operator
∂	Partial derivative
$\mathrm{Im}(\bullet)$	Imaginary part of $\bullet$
$\mathrm{Re}(\bullet)$	Real part of $\bullet$
$\langle\bullet\rangle$	Spatial average of $\bullet$
$\bar{\bullet}$	Temporal average of $\bullet$

List of Figures

List of Tables

Chapter 1: Introduction to Thermoacoustics

The meaning of the term *thermoacoustics* is, in the words of Nicholas Rott who laid much of the theoretical foundation for the field, fairly self-explanatory [1]. As its name suggests, thermoacoustics is a science that is concerned with the interactions between heat (thermo) and pressure oscillations in gases (acoustics). This field can be broken into two subcategories. The first is the forward effect which is concerned with the generation of pressure oscillations from heat. This effect is primarily used to create engines that are widely referred to as thermoacoustic engines in the literature. The second subcategory or reverse effect is concerned with using acoustic waves to pump heat. This reverse effect is primarily used to create refrigerators known as thermoacoustic refrigerators which are the topic at hand.

1.1 History of Thermoacoustics

Though attempts at applying the thermoacoustic effect to build useful devices have only been being carried out for the past few decades, observations and studies of is effect have been going on for quite some time. A number of publications which review the history of thermoacoustics are readily available in the literature [2, 3]. Higgins [4] conducted the first known experiments involving acoustic oscillations generated by heat back in 1777. Higgins noted that if a hydrogen flame was placed in the right position within an organ pipe, acoustic oscillations would take place.

An extension of Higgins work was carried out by Rijke [5]. Rijke placed a small, heated screen inside of an organ pipe and noted that acoustic oscillations

occurred. This tube is referred to as the Rijke Tube which is more completely discussed by both Tijani [3] and Feldman [6].

Lord Rayleigh [7] made record of a signing effect that glass blowers had for centuries observed from bulbs they had blown. Sondhauss [8] conducted related experiments by taking a glass ball with a neck attached and heating the junction between the ball and the neck as seen in Figure 1.1 below. In this picture sound is heard coming out of the neck after the heat has had time to warm the system up.

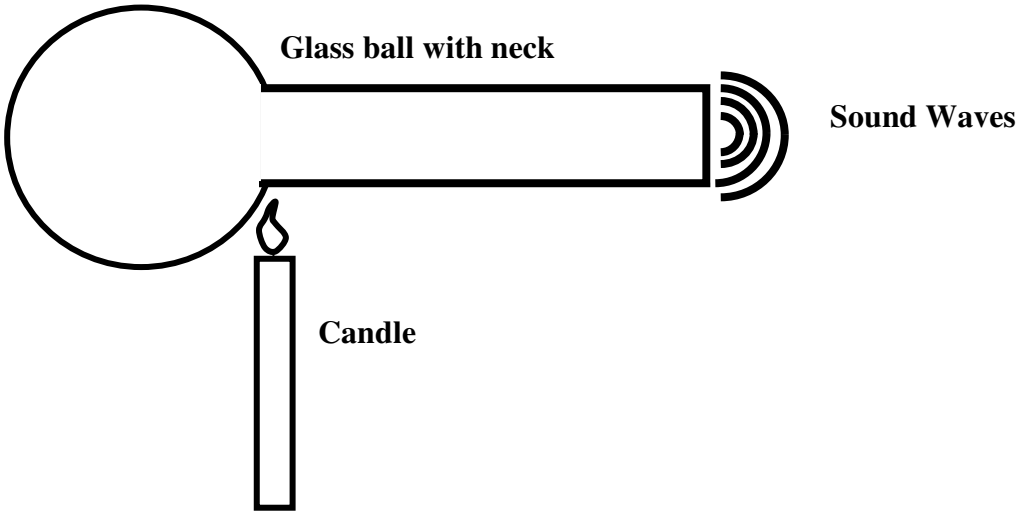

Figure 1.1: Sondhauss Tube

In the field of cryogenics what is known as Taconis oscillations has been observed to take place when tubes are sealed at one end and have their open end placed in liquid helium. This effect was first documented by Taconis [9] in 1949. Taconis oscillations are really an extension of the Sondhauss tube seen in Figure 1.1, with the difference being that Taconis' experiment cooled the open end of the tube while Sondhauss heated the closed end.

Solid theoretical understandings of the thermoacoustic effect do not appear as early in the literature. Perhaps the earliest writing on thermally-induced oscillations in a gas column was written by Rayleigh [7]. Rayleigh notes that if a gas is oscillating inside of a tube, the oscillation is encouraged if heat is added at an end of the pipe when the air inside is in the most compressed part of its phase, and also, if heat is taken away from the end of the pipe when the air is at its least compressed stage.

In 1969, Rott [10-14] laid the groundwork for a mathematical understanding of thermoacoustics in a series of papers which he wrote. In this series of papers he derives and solves linear equations which are the basis for thermoacoustic theory. Rott's work is the foundation upon which most of the present day mathematical models of thermoacoustics are built.

Two famous experimental studies triggered a lot of research using the reverse effect. The first was demonstrated by Gifford and Longsworth [15]. Gifford and Longsworth did experiments by using low frequency pressure pulses inside a tube from which they were able to achieve cooling. They named their device a "*pulse tube*" from which the term "*pulse tube refrigerator*" is derived.

A few years after Gifford and Longsworth built their pulse tube refrigerator, Merkli and Thomann [16] published their work on the thermoacoustic effect in a resonance tube. They performed experiments in which they used a tube closed at one end and placed a sinusoidal driven piston at the other end. When the system was driven at resonance, a cooling effect was observed.

The results from these experiments triggered Los Alamos National Laboratory (LANL) in New Mexico, U.S.A. to further investigate thermoacoustic cooling. The research efforts there were lead by J. C. Wheatley and G. W. Swift. Since the early 1980s until the present, numerous publications in the field of thermoacoustics have come out of LANL. One of the most notable publications is a book by Swift [17] in which he puts together all the basic theories of thermoacoustics. Some of Swift's other most notable publications on thermoacoustics are the following [18, 19, 20]. In recent years, thermoacoustics research has exploded and this research is being performed at many different research laboratories throughout the world. Swift is still very active in performing thermoacoustics research at LANL and could be called the current leader in the field.

1.2 Basics of the Thermoacoustic Effect

In this section, the thermoacoustic effect is introduced. A basic explanation as to how it works is given. The thermoacoustic effect will be discussed more rigorously in Chapter two.

1.2.1 Conversion of Heat to Acoustic Waves (The Forward Effect)

As was stated earlier, the forward effect is concerned with the generation of pressure oscillations from heat. A good way to visualize how this works is to think of a tube sealed at one end and open at the other that is filled with a gas like the one shown in Figure 1.2.

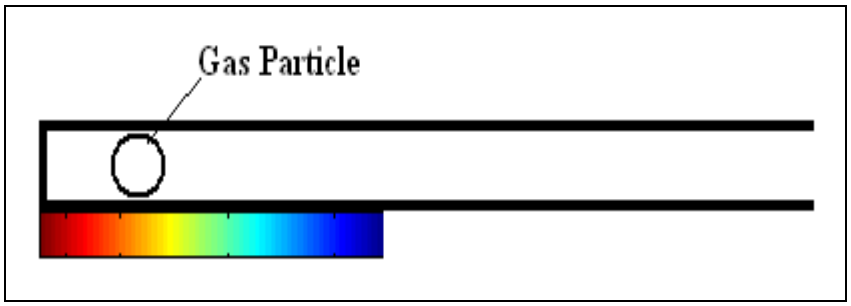

Figure 1.2: Thermoacoustic Engine Effect – Step 1

The colored spectrum in Figure 1.2 represents a temperature gradient applied to the wall of the channel. Since the channel wall is hotter than the gas particle at the position shown in Figure 1.2, heat will flow into the particle of gas. This heat flow will cause the gas to expand. Since the channel wall to the left of the gas particle in Figure 1.2 is hotter than that to the right, the gas which is to the left will become hotter than the gas particle of interest and thus expands more than the gas particle being observed. The gas to the right of the gas particle of interest will also expand, but to a lesser degree since the nearby wall is not as hot. This greater expansion from left to right will cause a pressure gradient from left to right as well, pushing all the gas particles to the right. The gas particle under observation now takes on the position and form observed in Figure 1.3 below.

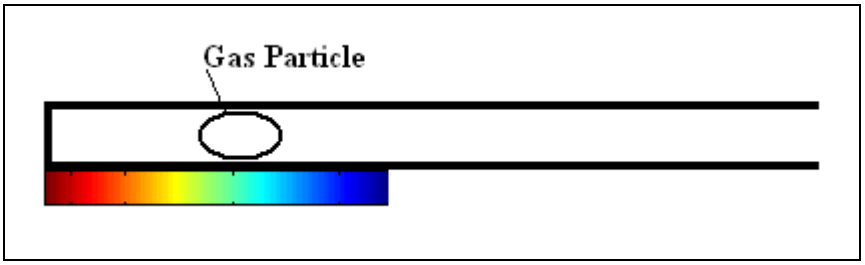

Figure 1.3: Thermoacoustic Engine Effect – Step 2

The gas particle seen above has both expanded and moved to the right. However, the gas particle is now hotter than the wall of the nearby channel. This temperature difference causes the gas particle to deposit heat to the channel wall, causing a cooling effect within the gas. This takes place all throughout the portion of the channel which is subjected to the imposed temperature gradient. After the gas particle has lost heat to the wall, it contracts as do all the other gas particles that were displaced along the temperature gradient. This causes a pressure vacuum which forces all the gas in the channel to oscillate back to the left to the position shown in Figure 1.2, starting the cycle all over again.

Though the motion of the gas particles is periodic in nature, the four step process described above captures the essence of the forward effect and makes understanding much easier. It can be applied to understand many of the historical examples of the thermoacoustic effect that were presented in section 1.1. This process, repeated over and over again, can be used to do work at the open end of the tube. This effect is almost always used to create engines which are referred to as thermoacoustic engines in the literature.

1.2.2 Pumping heat using acoustic waves (The Reverse Effect)

Pumping heat by using acoustic waves is almost always used to build thermoacoustic refrigerators though it has been used for a few other applications. This reverse effect is literally the reverse of the forward effect used with thermoacoustic engines that were discussed above. An easy way to grasp what goes on is to picture a tube closed at one end with a moving piston at the other end as shown in Figure 1.4.

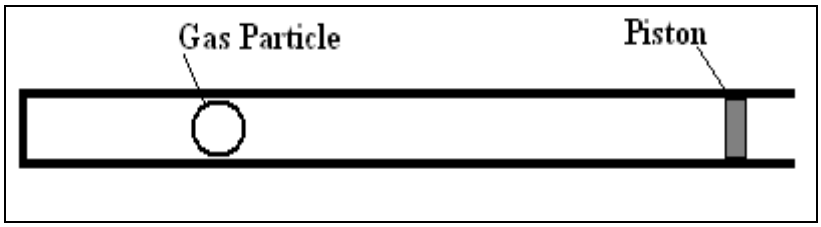

Figure 1.4: Gas in a sealed tube with a piston at one end

The gas is initially at rest inside the chamber. However, the refrigeration process will start to take place if the piston is actuated. In existing refrigerators, a sinusoidal actuation of the piston takes place. However, for simplicity a simplified 4 step process like the one used in the previous section will be described. As the piston in Figure 1.4 is moved to the left, all the air in the chamber will be forced to the left with it, being compressed as it moves over due to shrinking volume of the tube. This leads to the system being aligned as indicated in Figure 1.5.

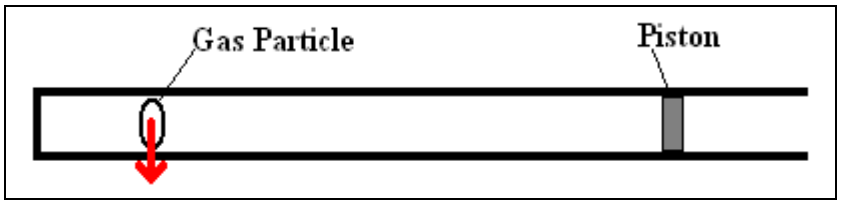

Figure 1.5: The piston is forced to the left, causing compression and heating of the gas

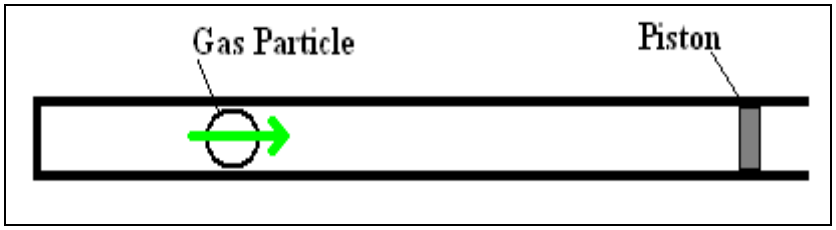

Figure 1.6: The piston is pulled back to the right, causing the gas to oscillate right as well

The compressed gas particle is seen after it has moved to the left. As described by the ideal gas law, the compressed gas particle becomes slightly hotter than the ambient temperature it was before the process began. The nearby wall, however, is still at the ambient temperature. This causes heat to be deposited from the gas onto the wall. After some heat has been deposited, the piston is pulled back to the right, causing all the gas to move to the right and expand as shown in Figure 1.6.

When the piston moves to the right, the volume of the cavity increases. However, the number of molecules of gas remains constant, so the gas expands as it moves to the right. This causes a cooling of the gas. When the gas has finished moving to the right it is cooler than the nearby wall of the tube. This causes heat to flow from the wall of the tube into the gas as shown in Figure 1.7.

After some time has elapsed, to allow heat to flow into the gas particle, the piston is moved back to the left, causing the cycle to start all over again. The rapid procession of this cycle causes heat to be moved from right to left in the example just described. Over time a steady state temperature gradient will develop where heat is pumped across it by using the gas as an agent.

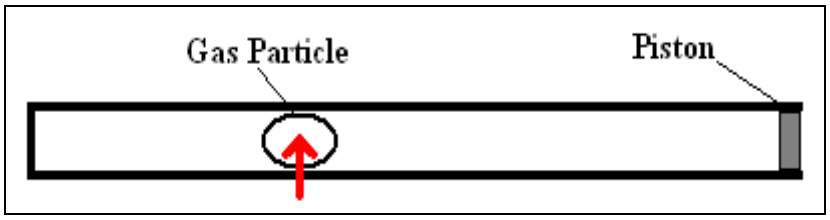

Figure 1.7: Heat flows from the wall of the tube into the expanded, cooled gas particle

For thermoacoustic engines, a temperature gradient must be maintained to get work out. For thermoacoustic refrigerators, work must be put into the system to maintain a temperature gradient. The examples described above give a good conceptual understanding of the underlying physics of thermoacoustic devices.

1.3 Existing thermoacoustic refrigerators

There are currently no commercial thermoacoustic devices in existence. Most of the thermoacoustic devices that have been made are in government research laboratories or universities. This section provides a brief review of some of the most well documented thermoacoustic refrigerators that have been built.

The first thermoacoustic device fabricated to do useful work was a thermoacoustic engine built at LANL by a team lead by Wheatley [19,20]. However, the first known thermoacoustic refrigerator was built by Hofler [21] who was a member of Wheatley's group in the building of the first thermoacoustic engine. Soon afterward, a thermoacoustic refrigerator known as the "*beer cooler*" was also built at LANL [18,22]. This refrigerator used a heat driven prime mover instead of a speaker to drive it.

At the Naval Postgraduate School, an extension of Hofler's refrigerator design was built to be launched on the Space Shuttle *Discovery.* This refrigerator is known as the Space ThermoAcoustic Refrigerator (STAR) [23]. A thermoacoustically driven thermoacoustic refrigerator (TADTAR) was also built at the Naval Postgraduate School by Adeff and Hofler [24]. This refrigerator used a lens to focus light from the sun to create heat for running a thermoacoustic engine. The output from this engine was used, in turn, to drive the thermoacoustic refrigerator,

completely eliminating all moving parts. With 100 Watts of input energy from the sun, 2.5 Watts of cooling power was obtained.

The Shipboard Electronics ThermoAcoustic Chiller (SETAC) was built to cool electronics aboard the *U.S.S. Deyo* [25, 26]. SETAC was able to operate at a maximum efficiency of a COP of 21% relative to a Carnot engine. However, when operated at the power necessary to cool the racks of electronics it was designed for, SETAC was only able to obtain a COP of 8% relative to a Carnot engine.

TRITON is one of the biggest thermoacoustic refrigerators ever built. It is named because it was designed to have the cooling power of a three ton air conditioner. Though TRITON is not well documented, information about it can be found on the website of the Pennsylvania State University [26].

Tijani [27] performed a number of studies on the effects of varying individual components of thermoacoustic refrigerators. He built a refrigerator based on the results of his research. The best COP relative to Carnot he was able to produce is 11% which was done by using helium as the working fluid.

A qualitative thermoacoustic refrigerator was built by Russel [28]. This refrigerator is quick, cheap, and easy to make. It is however, very inefficient because it was designed to be a qualitative example and not to obtain quantitative results.

Ben and Jerry's Ice Cream funded a project at the Pennsylvania State University to make a clean thermoacoustic refrigerator that would cool their ice cream freezers [26,29] This refrigerator has a cooling capacity of 119 W and an overall COP of 19% of Carnot's. Prototypes of this refrigerator are currently being used by Ben and Jerry's Ice Cream in the Boston and Washingtond, D.C. areas, and if

the prototypes are successful this may become the first commercially produced line of thermoacoustic refrigerators as Ben and Jerry's Ice Cream plans to switch all their stores over to the clean technology.

1.4 Scope of This Thesis

Nearly all of the thermoacoustic refrigerators in existence are driven by electromagnetic loud speakers. Many good numerical models exist for these refrigerators, which gives the engineer a powerful tool to use for design purposes. However, the performance of electromagnetic loudspeakers is greatly diminished at high frequencies. For this reason, piezoelectric drivers have been used for high frequency applications of thermoacoustic refrigeration [30]. Avoiding electromagnetic drivers may also be required for applications involving magnetic sensitive equipment. Unlike their electromagnetically driven counterparts, there are no known numerical models for piezoelectrically-driven thermoacoustic refrigerators.

In this thesis, a piezoelectrically-driven thermoacoustic refrigerator is built. A model is then developed for this system. This model provides a tool for designers to use with applications requiring piezoelectric actuation.

1.5 Summary

In this chapter, the author has presented the basic concepts of thermoacoustics, a brief review of the literature of thermoacoustic devices, as well as working principles of thermoacoustic engines, and refrigerators. The use of piezoelectric actuation as compared to a conventional electromagnetic actuation is also introduced and is the topic of the present thesis.

Chapter 2: Theory of Thermoacoustics

The first mathematical model of the thermoacoustic effect was developed by Rott [10-14]. Rott's model is a linear one which was later put together and reviewed by Swift [18]. In this chapter, concepts from thermodynamics, fluid mechanics, and acoustics are reviewed and later these concepts are used to derive and explain the equations governing the thermoacoustic effect.

2.1 Thermodynamics Review

The study of heat engines and refrigerators constitutes a major portion of the field of thermodynamics. Virtually every thermodynamics textbook covers these topics extensively. Therefore, it should come as no surprise that thermodynamics is at the heart of thermoacoustic theory, since the applications of the thermoacoustic effect are heat engines and refrigerators. This section covers selected principles from thermodynamics that are important to thermoacoustics.

2.1.1 The First Law of Thermodynamics

The first law of thermodynamics states that energy cannot be created or destroyed. Energy is simply transformed from one type to another. The total energy of a system is changed only by energy in the form of heat being added to the system or through work being done on the system. Note that heat was shown to be a form of energy by Joule in the mid nineteenth century [31]. The first law of thermodynamics is described mathematically as follows [33]:

$$\delta Q + \delta W = dE \tag{2.1}$$

In equation (2.1), Q is the heat added to the system, W is the work done on the system, and E is the total internal energy of the system.

When dealing with thermoacoustic applications, most of the heat transfer will occur through conduction. The assumption is made that the heat transfer rate is the following [34]:

$$\frac{dQ}{dt} = \dot{Q} = kA\frac{dT}{dx} \tag{2.2}$$

where k is the thermal conductivity at the boundary of the system, A is the cross sectional area perpendicular to the x direction, and T is the temperature.

The work done on the system comes from many sources including all forms of mechanical and electrical work. However, in the study of thermoacoustics and in thermodynamics in general, pressure-volume work is of the greatest concern. In the derivation of the governing equations of thermoacoustics all other forms of work are assumed to be much smaller than the pressure-volume work and so are neglected. Therefore, the work done on the system reduces to the following [35]:

$$\delta W = -p\delta V \tag{2.3}$$

where p represents the pressure and V represents volume. When work is done on a system, the system's volume decreases, causing the δV term in equation (2.3) to become a negative quantity and the δW term a positive quantity.

2.1.2 The Second Law of Thermodynamics

Though the first law requires that energy be conserved, it says nothing about the types of energy transformations which will take place. However, everyday human experiences quickly teach a person that there are some energy transformations which

will take place and some that will not. For instance, energy will flow out of a hot cup of coffee that is placed on a table in an ambient room, but heat from the ambient room will never flow into a cold cup of coffee and make it hot. The first law of thermodynamics is not violated in either case, and so the second law of thermodynamics is necessary to describe which energy flows and transformations will take place and which will not.

Every system has a scalar quantity called *entropy*. This quantity is related to how useable the energy within that system is. The entropy of a system is decreased if heat is removed from the system to the outside. Likewise, the entropy of a system is increased if heat is added to the system from the outside. The entropy of a system is also increased if an irreversible process takes place within it. For a system that is completely insulated from its surroundings, heat flow cannot take place into or out of the system. This means that the entropy of an insulated system can either stay the same or increase.

Energy transformations can be broken down into two categories. There are reversible energy transformations and irreversible energy transformations. An example of a reversible energy transformation is a ball being thrown up into the air. Initially the ball has a lot of kinetic energy which is transformed into gravitational potential energy as the ball gains altitude. Eventually the ball will reach a state at which all of its kinetic energy has been transformed into potential energy and the ball is as rest. At this point, the ball will start to transform its potential energy back into kinetic energy and proceed on its downward journey. In this example, kinetic energy was transformed into potential energy and then reversibly and freely transformed

back into kinetic energy. In these processes, the entropy of the system remains unchanged.

Irreversible processes however, cannot transform energy back and forth without some of that energy being converted to a less useable form. A common example of this is friction. If a book slides across a table, heat is generated due to friction and the book-table system has an entropy increase. However, though energy would still be conserved, the heat cannot directly be used to push the book back to its original position. This is an example of an irreversible process. It cannot happen because to do so would cause a decrease in the entropy of an isolated system, which defies the second law of thermodynamics.

The letter *S* is generally used to represent entropy. The exact value of a system's entropy is however, often not of interest. People are most often only concerned with how the entropy changes. Therefore, the following expression for the change in entropy is generally all that is important [36].

$$dS = \frac{dQ}{T} + (dS)_{gen} \tag{2.4}$$

where [37]:

$$(dS)_{gen} \geq 0 \tag{2.5}$$

Equations (2.1) and (2.4) are for closed systems only. When open systems are considered, additional terms are added to accommodate for the mass which moves across the system boundaries. The open system version of equation (2.1) is the following [38].

$$\delta Q + \delta W + \left(h + \frac{|\mathbf{v}|^2}{2} \right) dm = dE \tag{2.6}$$

where h is the enthalpy which is defined as the sum of the internal energy and the pressure times the volume, **v** is the velocity of the small mass particle, and dm is the mass which is flowing across the boundary. Likewise, for the open system equation (2.4) becomes the following [39]:

$$dS = \frac{dQ}{T} + sdm + (dS)_{gen} \tag{2.7}$$

2.2 Fluid Mechanics Review

Inside of every thermoacoustic device is a gas which is known as the working fluid. This gas oscillates within the thermoacoustic device. Understanding the physics of this fluid is important to understanding the thermoacoustic effect. Two very famous equations from fluid mechanics are especially important in thermoacoustics. These equations are the *continuity equation* and the *Navier-Stokes equation* which are reviewed below.

2.2.1 The Continuity Equation

The continuity equation is based on the assumption that mass is conserved within any control volume of the fluid. The change in the amount of mass within a fixed control volume can only be caused by the difference between the amount of fluid flowing into the control volume and the amount flowing out. This equation is expressed as follows [40]:

$$\frac{\partial \rho}{\partial t} + \nabla \cdot (\rho \mathbf{v}) = 0 \tag{2.8}$$

In equation (2.8) above, $\frac{\partial \rho}{\partial t}$ is the change in density with respect to time for an infinitesimal volume. The $(\rho \mathbf{v})$ in (2.8) is the total mass flow of the fluid at the point of the infinitesimal volume. The divergence operator acting upon the fluid flow becomes the difference between what is flowing into the infinitesimal control volume and what is flowing out. Thus the continuity equation given by equation (2.8) is indeed a statement of conservation of mass.

2.2.2 The Navier-Stokes Equation

The Navier-Stokes equation is simply a statement Newton's second law for fluids in which viscous effects cannot be neglected. Newton's second law states that the time rate of change of the momentum of a system is equal to the sum of the forces on it. For a viscous fluid, this is expressed mathematically as follows [41]:

$$\rho\left[\frac{\partial \mathbf{v}}{\partial t} + (\mathbf{v} \cdot \nabla)\mathbf{v}\right] = -\nabla p + \mu \nabla^2 \mathbf{v} \qquad (2.9)$$

The left hand side of equation (2.9) consists of the density times the acceleration. The acceleration is comprised of two parts, the temporal acceleration and the special acceleration. On the right hand side of equation (2.9) are the forces acting on the infinitesimal fluid volume. The first term is the pressure gradient while the second term is due to the viscous shearing force. Though other more rigorous and complete momentum equations for fluids do exist, the Navier-Stokes equation is more than sufficient for all the applications in thermoacoustics which are used in this thesis.

2.2.3 Laws of Thermodynamics for Fluids

The first law of thermodynamics can be applied to a control volume of fluid. The energy within a control volume of fluid is simply the internal energy plus the kinetic energy which is expressed mathematically as follows [42]:

$$\left(\rho\varepsilon + \frac{1}{2}\rho|\mathbf{v}|^2\right)dxdydz \tag{2.10}$$

Note that ε is the internal energy. According to the first law of thermodynamics, the change in energy must be equal to the heat flow into the system plus the work done on the system and the energy gained or lost by mass flow into and out of the control volume. The energy equation for a fluid control volume is then the following [43]:

$$\frac{\partial}{\partial t}\left(\rho\varepsilon + \frac{1}{2}\rho|\mathbf{v}|^2\right) = -\nabla\cdot\left[-k\nabla T + \mathbf{v}\cdot\sigma' + \left(\rho h + \frac{1}{2}\rho|\mathbf{v}|^2\right)\mathbf{v}\right] \tag{2.11}$$

The term on the left hand side in equation (2.11) is simply the time derivative of equation (2.10). The first term on the right hand side in equation (2.11) is due to the heat conduction into the control volume. The next term is the work done on the control volume where the stress tensor for the fluid is σ'. Finally, the terms inside the circle brackets and those terms which are multiplied by them are due to net energy flow due to mass crossing into the control volume.

2.2.4 Ideal Gasses

Inside of every thermoacoustic refrigerator or engine is a working fluid as will be discussed further in the next chapter. These working fluids are generally able to be

considered ideal gasses. Ideal gasses follow a few important and well known relations which are shown below ([45], [46], and [47] respectively):

$$p = \rho RT \tag{2.12}$$

$$c_p = \frac{R\gamma}{\gamma - 1} \tag{2.13}$$

$$c_v = \frac{R}{\gamma - 1} \tag{2.14}$$

Equation (2.12) is known as the ideal gas law, equation (2.13) is the constant pressure specific heat, and equation (2.14) is known as the constant volume specific heat. The gas constant R for any ideal gas is equal to the universal gas constant, $\Re = 8.314 J / mol \cdot K$, divided by the molar mass of the fluid. Also, γ is defined as the ratio of specific heats and it can be shown by combining equations (2.13) and (2.14) that it is equal to the ratio of the constant pressure specific heat to the constant volume specific heat.

2.3 Scales, Assumptions, and Notation

In this section, the length scales for thermoacoustics are introduced. Complex notation is then reviewed due to its widespread use in thermoacoustics literature and later use in this thesis. Finally, the assumptions used in the derivation of the governing equations of thermoacoustics are introduced.

2.3.1 Length Scales

The length scales of a thermoacoustic device play an important role in its performance. The important length scales are the wavelength λ [49], the thermal

penetration depth δ_k [50], and the viscous penetration depth δ_v [51] which are seen below.

$$\lambda = \frac{c}{f} \tag{2.15}$$

$$\delta_k = \sqrt{\frac{2k}{\omega \rho c_p}} \tag{2.16}$$

$$\delta_v = \sqrt{\frac{2\mu}{\omega \rho}} \tag{2.17}$$

In the equations above, c is the speed of sound, f is the excitation frequency, k is the thermal conductivity of the gas, and ω is the angular frequency. The acoustic wavelength is the distance at which a particular acoustic wave repeats itself. The thermal penetration depth is a metric describing how far heat can diffuse through the gas at the frequency driven. A fixed point will feel thermal effects from gas that is on the order of a thermal penetration depth away, but will not feel the effect of gas that is much further away.

The viscous penetration depth is related to the distance at which viscous effects can be felt. When gas is oscillating past a surface, viscous drag will take place. As with the thermal penetration depth, gas that is on the order of a viscous penetration depth from an object will experience viscous effects while gas that is much further away will not.

The ratio of these two penetration depths is known as the Prandtl number σ. This number is close to unity for most thermoacoustic working fluids which means that the viscous effects cannot be ignored. It is expressed below:

$$\sigma = \left(\frac{\delta_v}{\delta_\kappa} \right)^2 \tag{2.18}$$

2.3.2 Rott's Acoustic Approximation

Inside of every thermoacoustic device is an oscillatory flow across surfaces which have mean temperature gradients. Rott [10-14] made some simplifying assumptions which he was able to use to solve the equations describing oscillatory flow over non-isothermal plates. This groundwork laid by Rott was later used by Swift and is the basis for contemporary thermoacoustic theory. The assumptions are summarized below:

- The acoustic wavelength is much greater than the thermal and viscous penetration depths
- Viscosity remains constant (Not a function of temperature, density, etc…)
- The time dependences of the temperature, pressure, density, volumetric velocity, etc…, are sinusoidal
- The oscillatory part of the time dependant variables is small, causing second order terms and higher to be neglected
- Motion of the gas in the direction of the acoustic wave is much greater than transverse motions
- The mean of the oscillating variables is uniform across all cross sections through which the acoustic wave passes

2.3.3 Complex Notation

Due to the assumption in the last section that the time dependence of the oscillatory variables is sinusoidal, it is convenient to use what is known as *complex notation.* Complex notation allows the temporal part of the variables to be replaced by e^{jwt} because of their sinusoidal nature. Also, because the mean of the oscillating variables is uniform across every cross section through which the acoustic wave passes, the mean of these oscillating variables can be separated from the oscillating part and be written as a function of one variable. The direction in which the acoustic wave travels will be referred to as the *x* direction from here on, while the transverse directions will be denoted by *y* and *z*. An example of a variable and its equivalent in complex notation is seen below:

$$T(x, y, z, t) = T_m(x) + \mathrm{Re}\left[T_1(x, y, z)e^{jwt}\right] \tag{2.19}$$

In equation (2.19), the left hand side is the normal way in which the temperature would be written. However, on the right hand side the mean temperature is only a function of *x*, allowing it to be separated from the oscillatory part. The oscillatory part has the time dependence replaced with e^{jwt}, and the real part of this is taken. The subscript 1 indicates that it is the first order term, and all higher order terms are neglected because of the linear nature of the theory. The *Re* will often be omitted in the future from terms with the subscript 1. Note that for the sake of brevity, terms with the subscript 1 will be assumed to be the variable as a function of the three special directions multiplied by the temporal part as follows:

$$\xi_1(x, y, z)e^{j\omega t} = \xi_1 \tag{2.20}$$

Complex notation is especially convenient to describe the displacement ξ using complex notation because it has a mean of zero. This means that time derivatives are simply equal to the product of the complex number, angular frequency, and the displacement itself as follows:

$$\frac{\partial \xi_1}{\partial t} = j\omega\xi_1 \tag{2.21}$$

The result in equation (2.21) allows temporal differential equations using normal notation to be turned into algebraic equations in time using complex notation. For this reason, complex notation is widely used throughout thermoacoustics literature and will be used often throughout this thesis.

2.4 Theory of Thermoacoustics

There are three governing equations used to model thermoacoustic devices. These equations are derived from the continuity, Navier Stokes, and energy equations which are equations (2.8), (2.9), and (2.11). This section derives the thermoacoustic versions of these equations which are necessary for modeling parts of thermoacoustic devices where mean temperature gradients exist. This derivation is done using the assumptions from the previous section.

2.4.1 Thermoacoustic Continuity Equation

The continuity equation expressed above as equation (2.8) is repeated once again as follows:

$$\frac{\partial \rho}{\partial t} + \nabla \cdot (\rho \mathbf{v}) = 0 \tag{2.22}$$

This equation is a function of the density and the velocity of the fluid. These two variables are expressed in complex notation using the assumptions from the last section as follows:

$$\rho(x, y, z, t) = \rho_m(x) + \rho_1(x, y, z)e^{j\omega t} = \rho_m + \rho_1 \tag{2.23}$$

$$\mathbf{v}(x, y, z, t) = \mathbf{v}_1(x, y, z)e^{j\omega t} = \mathbf{v}_1 \tag{2.24}$$

Recall that the mean velocity is zero which is why it does not appear in (2.24). These variables can then be put into equation (2.22) to obtain the following:

$$\frac{\partial}{\partial t}(\rho_m + \rho_1) + \nabla \cdot ([\rho_m + \rho_1]\mathbf{v}_1) = 0 \tag{2.25}$$

The mean density has no temporal dependence which means:

$$\frac{\partial}{\partial t}[\rho_m(x)] = 0 \tag{2.26}$$

Also, because of the assumption that the oscillating parts of the variables are very small, the second order term in the product between the density and the velocity is assumed to be negligible. Using this fact along with equation (2.26) allows equation (2.25) to become the following:

$$\frac{\partial \rho_1}{\partial t} + \nabla \cdot (\rho_m \mathbf{v}_1) = 0 \tag{2.27}$$

or $$j\omega\rho_1 + \nabla \cdot (\rho_m \mathbf{v}_1) = 0 \tag{2.28}$$

The velocity vector is made up of three components, one in the *x* direction, one in the *y* direction, and one in the *z* direction as follows:

$$\mathbf{v}_1 = u_1\mathbf{i} + v_1\mathbf{j} + w_1\mathbf{k} \tag{2.29}$$

It is assumed that the velocity in the x direction is much greater than the velocities in the y and z directions. Therefore, the product of the mean density and the velocity vector can neglect the terms that are not on the x direction as follows:

$$\rho_m \mathbf{v}_1 = \rho_m \left(u_1 \mathbf{i} + v_1 \mathbf{j} + w_1 \mathbf{k}\right) \approx \rho_m u_1 \tag{2.30}$$

Putting the result in equation (2.30) back into equation (2.28) results in the following:

$$j\omega\rho_1 + \frac{d}{dx}\left(\rho_m u_1\right) = 0 \tag{2.31}$$

Equation (3.31) can be integrated across the cross sectional area of the refrigerator channel to obtained the special averaged version of this equation as follows [52]:

$$j\omega\langle\rho_1\rangle + \frac{d}{dx}\left(\rho_m \langle u_1\rangle\right) = 0 \tag{2.32}$$

In equation (2.32), the sharp brackets $\langle\ \rangle$ around a variable indicate a spatial average over the cross sectional area of the channel. At this point it is useful to express the density in terms of the temperature and the pressure. This expression is derived from the ideal gas law as follows:

$$\left(p_m + p_1\right) = \left(\rho_m + \rho_1\right)\left(T_m + T_1\right)R \tag{2.33}$$

Expanding this equation and dropping the second order term allows equation (2.33) to be simplified to the following:

$$\left(p_m + p_1\right) = \left(\rho_m T_m + \rho_1 T_m + T_1 \rho_m\right)R \tag{2.34}$$

or $$p_1 = \left(\rho_1 T_m + T_1 \rho_m\right)R \tag{2.35}$$

or $$\rho_1 = \frac{p_1}{T_m R} - \frac{T_1 \rho_m}{T_m} \tag{2.36}$$

Hence, $\langle \rho_1 \rangle = \frac{p_1}{T_m R} - \frac{\langle T_1 \rangle \rho_m}{T_m}$ (2.37)

Equation (2.37) can be put back into equation (2.33) as follows:

$$j\omega\left(\frac{p_1}{T_m R} - \frac{\langle T_1 \rangle \rho_m}{T_m}\right) + \frac{d}{dx}\left(\rho_m \langle u_1 \rangle\right) = 0 \tag{2.38}$$

An expression for the spatially averaged temperature $\langle T_1 \rangle$ is now required. This expression is derived by applying the first law of thermodynamics to a control volume. Equation (2.1) can be expressed in a temporal form as follows:

$$\frac{dQ}{dt} + \frac{dW}{dt} = \frac{dE}{dt} \tag{2.39}$$

Expressions for the heat flux Q and the work W done on the control volume were found in equations (2.2) and (2.3) respectively. The internal energy is a function of the temperature according to the well known equation:

$$E = \rho c_p T \tag{2.40}$$

Equations (2.2), (2.3), (2.38), and (2.40) are now combined to obtain the following:

$$\frac{d}{dt}\left(\rho c_p T\right) = \nabla \cdot k \nabla T + \frac{\partial p}{\partial t} \tag{2.41}$$

or $$\rho c_p \frac{\partial T}{\partial t} + \rho c_p \mathbf{v} \cdot \nabla T = \nabla \cdot k \nabla T + \frac{\partial p}{\partial t} \tag{2.42}$$

Recalling the assumption that the velocity in the x direction is much greater than the velocities in the y and z directions and that the temperature gradients in the x direction are much smaller than the temperature gradients in the y and z directions allow equation (2.42) to be simplified to the following:

$$\rho c_p \frac{\partial T}{\partial t} + \rho c_p u_1 \frac{\partial T}{\partial x} = k\left[\frac{\partial^2 T}{\partial y^2} + \frac{\partial^2 T}{\partial x^2}\right] + \frac{\partial p}{\partial t} \tag{2.43}$$

Using the assumptions stated above and replacing the temporal derivatives with $j\omega$ allows equation (2.43) to be simplified to the following [53]:

$$\rho_m c_p\left(j\omega T_1 + u_1 \frac{dT_m}{dx}\right) - j\omega p_1 = k\left[\frac{\partial^2 T_1}{\partial y^2} + \frac{\partial^2 T_1}{\partial x^2}\right] \tag{2.44}$$

The solution of this second order differential equation for T_1 is a function of the channel geometry across which the thermoacoustic equations are being solved. The solution is expressed for arbitrary geometries in the following way [54]:

$$T_1 = \frac{1}{\rho_m c_p}(1 - h_\kappa) p_1 - \frac{1}{j\omega A}\frac{dT_m}{dx}\frac{(1 - h_\kappa) - \sigma(1 - h_v)}{(1 - f_v)(1 - \sigma)} U_1 \tag{2.45}$$

In equation (2.45), h is a function of the y and z directions as well as the penetration depth where the κ subscript denotes that the thermal penetration depth is to be used and the v subscript indicates that the viscous penetration depth must be used. The variables f_κ and f_v are the spatial averages of h_κ and h_v respectively. These functions have been solved for a number of geometries by Swift [55].

The spatially averaged version of equation (2.45) is found by simply replacing all the h functions with their spatially averaged counterparts. If this is done along with putting the constant pressure specific heat in terms of the ratio of specific heats, the following is obtained:

$$\langle T_1 \rangle = \frac{\gamma - 1}{\rho_m R\gamma}(1 - f_\kappa) p_1 - \frac{1}{j\omega A}\frac{dT_m}{dx}\frac{(1 - f_\kappa) - \sigma(1 - f_v)}{(1 - f_v)(1 - \sigma)} U_1 \tag{2.46}$$

Equation (2.46) is now combined with equation (2.38), and a good amount of algebra is carried out to obtain the following thermoacoustic continuity equation:

$$dU_1 = \frac{j\omega A dx}{\gamma p_m}\left(1+(\gamma-1)f_\kappa\right)p_1 - \frac{(1-f_\kappa)-\sigma(1-f_v)}{(1-f_v)(1-\sigma)}\frac{dT_m}{dx}U_1 dx \qquad (2.47)$$

Equation (2.47) is a first order differential equation which describes how the volumetric flow changes as a function of pressure, volumetric flow, and the mean temperature gradient. This dependence on the mean temperature gradient is what causes the thermoacoustic effect to take place.

2.4.2 Thermoacoustic Momentum Equation

The thermoacoustic momentum equation is much simpler to derive than the thermoacoustic continuity equation. In fact, the thermoacoustic momentum equation is not dependant on the mean temperature gradient. Its derivation is quite straight forward starting from equation (2.9) which is the Navier Stokes equation repeated below.

$$\rho\left[\frac{\partial \mathbf{v}}{\partial t} + (\mathbf{v}\cdot\nabla)\mathbf{v}\right] = -\nabla p + \mu\nabla^2\mathbf{v} \qquad (2.48)$$

Applying the thermoacoustic assumptions causes this equation to become a lot simpler. The second term on the left hand side completely drops out because it is made up of second order terms. Many of the velocity components are also dropped because of the assumptions regarding certain quantities being insignificant up next to others. These simplifications result in the following [56]:

$$\rho_m j\omega u_1 = -\frac{dp_1}{dx} + \mu\left[\frac{\partial^2 u_1}{\partial y^2} + \frac{\partial^2 u_1}{\partial z^2}\right] \qquad (2.49)$$

Solving this second order differential equation for u_1 results in the following [57]:

$$u_1 = \frac{j}{\omega \rho_m}\left[1 - h_v\right]\frac{dp_1}{dx} \tag{2.50}$$

If equation (2.50) is integrated over the cross sectional area of the channel in which it is applied, the following momentum equation results [58]:

$$dp_1 = -\frac{j\omega \rho_m dx}{A\left(1 - f_v\right)}U_1 \tag{2.51}$$

Equation (2.50) is a first order differential equation describing how the pressure changes as a function of the volumetric flow and geometrical properties of the channel.

2.4.3 Thermoacoustic Energy Flow

The objective of most thermoacoustic models is to describe how the energy flows through a thermoacoustic device. This section derives a third equation describing the total power flow through a thermoacoustic device which can be used with the thermoacoustic continuity and momentum equations. It should be kept in mind that the version of the equation derived in this section appears in many forms throughout the literature depending on the application. However, this section will derive the version used later in this thesis.

One of the assumptions made earlier was that first order terms were small so second order terms could be neglected. This assumption must be removed for the energy flow because there are no first order terms involved. The focus of this section will be on second order terms and all variables that are second order will contain the subscript 2.

From the energy equation for a fluid, equation (2.11), it is easy to see that the energy flux or total power flux H is the following:

$$\dot{H} = -k\nabla T + \mathbf{v}\cdot\sigma' + \left(\rho h + \frac{1}{2}\rho|\mathbf{v}|^2\right)\mathbf{v} \tag{2.52}$$

This equation is readily simplified by noting that the kinetic energy term on the far right is third order and higher so it can be dropped because those higher order terms are assumed to be very small. Also, the velocity in the x direction is once again assumed to be much greater than the velocities in the transverse directions, so the velocity vector is simplified for the enthalpy flow term. Also, due to the sinusoidal nature of the time dependence of the variables, an average over one period is assumed and denoted by the over bar in the equations below. The second order power flow across the cross sectional area of a duct can then be written down as follows [59]:

$$\dot{H}_2 = \int\left(-\overline{k\frac{\nabla T}{dx}} + \overline{\mathbf{v}\cdot\sigma'} + \overline{\rho h u}\right)dA \tag{2.53}$$

Rott's acoustic approximation can now be used to simplify this equation. Because all the terms inside the integral are time averaged, the first order parts of all the variables are zero. Keeping this in mind and examining the first term which is due to thermal conduction, it is assumed that the second order part is much less than the first order part, allowing the following simplification [60]:

$$\int\left(\overline{k\frac{\nabla T}{dx}}\right)_2 dA \approx \left(Ak + A_{solid}k_{solid}\right)\frac{dT_m}{dx} \tag{2.54}$$

The second term in equation (2.53) is due to the stress tensor and it is assumed that this term is of the same order of magnitude as the viscous penetration depth while the last term in equation (2.53) is on the order of the acoustic wavelength. This

means that the second term can be neglected up next to the third. The third term is evaluated as follows [61]:

$$\int \left(\overline{\rho h u}\right)_2 dA = \int \left(\overline{\rho u}\right)_2 h_m dA + \int \overline{\left(\rho u\right)_1 h_1} dA \tag{2.55}$$

For a standing wave refrigerator or engine:

$$\int \left(\overline{\rho u}\right)_2 dA = \dot{m} = 0 \tag{2.56}$$

This means that equation (2.54) is simplified as follows [62]:

$$\int \left(\overline{\rho h u}\right)_2 dA = \frac{1}{2}\rho_m \int \mathrm{Re}\left[h_1 \tilde{u}_1\right] dA \tag{2.57}$$

Combining the above results means that [63]:

$$\dot{H}_2(x) = \frac{1}{2}\rho_m \int \mathrm{Re}\left[h_1 \tilde{u}_1\right] dA - \left(Ak + A_{solid} k_{solid}\right)\frac{dT_m}{dx} \tag{2.58}$$

The enthalpy as a function of temperature and pressure is then the following [64]

$$dh = c_p dT + \frac{\left(1 + T\beta\right)dp}{\rho} \tag{2.59}$$

At first order, this becomes:

$$h_1 = c_p T_1 \tag{2.60}$$

This result can be plugged back into (2.58) to obtain the following [65]:

$$\dot{H}_2(x) = \frac{1}{2}\rho_m c_p \int \mathrm{Re}\left[T_1 \tilde{u}_1\right] dA - \left(Ak + A_{solid} k_{solid}\right)\frac{dT_m}{dx} \tag{2.61}$$

Expressions for T_1 and u_1 were found in equations (2.45) and (2.50) respectively. If these results are plugged into (2.61), and the integration is carried out the following equation results [66]:

$$\dot{H}_2 = \frac{1}{2}\rho_m c_p \,\mathrm{Re}\left[p_1 \tilde{U}_1 \left(1 - \frac{f_k - \tilde{f}_v}{(1+\sigma)\left(1-\tilde{f}_v\right)} \right) \right] + \frac{\rho_m c_p \left|U_1\right|^2}{2A\omega\left(1-\sigma^2\right)\left|1-f_v\right|^2} \mathrm{Im}\left(f_k + \sigma \tilde{f}_v \right) \frac{dT_m}{dx} - \left(Ak + A_{solid} k_{solid} \right) \frac{dT_m}{dx} \tag{2.62}$$

Equation (2.62) describes the energy flow through standing wave thermoacoustic devices only. The energy equation used in unison with the thermoacoustic continuity and momentum equations is the basis for most if not all models of thermoacoustic devices.

2.5 Summary

This chapter has presented a brief review of the basics of thermodynamics and fluid mechanics as applied to thermoacoustic devices. A discussion of the spatial scales, basic assumptions, and notation is then introduced. Finally, the basic equations which govern the operation of thermoacoustic devices are presented with emphasis on describing the temperature, flow and power fields.

Chapter 3: Thermoacoustic Refrigerator Design

The design of thermoacoustic refrigerators is a field where a lot of research is currently being carried out. This literature contains many ongoing debates as to what the best design techniques may be. This chapter starts off with a basic design strategy for thermoacoustic refrigerators, and then goes on to discuss the individual components in detail, reviewing the relevant literature on the topic.

3.1 Design Overview

Thermoacoustic refrigerators can generally be broken up into four parts. These parts are known as the driver, the resonator, the stack, and the heat exchangers and are labeled for an example refrigerator in Figure 3.1:

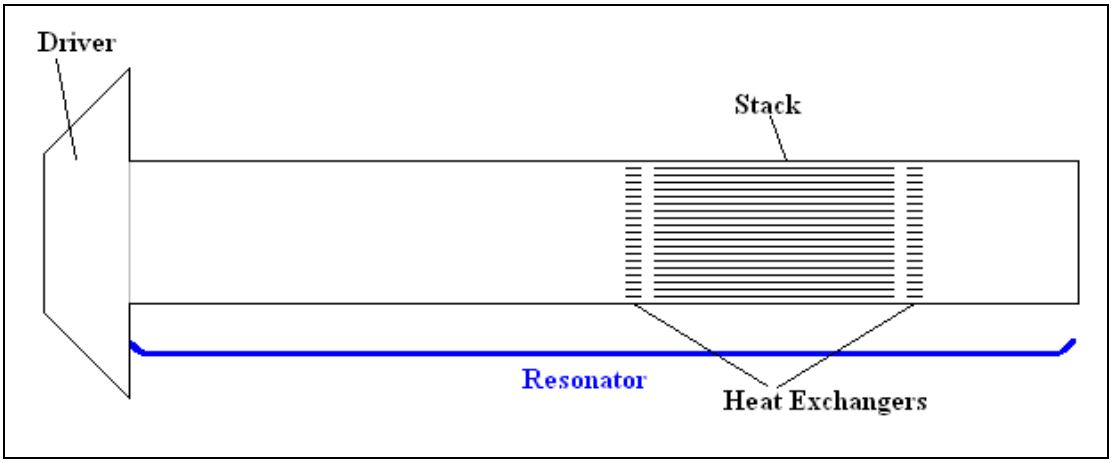

Figure 3.1: Parts of a thermoacoustic refrigerator

In Figure 3.1, the parts are shown for a common thermoacoustic refrigerator setup. However, there are many different thermoacoustic refrigerators in existence, some of which look nothing like the thermoacoustic refrigerator shown in Figure 3.1.

This being said, every design in some way carries out the four basic functions shown above.

The driver creates either a standing or traveling wave in the refrigerator. The wave created by the driver is generally at or near the resonant frequency of the resonator in which the wave oscillates. The stack is located at some point within the resonator and exists to create more surface area across which the thermoacoustic effect can take place. Finally, the heat exchangers are used to take heat from a refrigerated region and dump heat to the outside. These components are each described individually in detail in the later sections.

Russel [28] describes a cheap and easy to build thermoacoustic refrigerator. This refrigerator is for demonstration purposes and so is not very powerful or efficient. However, it is an excellent starting point for those interested in the field.

Tijani [67] published a paper describing in detail the process used to design a thermoacoustic refrigerator from start to finish. He starts off by designing the stack in such a way as to be able to meet the cooling requirements. This stack design is performed by first making choices for the average pressure, frequency, dynamic pressure, and working gas. After these variables have been selected, the material, geometry, and position of the actual stack is designed and optimized. The resonator is then designed under the constraints of the natural frequency and minimizing loss at the walls. The heat exchangers are then designed though the author concedes that not much is known about heat exchangers in oscillatory flow with zero mean displacement. The acoustic driver is then the final part of the refrigerator to be

designed. In another publication [68], Tijani describes in detail how the refrigerator parts were manufactured and built.

In an attempt to optimizing the design of thermoacoustic refrigerators, Wetzel [69] developed an algorithm for optimizing the design of thermoacoustic refrigerators. The developed algorithm splits the optimization process into the four basic parts discussed above. Lengthy discussions are given about optimization of the stack and resonator while admitting that the heat exchangers of thermoacoustic refrigerators are an issue that little is known about, and the optimization of the driver is a separate issue that goes far beyond just thermoacoustic refrigerators. It is concluded that efficient thermoacoustic refrigerators that are competitive with traditional refrigerators are theoretically possible if hang ups such as better heat exchangers can be overcome.

3.2 Refrigerator Parts

Focusing on the complete design of a thermoacoustic refrigerator can be overwhelming. It is often much easier to examine the different components of the design individually. This section reviews the literature for the various parts of thermoacoustic refrigerators individually.

3.2.1 Driver

The driver in a thermoacoustic refrigerator is used to create the acoustic waves within a thermoacoustic refrigerator. Electromagnetic speakers are commonly used as the drivers in thermoacoustic refrigerators, though other types of drivers are also used. Piezoelectric speakers are used in applications that require high driving

frequencies. A thermoacoustic engine is used with the TADTAR built by Adeff and Hofler [24]. Reid and Swift [70] use an oscillating piston in one of their designs.

A study of the choice and design of electrodynamic drivers for thermoacoustic refrigerators was carried out by Wakeland [71] at *The Pennsylvania State University*. Though Wakeland admits that not every aspect of the driver selection for thermoacoustic refrigerators is addressed, he comes to four conclusions. Wakeland's first conclusion is that the ratio $(Bl)^2/(R_e R_m)$ should be maximized where l is the length of the coil used to actuate the driver, B is the inductance of that coil, R_e is the electrical resistance of the driver, and R_m is the mechanical resistance of the driver. His next conclusion is that the stiffness in the suspension of the driver should be chosen so as to make the combined mechanical and electrical impedances completely real for the operating frequency of the refrigerator. He goes on to conclude that the electroacoustic efficiency should be maximized by selecting a piston sized so that impedance matching between the mechanical and acoustic loads takes place. Wakeland's final conclusion is for the scenario where the driver cannot be altered. In such cases, the operating frequency can be adjusted so as to achieve impedance matching.

Building of Wakeland's second conclusion, Tijani [72] developed a method to easily manipulate the mechanical impedance of the speaker so as to make the combined electrical and mechanical impedance of the system real. A variable volume of gas was attached to the back side of a speaker. This volume of gas creates a spring force on the speaker diaphragm which is a function of the volume. By adjusting the

volume, the imaginary part of the total impedance was eliminated and Tijani demonstrates that the highest efficiency does indeed occur for this case.

Li [73] develops a proportional-integral (PI) feedback control algorithm to control the frequency at which thermoacoustic drivers operate at. This frequency can change throughout the transient phases of operation because the natural frequency of the refrigerator is a function of the sound speed in the gas, which changes with temperature. The controller developed by Li and his colleagues measures both the acoustic and electric powers and seeks to optimize the efficiency which is defined as the acoustic power output over the electric power input.

Li *et al.* [74] expanded on their work to include a piston at the back of the resonator cavity which makes the resonator size to be another controllable variable along with the speaker frequency. The objective of this design was to maximize the cooling power. They demonstrated that their controller is able to find the optimal driver frequency and resonator size, as well adjust to changing conditions within the refrigerator.

3.2.2 Resonator

The purpose of the resonator in a thermoacoustic refrigerator is to contain the working fluid in a thermoacoustic refrigerator, and to cause it to have a desired natural frequency.

Resonators are generally either half or quarter wavelength resonators. Quarter wavelength resonators are made with tubes by sealing one end and making the length approximately one quarter of the desired resonant frequency wavelength. The open end of the tube is simulated by attaching a large volume to the end. This large

volume creates the boundary condition of zero pressure at the end, causing the end of the tube to be a pressure node and velocity anti-node while the beginning of the resonator is approximately a velocity node and a pressure anti-node. This means that the natural frequency of such a resonator will have a wavelength four times the resonator length from which quarter wavelength resonators derive their name. An example of a quarter wavelength resonator is pictured in Figure 3.2.

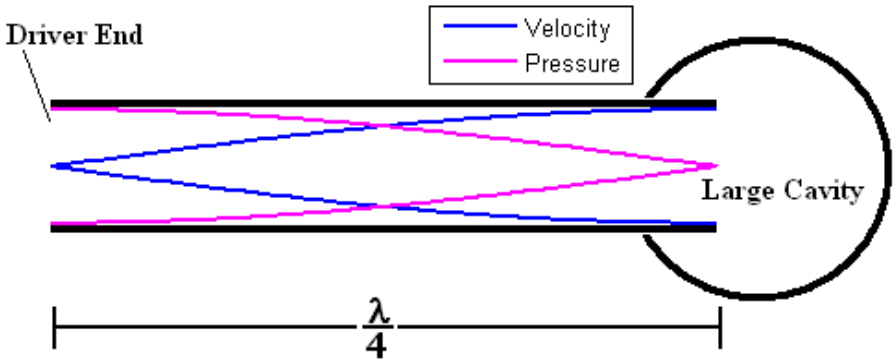

Figure 3.2: A quarter wavelength resonator

Half wavelength resonators are roughly a long tube that is closed at the end. The closed end means that the gas inside the resonator cannot move, creating a velocity node and pressure anti-node. The driver at the beginning of the tube also creates a velocity node and pressure anti-node, causes the natural frequency of such a cavity to be half the acoustic wavelength. These resonators are depicted in Figure 3.3.

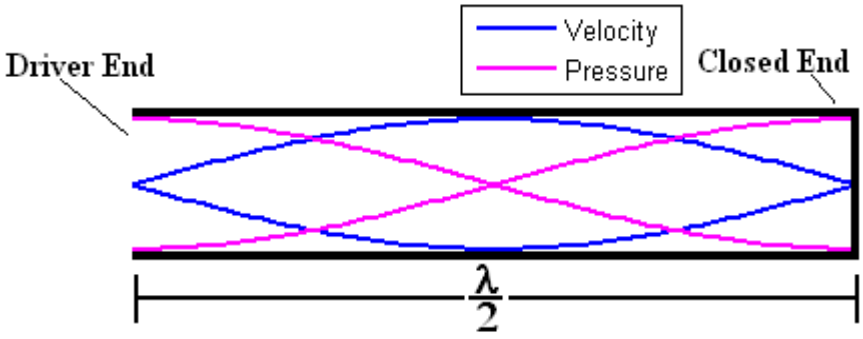

Figure 3.3: A half wavelength resonator

In Figures 3.2 and 3.3, it should be noted that these are idealized cases. Real thermoacoustic resonators are generally close to either half or quarter wavelength resonators but are not exact because ideal resonators are hard to build and are not always the best possible choice as is now discussed. Also, the assumption that the driver is a velocity node and pressure antinode is made. The validity of this assumption is very much a function of the driver and how it is attached to the resonator.

Gardner and Swift [75] discuss the use of inertance in thermoacoustic refrigerators. They note that maximum acoustic efficiency takes place when the acoustic impedance is purely real. Since many refrigerators have a large compliance tank at the end of the resonator which causes a negative imaginary component of impedance to appear, inertance can be used to introduce a positive imaginary part to the impedance to counteract this phase shift and make the impedance purely real once again. However, recalling the work done by Wakeland [71] discussed in the previous section, the overall impedance of the speaker coupled to the resonator is really what should be examined. Therefore, using inertance is another tool for tuning the overall impedance to being purely real, but it should be adjusted with the coupling to the driver kept in mind.

Tijani [67] notes that the acoustic power loss is proportional to the surface area of the resonator. If a quarter wavelength resonator is used, the surface area of the resonator is approximately half that of the half wavelength resonator, and so is more efficient. He also notes that at the end of the tube where the transition to the large compliance volume occurs in a quarter length resonator could cause losses due to turbulence generated by the steep transition. To solve this problem, he proposed a cone shaped tapering out to the buffer volume. He found that the optimal half-angle of the tapering from the resonance tube to the compliance volume is 9 degrees.

Hofler [76] notes that when the cross sectional area of the stack requires a certain diameter tube on a quarter wavelength resonator, the surface area of the remaining part of the resonator past the stack can be reduced by using a smaller diameter tube. This smaller diameter tube reduces the losses that are proportional to the surface area of the resonator. However, as the diameter of the second tube is shrunk in ratio to the diameter of the first tube, the thermal losses increase monotonically while the viscous losses have a steep drop off and then steady out.

Tijani [67] claims that the optimal ratio is for the second tube's diameter to be 0.54 times the first tube's diameter. He also once again suggests having a cone taper between the two tubes to prevent turbulence. Finally, Tijani notes that straight tubes have harmonic resonant frequencies that are integer numbers of the first natural frequency. If nonlinear effects arise, they will often excite these higher harmonics if straight tubes are used. Therefore, though straight tubes are the simplest resonators they are often very inefficient. Tijani's resonator design taking these effects into account is displayed in Figure 3.4.

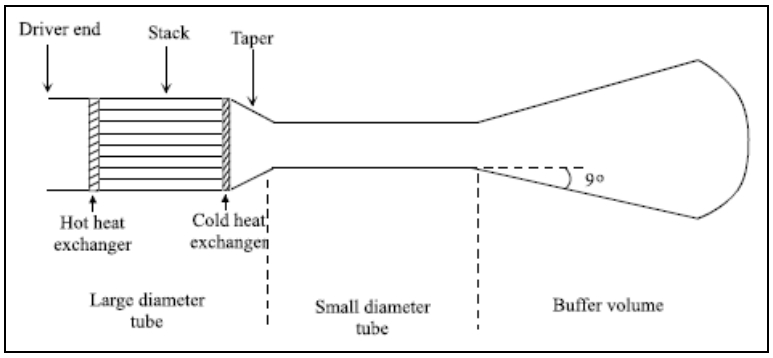

Figure 3.4: Taken from [67]. Optimized resonator for a thermoacoustic refrigerator

3.2.3 Stack

The stack is the heart of the thermoacoustic refrigerator. This is where the thermoacoustic effect takes place and is perhaps the most sensitive part of the design as small changes in stack dimensions can lead to huge changes in performance.

One of the biggest engineering decisions made with stack design revolves around the tradeoff between efficiency and cooling power. This tradeoff arises because there is a point within the resonator at which the pressure and velocity oscillations work together to maximize the thermoacoustic effect. However, this location is an infinitesimally small cross section which would produce no cooling power if the stack were operated at this point only. As the stack is made longer, the cooling power increases but the efficiency decreases because the further cross sections of the stack are from the optimal point, the less efficient they operate. Tijani *et al*. [67] showed that for every stack length there is an optimal placement and suggests that the optimal placement is generally close to half way between the velocity and pressure nodes.

Stack spacing is another important aspect of stack design. As the surface area within the stack is increased, the power density also increases because the thermoacoustic effect takes place at the surface. However, if the surface area

becomes too dense the thermal contact between the working fluid and the stack will be too strong which will prevent the thermoacoustic effect from taking place. Tijani *et al*. [77] systematically investigated the optimal stack spacing for parallel plate stacks by building and comparing the performances of a number of stacks with varied spacing. The results showed that 2.5 thermal penetrations was the optimal spacing for his refrigerator.

The stack material and thickness are also important design considerations. A material that has a low thermal conductivity is desired because heat conducting across the stack works against the refrigerator. However, the material must also have a heat capacity much larger than the heat capacity of the working fluid so that the temperature gradient may be created and remain. Mylar [77] and 35 mm camera film [78] are some examples of materials used in the literature.

The material must be thick enough to provide sufficient heat capacity but the thickness should be minimized with this restraint in mind to reduce the blockage caused by the stack plates. Another adverse effect of the stack becoming too thick is the formation of eddies at the ends of the stack which cause loss. Blanc-Benon *et al*. [79] developed computational model for the flow at the end of a thermoacoustic stack and validated the results by taking particle image velocimetry (PIV) measurements. Their work shows that, as the plates of a thermoacoustic stack get thicker, the formation of eddies do indeed take place.

3.2.4 Heat Exchangers

A great wealth of research and literature exists for heat transfer under constant flow. However, the flow within thermoacoustic refrigerators is oscillatory with no

mean displacement of the gas particles. Paek *et al*. [80] noted that very little research has been performed on heat transfer under such conditions and most of the research that has been performed was done on thermoacoustic refrigerators. This makes educated designs of heat exchangers in thermoacoustic refrigerators rather challenging.

The heat exchangers are generally made out of copper and often have similar cross sectional profiles as the stack. Tijani *et al*. [67] notes that the porosity of the heat exchanger should match that of the stack in order to maintain the velocity of the flow through the stack. He also notes that the length of the heat exchanger should be on the order of the maximum displacement of the gas particles.

Nosfar *et al.* [81] constructed a heat exchanger with the same shape as a parallel plate stack. They developed a model for this heat exchanger and tested it. Their experimental results loosely follow their theory with lots of error. However, their results do show that the heat transfer coefficient for the heat exchanger is higher under greater mean pressures and at the resonant frequency where the highest dynamic pressure takes place. They assume that this higher heat transfer coefficient is due to a greater number of gas particles being in contact with the heat exchanger surface.

Paek *et al*. [80] studied a heat exchanger in a thermoacoustic refrigerator with water flowing through micro fluidic channels. They developed a model for the non-dimensional heat transfer coefficients for oscillating flows. They propose that if the flow is assumed to be steady instead of oscillatory, a modified acoustic-Reynolds number can be used to predict heat transfer in their heat exchanger. They compare

models for their heat exchanger for constant and oscillatory flows. Though they are able to somewhat predict heat transfer coefficients, the error with the oscillatory model is seen to be many times higher than the case where constant flow was modeled and used.

3.2.5 Working Fluid

Another important design consideration is the choice of the working fluid which fills the resonator. Both the viscous and thermal penetration depths as well as the natural frequency of the resonator are dependent on the choice of working fluid. Belcer *et al*. [82] points out that a high ratio of specific heat and small Prandtl number are desirable characteristics of the working fluid. The Prandtl number is of particular interest because it is equal to the square of the ratio of the viscous penetration depth to the thermal penetration depth. A small Prandtl number means that the viscous effects are small compared to the thermal effects.

Belcer *et al*. [82] explore this concept further. He suggested that when mixing two binary gases, the minimum Prandtl number occurs when the lighter gas is approximately 66% by volume. He tests his theory and gets reasonable results. However, he concludes that the design applications must be taken into account before selecting a fluid for thermoacoustic devices, citing the example that when small temperature differences are the design goal, mixtures including polyatomic gases with small specific heat ratios may be desired.

Tijani *et al*. [83] conducted numerous experiments with different gas mixtures used as the working fluid in thermoacoustic refrigerators. Their experiments centered around mixing helium with other noble gases (*Xe, Kr, Ar, Ne*) and studying the effect

of the resulting Prandtl numbers on refrigerator performance. They found that though the Prandtl number decreases as the mole fraction of helium to the other noble gas is decreased, the density of the overall working fluid increased. This increase in working fluid density reduces the cooling power of the system. Because of this tradeoff between efficiency and cooling power comes into play, the authors conclude that the optimal working fluid for helium-noble gas mixtures depends on the design goals of a specific refrigerator.

Giacobbe [84] introduced methods for calculating the Prandtl number, viscosity, and thermal conductance of mixtures of gases. His paper describes experiments using mixtures of helium and other noble gases to validate his theoretical work. His results are in good agreement with his theory which allows this method to be used to obtain good estimations of the Prandtl number for gas mixtures to be made.

3.3 Modeling

As with most fields of engineering these days, computational models are very important in the field of thermoacoustics. A lot of different thermoacoustic computational tools exist today. Most but not all of these tools simplify the problem by making the assumption of a one dimensional flow. Though a thorough review of the computational tools is not carried out here, a brief overview of some of the most important thermoacoustic computer simulations is presented.

3.3.1 Numerical Modeling

Worlikar *et al*. [85] developed a numerical model for thermoacoustic refrigerators. They point out that in the region of the stack, the flow cannot be

assumed to be one dimensional due to effects such as vortex shedding. They also pointed out that because the resonators length is not insignificant next to the acoustic wavelength, nonlinear effects should be taken into account. They used two separate codes, one for the areas away from the stack and one for the area near the stack. The code for the areas away from the stack assumes one dimensional flow while the code for the areas near the stack assumes that the spatial dependence of the acoustic wave is negligible because the stack is small compared to the acoustic wave. They are able to achieve results similar to experiments using these two codes for low Mach numbers.

Further studies were carried out by Worlikar *et al*. [86] in which they created a two dimensional code of a thermoacoustic refrigerator. They were able to obtain very good results for low drive ratios (<1.5%) but their simulated results start to diverge from experimental results at higher drive ratios. They noted that at lower drive ratios, the simulation follows linear theory and the flow is largely one dimensional. However, as the drive ratio increases, their simulation predicts that the flow departs greatly from being one dimensional which is one of the reasons that linear models break down at high drive ratios.

Marx and Blanc-Benon [87] performed numerical simulations on stack-heat exchanger coupling in a thermoacoustic refrigerator. Due to their simulations being very computationally expensive, they simplify their model by using a two dimensional model which includes one zero-thickness plate and half of a channel. This allows for symmetric boundary conditions at the wall and saves a lot of computational time. Marx and Blanc-Benon observed nonlinear effects consisting of

non-sinusoidal temperature oscillations at the edge of the zero-thickness plate even in cases where an isothermal plate was used for any Mach number. At higher Mach numbers, they observed nonlinear distortion of the temperature oscillations away from the plate. This has the important consequence of having the energy flux vary proportionally with the Mach number instead of the square of the Mach number for cases where the Mach number is high. Marx and Blanc-Benon also included heat exchangers and found that the heat exchangers must be close to the particle displacement within the refrigerator in order to avoid loss of efficiency.

3.3.2 DELTAEC

Many commercial numerical integration tools are available. Best known of these tools is the software package Design Environment for Low-amplitude Thermoacoustic Energy Conversion or DELTAEC [88] (Formerly known as DELTAE). This software package was produced at Los Alamos National Laboratories by part of the group which works on thermoacoustics of which G. Swift is most notable. The software and users manual can be downloaded for free which has lead to the widespread use of this software throughout the literature.

DELTAEC numerically integrates the continuity, momentum, and energy equations (derived in chapter 2) for thermoacoustic devices. It uses a simplified one dimensional approximation and assumes that the amplitude of oscillation is low and has sinusoidal time dependence. Poese and Garret [89] experimentally found that DELTAEC starts to lose accuracy for ratios of pressure amplitude to mean pressure above 3%.

Models are comprised of a number of segments which are pieced together by the user. These segments reflect the physical properties of the refrigerator and assume the problem is one dimensional throughout the segment. Segments are linked together much in the way electric circuits are often drawn. DELTAEC is discussed in further detail in chapter 5.

3.3.3 Lumped Element Modeling

Another modeling tool used extensively throughout thermoacoustics is lumped element modeling. Lumped element modeling divides the device into elements which have spatial dimensions that are much smaller than the acoustic wavelength. This allows the spatial dependence of the elements to be approximated as constant so that the individual elements are only functions of time and neighboring elements.

Lumped element modeling is often used to conceptually model thermoacoustic devices though models aimed at numerical accuracy exist as well. Swift [17] gives derivations for one dimensional lumped element models in the presence of temperature gradients. This modeling technique creates electric circuit analogies for thermoacoustic devices where the voltage is analogous to pressure and the current is analogous to the volumetric flow rate. These models are good for conceptualizing what is going on inside of thermoacoustic devices.

3.4 Other design considerations

Many of the other most notable publications on thermoacoustic refrigerator design fail to fit under any of the categories discussed above. Some of these

publications are, however, still very important to the thermoacoustic literature. The most notable of these publications are discussed in this section.

Reid *et al*. [90] suggested that eliminating heat exchangers in thermoacoustic refrigerators could greatly increase the efficiency. They conducted experiments with a thermoacoustic refrigerator in which a slow and constant flow of gas is superimposed on the refrigerator. They computed theoretical results in which they predicted that there will be a higher cooling power and greater efficiency for the refrigerator with flow going through it. Their results showed these trends to be true and agree fairly well with their theoretical predictions.

Hiller and Swift [91] experimented with condensation in a thermoacoustic refrigerator with a steady air flow going through it. Air was introduced into the hot end of the refrigerator near its dew point. The air was then forced through the stack where it was cooled, causing water to condense. Hiller and Swift proposed two models for this condensation, the first assuming that a mist formed within the stack while the second assumed that water condensed on the sides of the stack directly. They ran experiments and measured the temperature through the stack. The experiments were in support of the '*wet-wall model*' which assumed the water condensed directly to the sides of the stack.

Swift *et al*. [92] proposed a refrigerator design aimed at recovering some of the energy wasted in the form of exhausted heat. They introduced the use of acoustic transmission lines to feed acoustic power from the hot end of a refrigerator back to the driver. A model was built with the intent of demonstrating the feasibility of the principles. Experimental results showed that such refrigerator designs were indeed

feasible which made Swift *et al*. feel optimistic about future designs along the same lines which would produce higher efficiencies.

Reid and Swift [93] did experiments with what they called a flow-through thermoacoustic refrigerator. In this refrigerator, the cold heat exchanger is eliminated by using the air one wishes to cool as the working fluid itself. Reid and Swift argue that the flow-through thermoacoustic refrigerator has a greater potential for efficiency for two reasons. The first of these reasons is that one of the heat exchangers is eliminated. The second is that the air that is to be cooled is in contact with the entire stack instead of just the coldest end, creating a greater contact surface between the air and the stack.

3.5 Summary

This chapter has presented a survey of the basic design strategies for thermoacoustic refrigerators, and a discussion of the important design features of the individual components with emphasis on their effect of the overall performance of the thermoacoustic refrigerators. The different design and predictive tools of thermoacoustic refrigerators are then presented, in details, along with their merits and limitations. Particular focus is given on the DeltaEC which is developed by Los Alamos National Laboratories because of its ability to analyze thermoacoustic refrigerators with various types of drive systems.

Chapter 4: Piezoelectrically-driven Thermoacoustic Refrigerator

A piezoelectrically-driven thermoacoustic refrigerator was designed, built, and tested so that a model could later be developed. This chapter first discusses the design choices made for this refrigerator. It then goes on to detail the design and describe the construction process. Finally, it discusses the operation of this piezoelectrically-driven thermoacoustic refrigerator and shows the experimental results which the model in the fifth chapter is validated against.

4.1 Refrigerator Design

The starting point for the design of this thermoacoustic refrigerator was the driver as it was required to be piezoelectric. This is the reverse of most thermoacoustic refrigerator designs discussed in chapter 3 where the driver selection comes much later in the design process. Once a suitable driver was selected, the choice of the resonator and stack followed as detailed in the following sections.

This refrigerator was designed to be low cost and easy to assemble and study so that it can be modeled. Once models are created and validated, more expensive and difficult to construct piezoelectrically-driven thermoacoustic refrigerators will then be able to be modeled before massive amounts of effort are put in to construct them.

4.1.1 Piezoelectric Driver Selection

Most piezoelectric drivers consist of a metallic diaphragm with piezoelectric material deposited on it. Electrodes are then attached to the two sides of the

piezoelectric material. When voltage is applied across the electrodes, the piezoelectric material expands or contracts while the metal diaphragm is not affected by the voltage. The mismatch in expansion and contraction between these two materials which are bonded together causes a bending moment in the diaphragm. If an AC signal is applied, the diaphragm oscillates back and forth at the frequency of the signal, causing the air around it to oscillate as well. Such a speaker and the process by which it oscillates are shown in Figures 4.1 through 4.3.

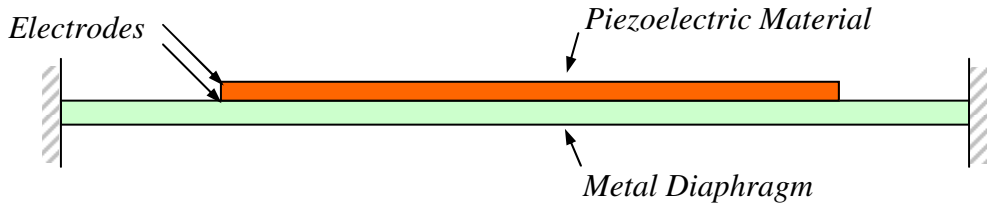

Figure 4.1: Side view of piezoelectric speaker with no voltage applied

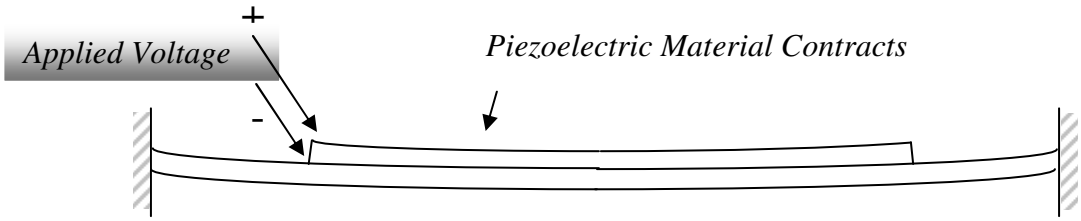

Figure 4.2: When voltage is applied, the diaphragm deflects

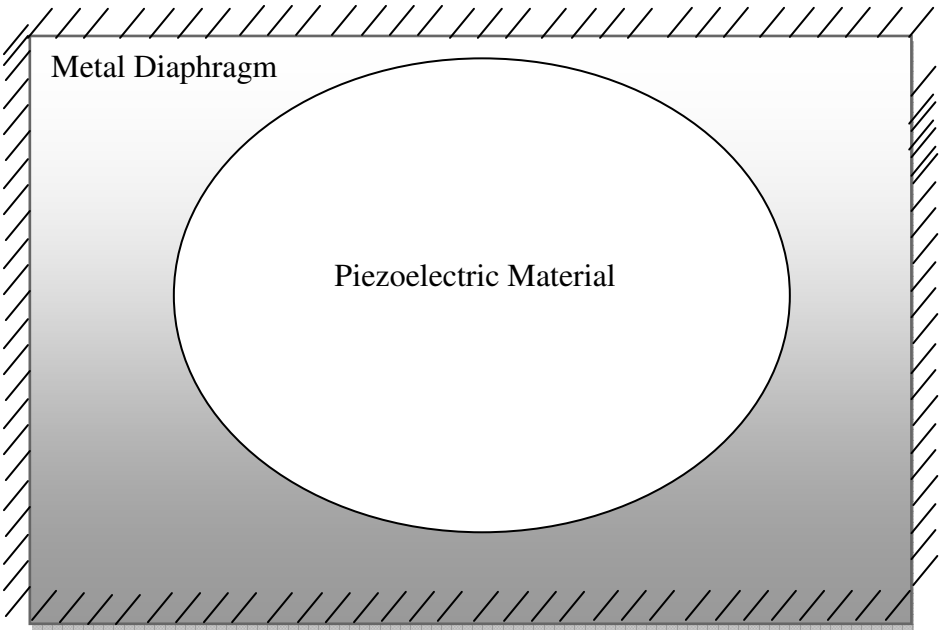

Figure 4.3: Top view of piezoelectric speaker

Piezoelectric speakers can output considerable amount of acoustic power at high frequencies (on the order of a few kilohertz). However, because their displacement is limited, they have difficulty generating significant acoustic power at lower frequencies (On the order of a few hundred Hertz). Because small dimensions go along with high resonant frequencies, building such a small refrigerator would have been difficult and expensive. This made it necessary to use a lower resonant frequency with the refrigerator.

Attempts to make a thermoacoustic refrigerator with an easily measurable cooling out of classic piezoelectric speakers turned out to be futile. Because of this, the commercially available PZ-94 Harsh Environment Speaker made by ISL Products was used. This speaker, pictured in Figure 4.4, is a piezoelectrically-driven speaker.

Its frequency response function is shown in Figure 4.5. Figures 4.6 and 4.7 details how this speaker works.

Figure 4.4: ISL Products PZ-94 Harsh Environment Speaker (Picture from [94])

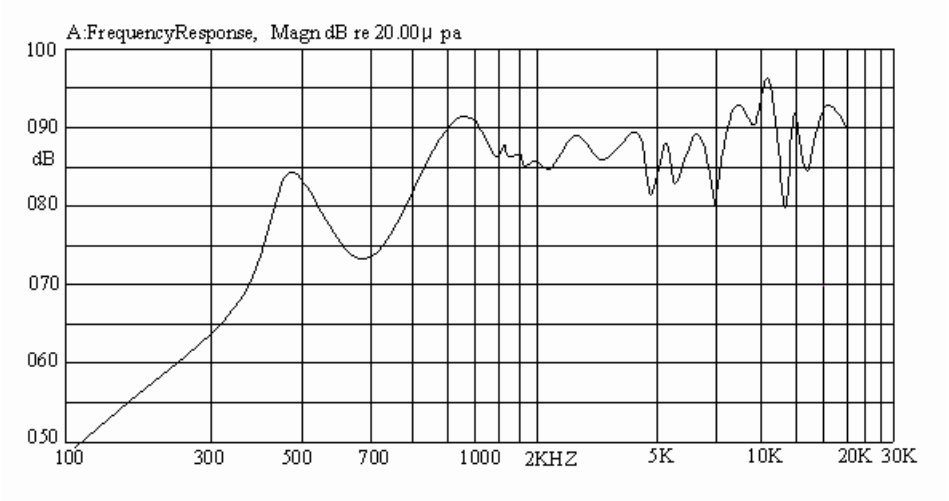

Figure 4.5: Frequency Response of the PZ-94 Harsh Environment Speaker (Picture from [94])

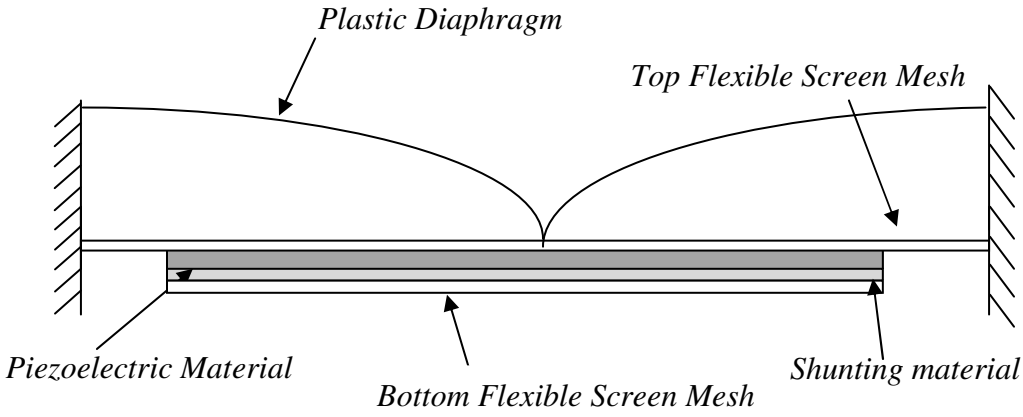

Figure 4.6: Cross section view of PZ-94 Harsh Environment Speaker

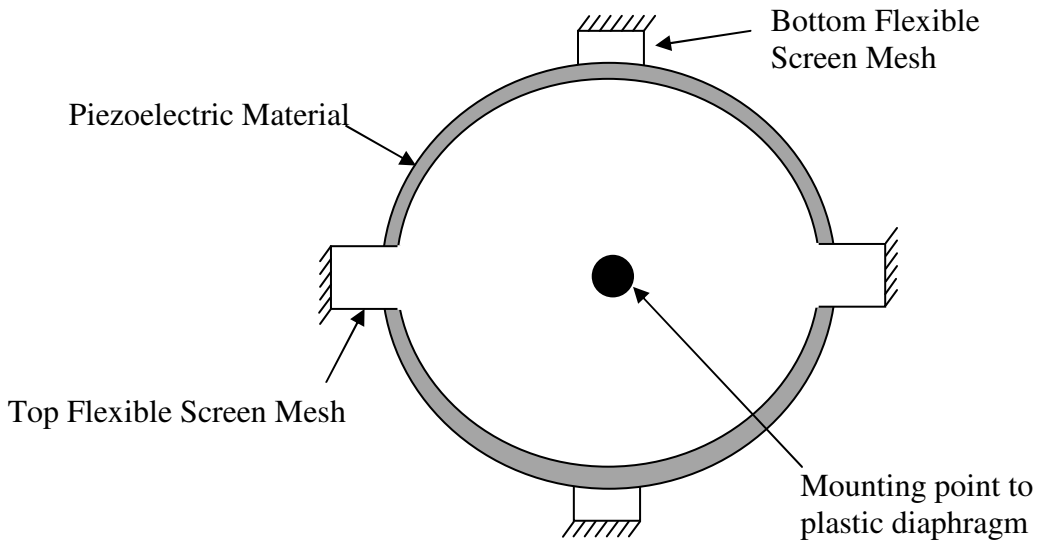

Figure 4.7: Top view of PZ-94 Harsh Environment Speaker with diaphragm removed

The speaker design shown in the figures above allows this piezoelectric speaker to achieve higher displacements than the previously discussed standard type. The flexible screen meshes are used as both electrodes and mounting mechanisms. When a voltage is applied across the top and bottom screens, the piezoelectric material expands or contracts (depending on the voltage direction) while the shunting material remains the same. This causes a moment to be created between the two, causing the whole disk to deflect. When this deflection takes place, the flexible mesh holding the piezoelectric disk in place allows the whole disk to be displaced slightly. As the piezoelectric disk is excited by an AC current, the rapid deflection of the disk

in both directions causes the whole disk to move back and forth through the air. This motion in turn pushes the plastic diaphragm back and forth, generating an acoustic power output with a much higher displacement than would be achievable by conventional piezoelectric disks.

This design allows for the first speaker resonance to be much lower. The first resonance is seen in Figure 4.8. Scans over the surface of the speaker were made using a scanning laser Doppler vibrometer to confirm the first resonance and mode shape. The results of a scan of the piezoelectric speaker diaphragm driven at 400 Hz are shown in Figure 4.8. This confirms that this frequency is driving the first mode for a circular disk, which is the desired mode because the displacement is all in one direction so the speaker is nowhere working against itself as it would be for higher mode shapes.

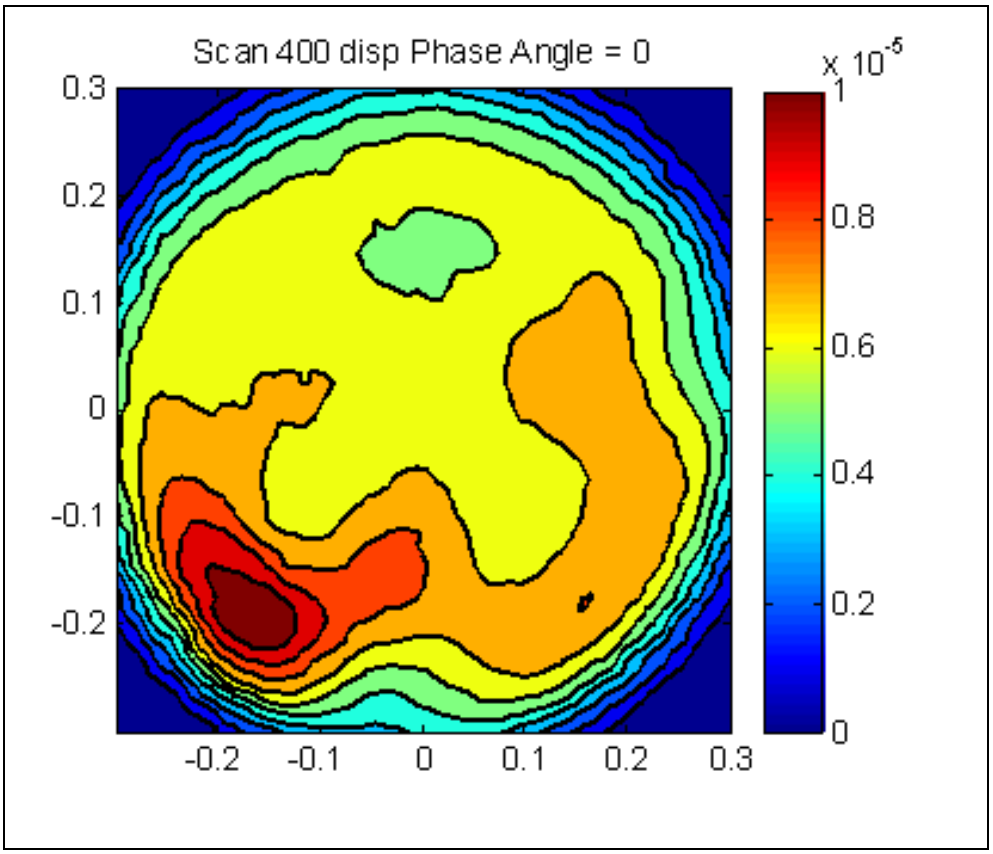

Figure 4.8: Maximum displacement of piezoelectric speaker face when driven at 400 Hz

Scans were made across many frequencies and phase angles were also recorded. The magnitude and phase of the volumetric flow rate are plotted against the frequency is Figures 4.9 and 4.10 respectively. These figures show that at low frequencies, the speaker acts like a single degree of freedom system with a damping ration of 0.05 which is represented by the green line in Figure 4.9 and the red line in Figure 4.10. The blue line in Figure 4.9 plots the average volumetric flow rate where more than one set of data was taken.

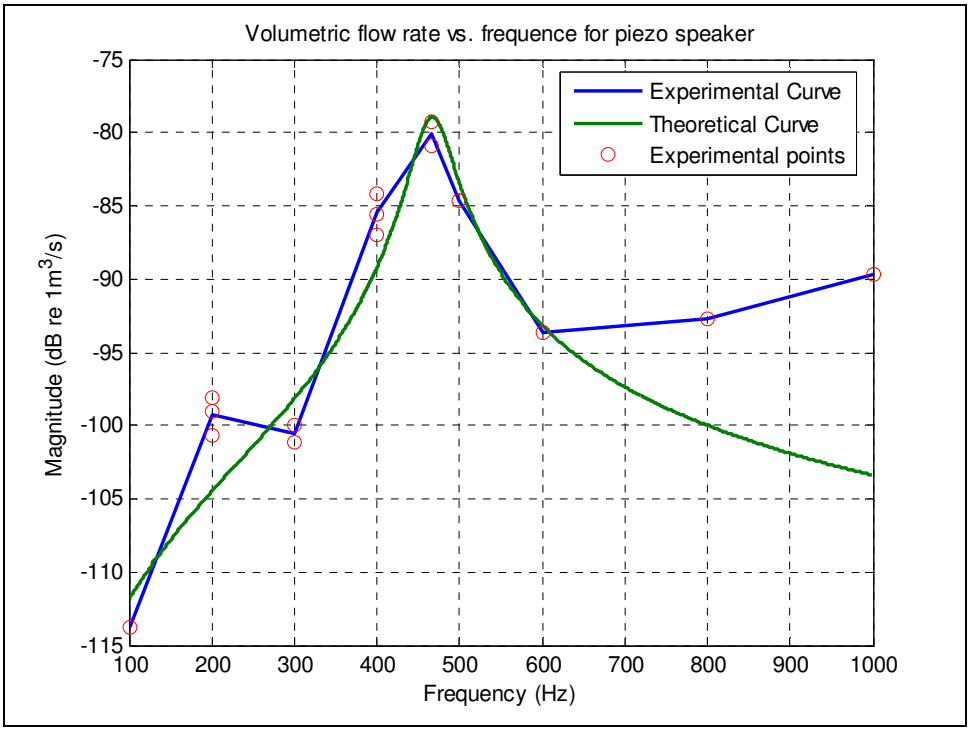

Figure 4.9: Volumetric Flow vs. Frequency

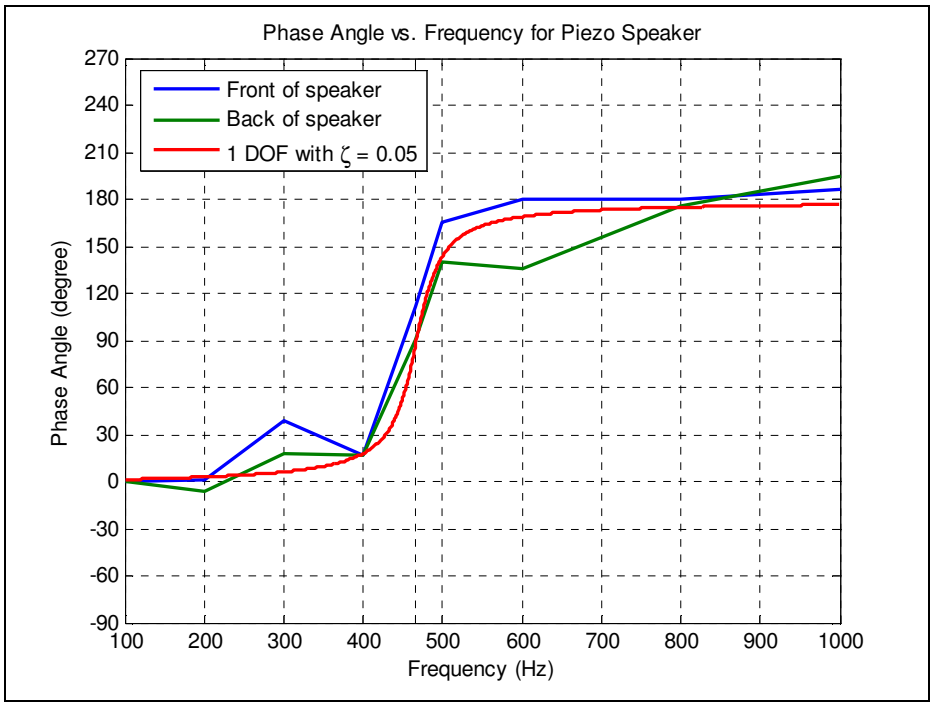

Figure 4.10: Phase between Voltage Input and Speaker Diaphragm

The first natural frequency allows significant acoustic power to be delivered to the resonator while at the same time lets the sizing of the rest of the thermoacoustic refrigerator to be big enough that it can be constructed easily. Also, modeling will be much simplified for this speaker at low frequencies because its behavior resembles a single degree of freedom system. For these reasons, the *ISL Products PZ-94 Harsh Environment Speaker* was selected as the driver for this piezoelectrically-driven thermoacoustic refrigerator.

4.1.2 Stack Design

Most thermoacoustic refrigerator stack designs are driven by cooling power requirements. For this design however, easily measurable cooling was the only requirement. Therefore, the stack and resonator designs were based off of the design given by Russel and Weibull [28].

The stack needed spacing on the order of 2 to 4 thermal penetration depths. The calculation of the thermal penetration depth is given in equation (2.16) above and is repeated below after substituting in frequency instead of angular frequency.

$$\delta_k = \sqrt{\frac{\kappa}{\pi f \rho c_p}} \tag{4.1}$$

The variables that make up the thermal penetration depth are functions of the gas properties and the frequency. Air at room temperature was selected as the working fluid for this refrigerator. The properties for air at room temperature to be used in equation (4.1) are as follows [95].

$$\text{Thermal Conductivity } \kappa = 0.0257 \frac{W}{m \cdot K} \tag{4.2}$$

$$\text{Density } \rho = 1.205 \frac{kg}{m^3} \tag{4.3}$$

$$\text{Specific Heat Capacity } c_p = 1005 \frac{J}{kg \cdot K} \tag{4.4}$$

These variables are then used with equation (4.1) where f is the driving frequency of the refrigerator. This yields the following:

$$\delta_k = 1.3 \times 10^{-4} m \tag{4.5}$$

Recalling from chapter 3 that the stack spacing should be around 2.5 thermal penetration depths, the targeted stack spacing is $3.25 \times 10^{-4} m$ or $0.325 mm$. A coil design for the stack was then selected for ease of manufacturing. The cross section of the stack was then required to be round. The stack cross sectional area selected to be much smaller than the speaker diaphragm was chosen in order to increase both pressure and volumetric flow rates in the resonator. The final selection was 0.875”

(2.14 *cm)* diameter was used because the plastic tubes used for the resonator come in that standard size. The stack length was selected to be 35 mm following Russel and Weibull [28].

4.1.3 Resonator Design

The resonator design was driven by the need to have a natural frequency near to 400 Hz so as to line up with the speaker natural frequency. It also needed to interface with the speaker and stack cross sections. Finally, it had to be easy to manufacture.

A simple tube was selected to be used as the resonator geometry. This tube made manufacturing very simple. It also made for easy calculation of the resonator natural frequency. At the driver end, the resonator was expanded to meet the speaker as shown in Figure 4.11. The other end was plugged with an aluminum cap as this is the hot end of the refrigerator and the aluminum would help heat to leave the system.

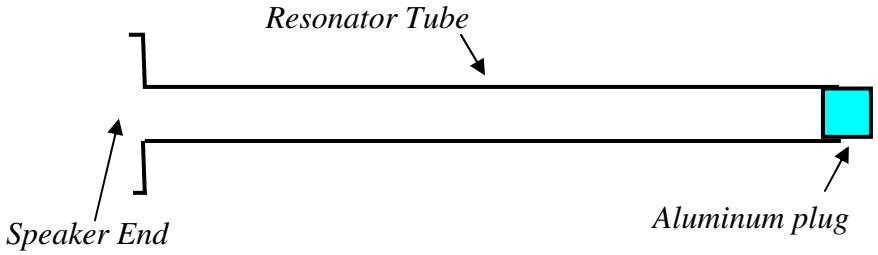

Figure 4.11: Resonator Design

The resonator shown above is a quarter wavelength resonator. This is because the end of the resonator with the aluminum plug is a pressure anti-node and velocity node. The end near the speaker has close to (but not exactly) the opposite boundary conditions (pressure node and velocity anti-node). The approximate resonator length is calculated as follows:

$$L = \frac{vel}{4f} = \frac{343 m/s}{4 \cdot 400/s} = 21.4 cm \tag{4.6}$$

The resonator length was varied somewhat after experiments were performed and the final resonator length was 9.45" (24 *cm*) which brought the natural frequency to 395 Hz. This variance in length is a result of the resonator boundary conditions at the speaker end being approximate.

The resonator cross section had to be round due to the stack. For ease of manufacturing, a 1" (2.54 *cm*) outer diameter, 0.875" (2.14 *cm*) inner diameter tube was to be used. The placement of the top of the stack was selected to be 1.85" (4.70 *cm*) from the speaker end of the resonator so that it would be well placed between the velocity and pressure nodes. The aluminum plug was simply selected to seal the end of the tube tightly.

4.2 Construction

The stack and resonator were made in house out of cheap, every day materials as detailed in the following sections. The driver was purchased as it is available commercially (model PZ-94, ISL Products International Ltd., Syosset, NY). Thermocouples and a piezoelectric buzzer were added so that the system could be measured during operation. A mount was built to hold the driver in place and is shown in the section on assembly.

4.2.1 Stack Construction

The stack spiral was made using 35 *mm* camera film. To enforce the spacing between the layers, nylon fishing line with a diameter of 0.35 *mm* was glued across the film as shown in Figure 4.12. After the glue dried, the film was rolled up as seen

in Figure 4.13, and glued at the very end. The diameter of the rolled up stack is 0.875" (2.22 cm) and its height is 1.38 in (3.5 cm). The strip of film before being rolled up is approximately 20 in (50.8 cm).

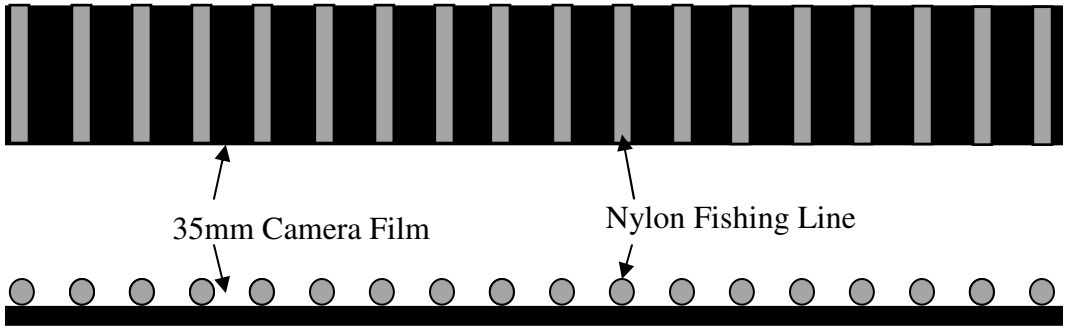

Figure 4.12: Top and side views of the stack before it is rolled up

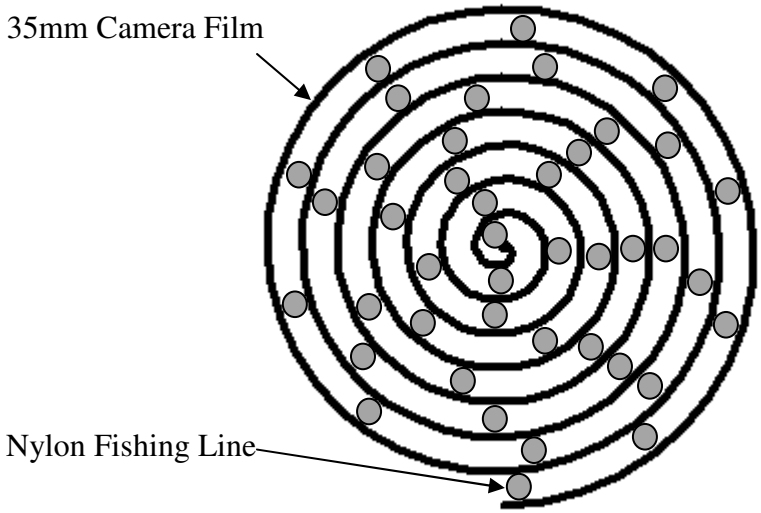

Figure 4.13: Cross sectional view of the stack after it has been rolled up

4.2.2 Resonator Construction

The resonator was constructed from acrylic tubing with a 1" (2.54 *cm*) outer diameter and 0.875" (2.22 *cm*) inner diameter. An aluminum cap was machined to fit into the end of the tube. An acrylic base plate was used to create an interface between

the speaker and the resonator, which was fastened to the resonator tube using an adhesive. Holes were drilled in the base plate which matched the speaker mounting holes for easy attachment to the speaker. The resonator is pictured in Figure 4.11.

4.2.3 Assembly

The stack was positioned inside the resonator tube by sliding it in from the top. The stack was pushed down until its top was 1.85" (4.70 *cm*) from the top of the resonator. Two small holes were then drilled in the side of the resonator so that thermocouples could be used to measure the internal temperature, one hole above the stack and one hole below it. Thermocouples were placed just through the holes and glue was used to both hold them in place and to reseal the holes. The aluminum cap was then placed at the top of the resonator.

The speaker was placed in the mount which had been made for it. The resonator was then placed above the speaker and screws were used to fasten the whole thing together. Figures 4.14 show the assembled refrigerator. The dimensions of the refrigerator are displayed in Figure 4.15.

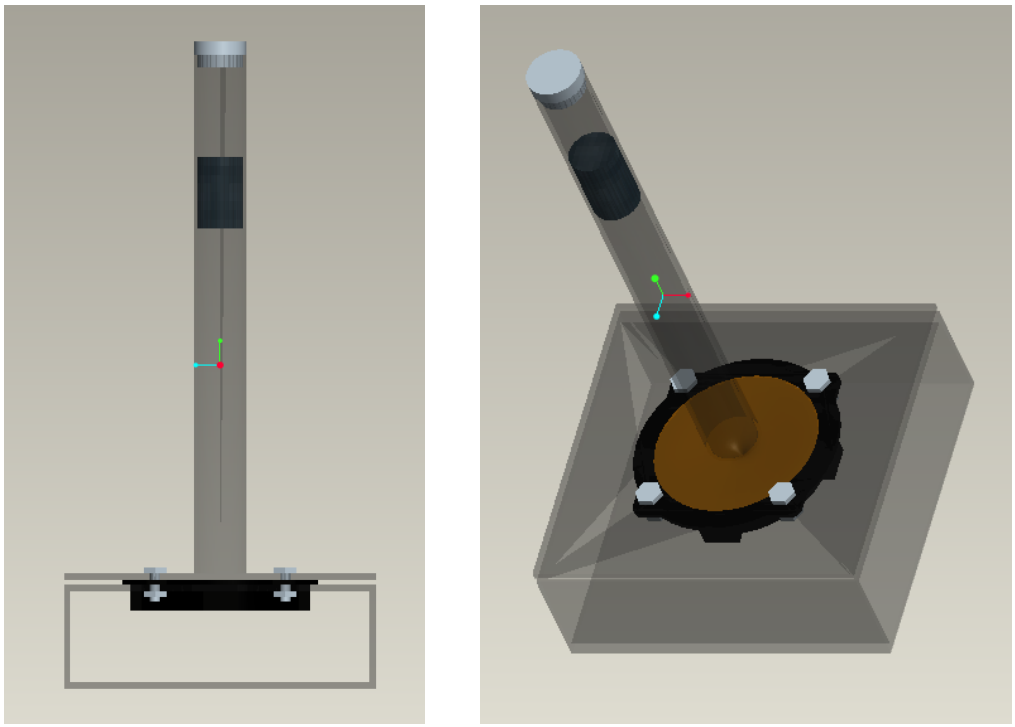

Figure 4.14: The assembled piezoelectrically-driven thermoacoustic refrigerator

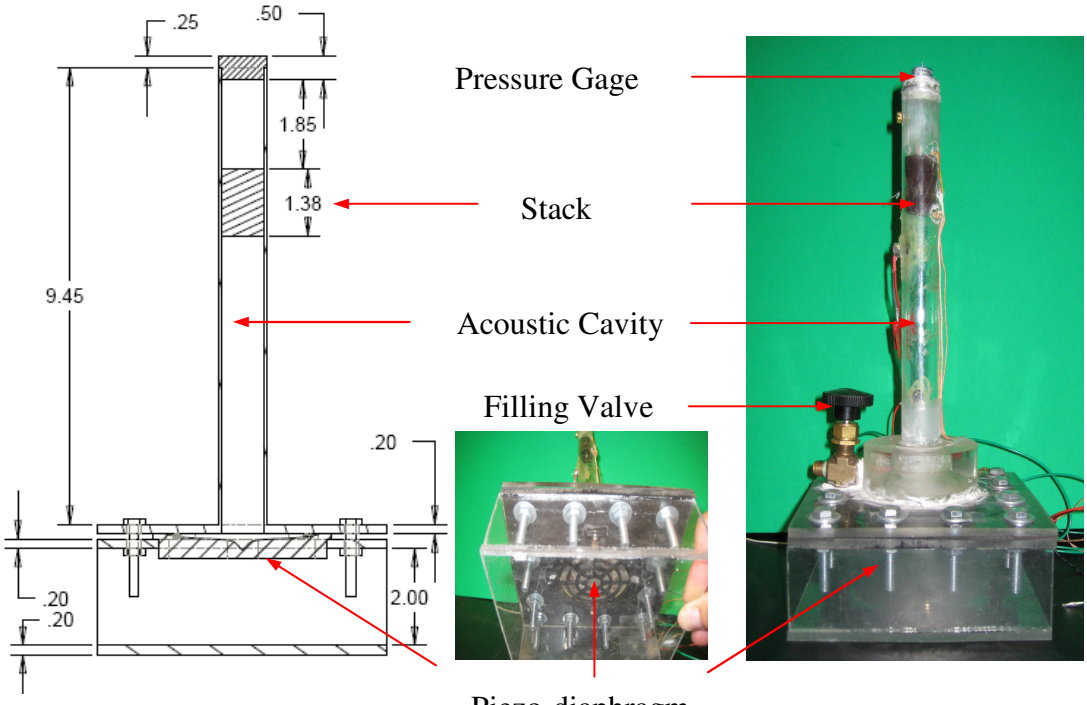

(a) – schematic drawing (b) - photograph

Figure 4.15: Dimensions of the piezoelectrically-driven thermoacoustic refrigerator

4.3 Operation

4.3.1 Setup

A signal generator was used to generate the 395 Hz sinusoidal input signal to drive the piezoelectric speaker. An amplifier was then used to bring the signal up to the desired amplitude. This amplified signal drove the piezoelectric speaker which was the input to the refrigerator.

The temperature difference across the stack was the measured output. This temperature difference was measured by the thermocouples placed at either end of the stack. The signals put out from the thermocouples were fed into an A/D board which passed the digital data into a computer for processing. A layout of the test set-up is shown in Figure 4.16.

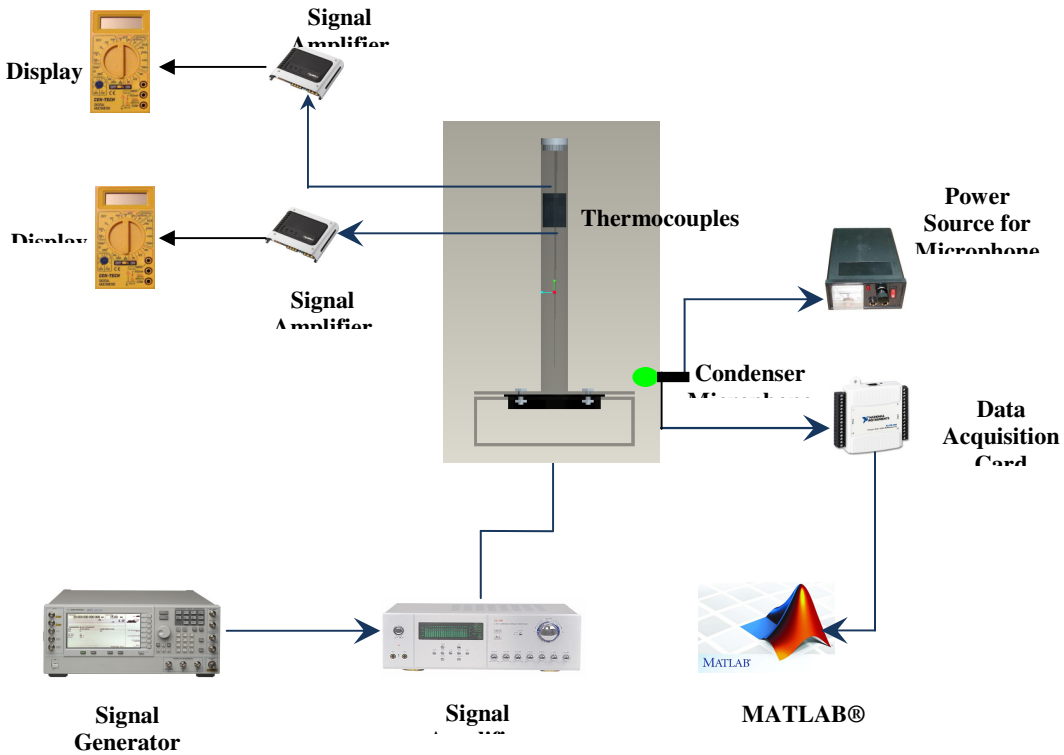

Figure 4.16: Layout of the test setup

A thermal camera (model ThermaCAM® SC 3000, from FLIR Systems, Boston, MA) was also used to collect data on the refrigerator. The thermal camera was used to provide data on the outside of the refrigerator. Because the walls of the resonator were thin, enough heat conducted to the outside surface to be able to gain visual information as to what was going on inside the refrigerator. However, all the model verification in the following chapter is based off the thermocouple data because the outside of the refrigerator is not contained in the models.

4.3.2 Operation of the Refrigerator

The refrigerator was driven by a 395 Hz signal with a 38 Vrms amplitude which drew a root mean square value of 200 mA of current. With the refrigerator at ambient temperature, the experiment was begun by flipping a switch on the amplifier which had been preset to the driving level. The input signal amplitude and frequency were then left constant throughout the experiment.

The thermocouple readings were sampled at a rate of 100 Hz. The recorded data was processed by taking the average thermocouple reading over each second which reduced the effective sampling rate to 1 Hz as well as noticeably reducing the signal noise. The thermocouple readings were monitored in real time so that steady state conditions could be determined. The thermal camera was also set to record throughout the experiment. The pictures were recorded with a sampling rate of once every fifteen seconds.

4.3.3 Obtained Data

a. Excitation at Resonant Frequency of 395Hz

In this case, the refrigerator was at its resonant frequency of 395 Hz by a root mean square voltage and current of 38 V and 200 mA respectively, *i.e.* input power is 7.6 watts. The thermocouple and thermal camera data obtained at various times throughout the operation of the refrigerator are shown in Figures 4.17 through 4.21. It should be kept in mind that the thermocouples are measuring the internal temperatures just above and just below the stack, while the thermal camera is seeing the temperature of the exterior surface of the refrigerator and has significantly less variation from the ambient temperature than the inside of the refrigerator.

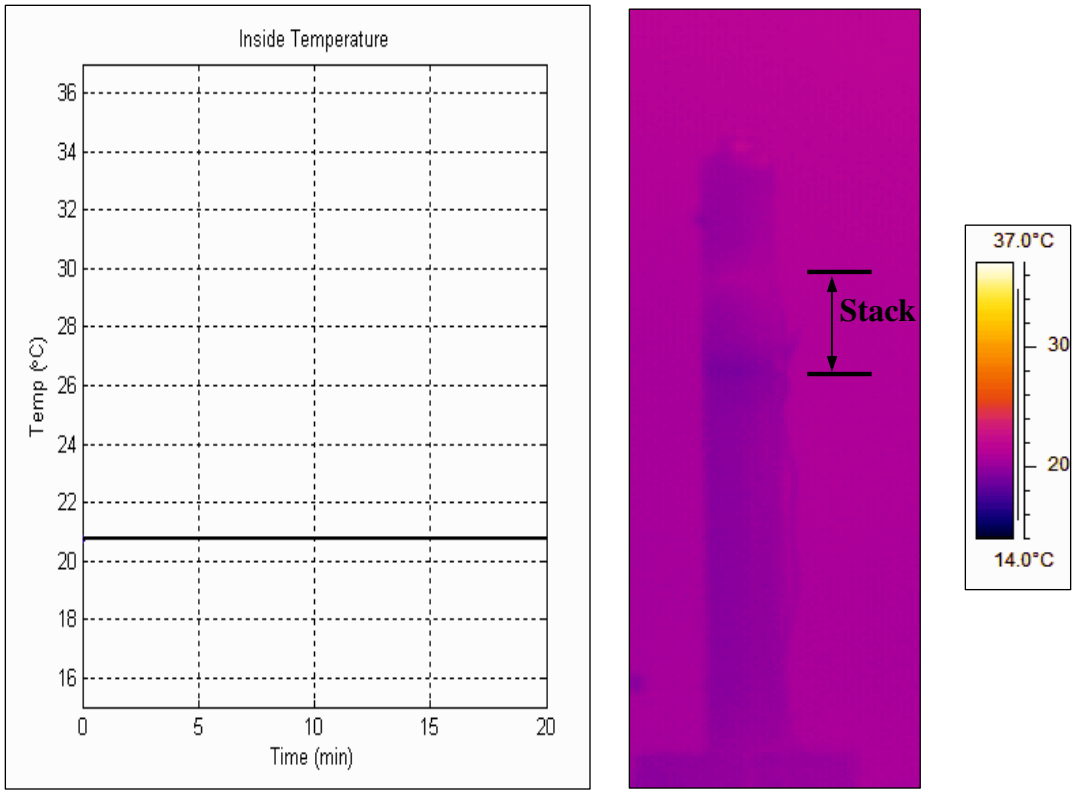

Figure 4.17: Refrigerator data at the beginning of the experiment

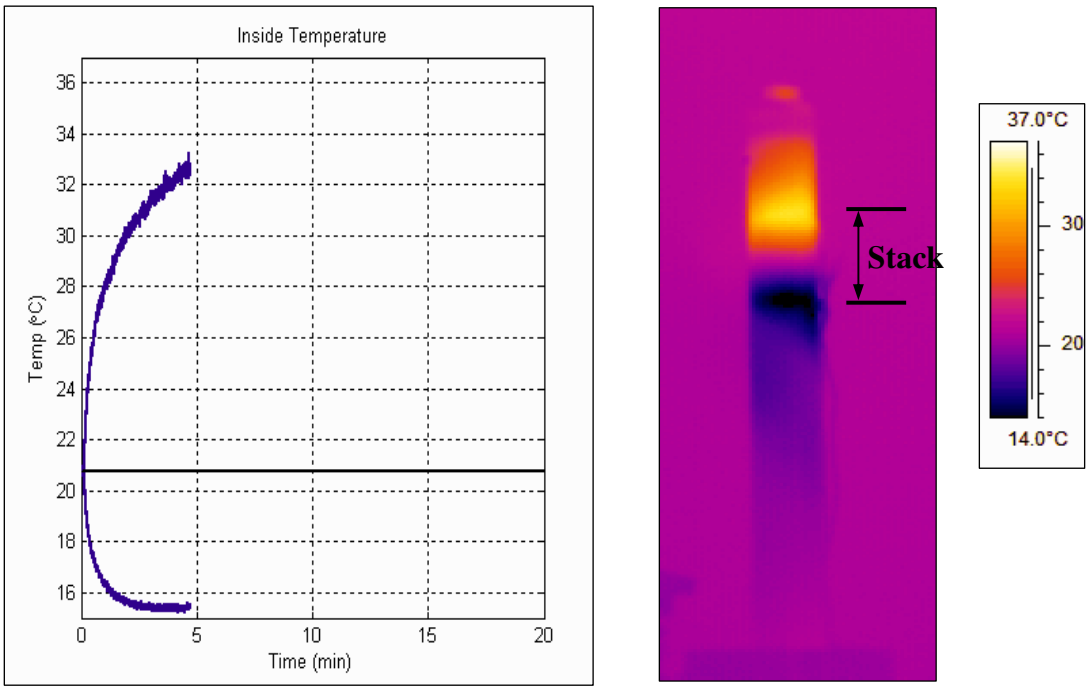

Figure 4.18: Refrigerator data after 4.75 min

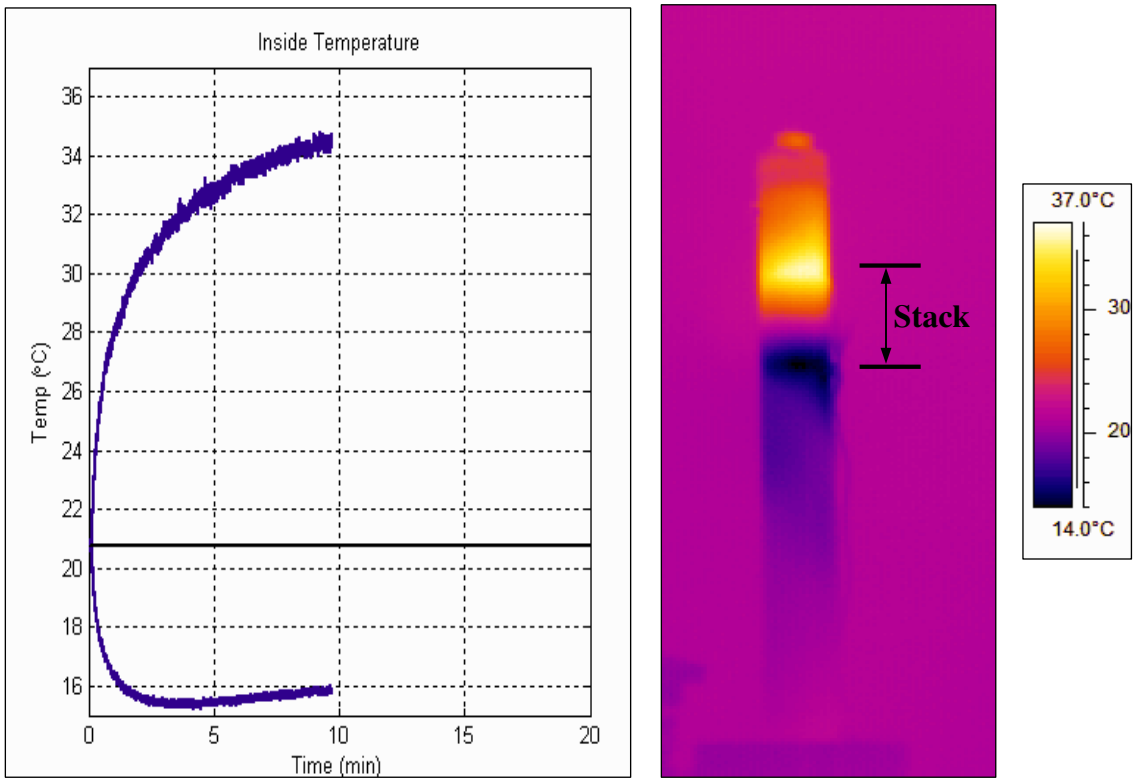

Figure 4.19: Refrigerator data after 9.5 min

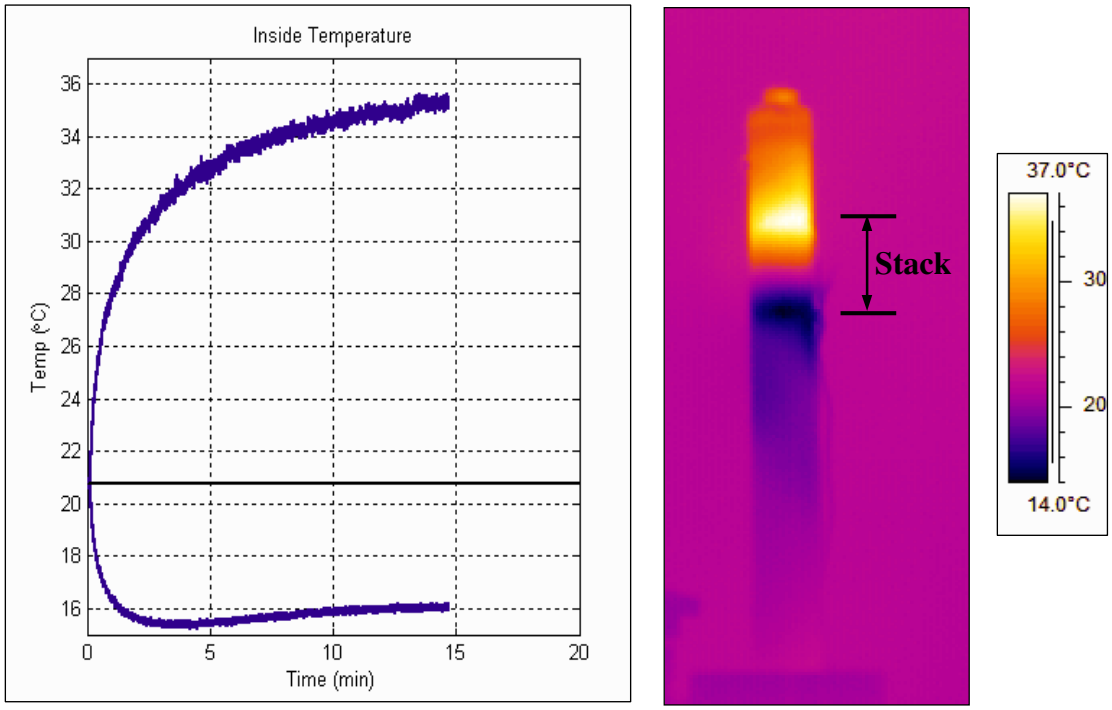

Figure 4.20: Refrigerator data after 14.25 min

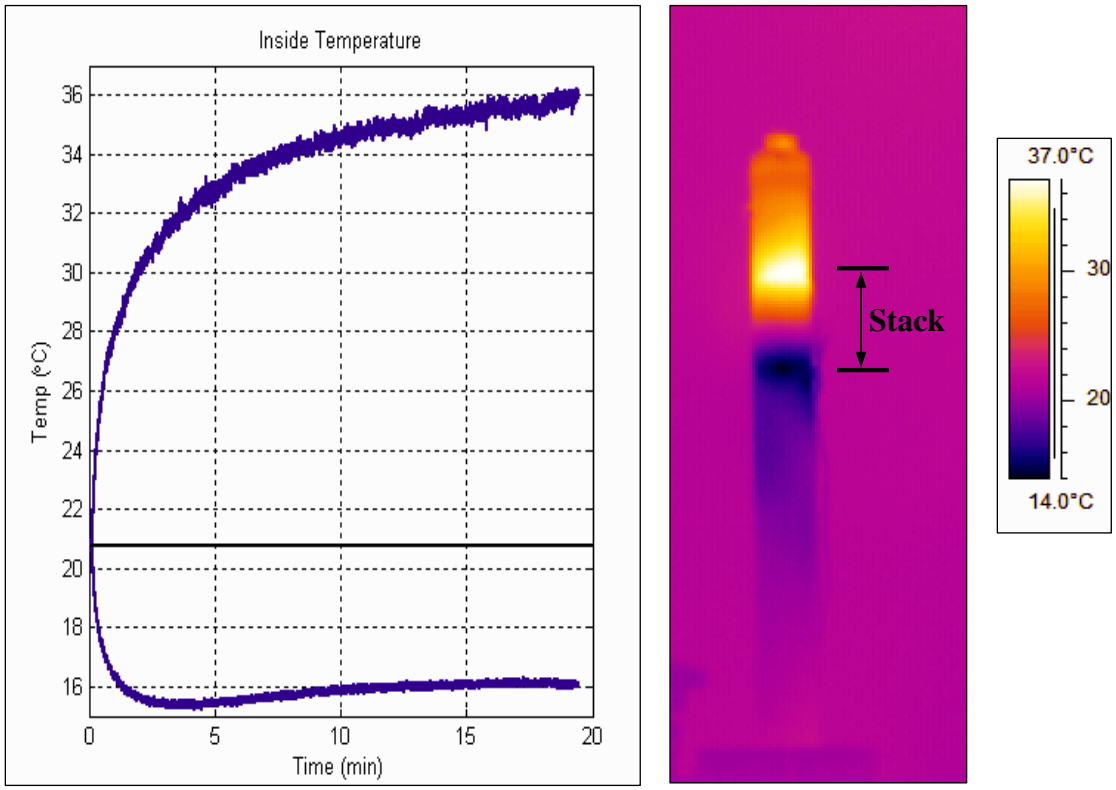

Figure 4.21: Refrigerator data after 19 min

b. Excitation off-Resonance at Frequency of 380Hz

When the refrigerator was driven off resonance at an excitation frequency of 380 Hz, the time histories of the cold and hot temperatures are shown in Figure (4.22) for different input power. It is evident that a slight shift of the excitation frequency from the resonance results in a dramatic drop of the temperature difference, between the temperatures just above and just below the stack which is generated by the refrigerator. Note that for an input power of 7.6 W, the refrigerator operating at 395Hz produces a temperature difference of 20 degrees C as shown in Figure (4.21), while operation at 380Hz results in temperature difference of only 11 degrees C as displayed in Figure (4.22).

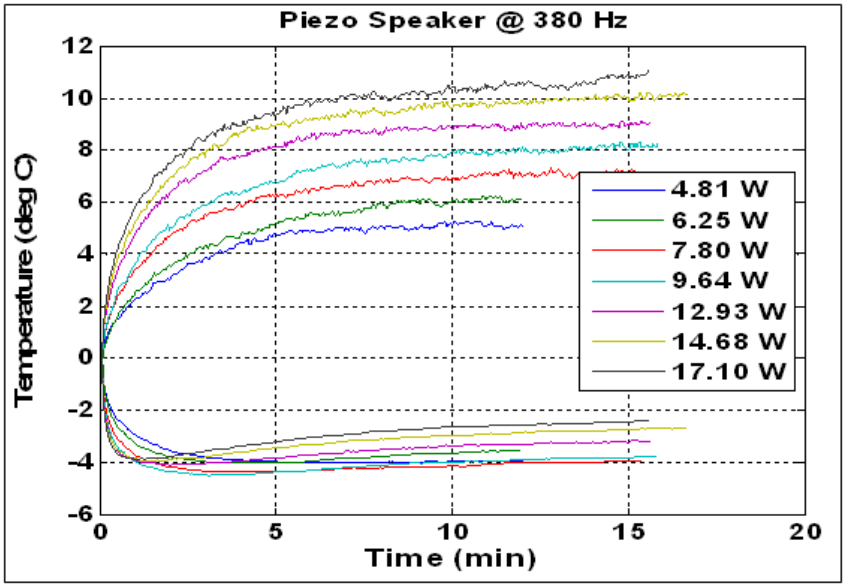

Figure 4.22: Response of piezelectric driven TAR at various power levels

4.3.4 Comparison to a Electromagnetically Driven TAR

The piezoelectrically-driven thermoacoustic refrigerator's performance was compared to a comparable electromagnetically driven refrigerator by replacing the piezoelectric driver with an electromagnetic driver. The electromagnetically driven thermoacoustic refrigerator was then run at multiple power levels and compared to results of the piezoelectrically-driven thermoacoustic refrigerator at different power levels.

Figure (4.23) shows photographs of the electromagnetically driven refrigerator which has a resonator that replicates exactly that of the piezoelectrically-driven thermoacoustic refrigerator. Because of the dynamics of the electromagnetic speaker, the resonant frequency of the electromagnetic driven thermoacoustic refrigerator is found to be 305Hz. Figure (4.24) shows the time histories of the resulting cold and hot temperatures for different input power.

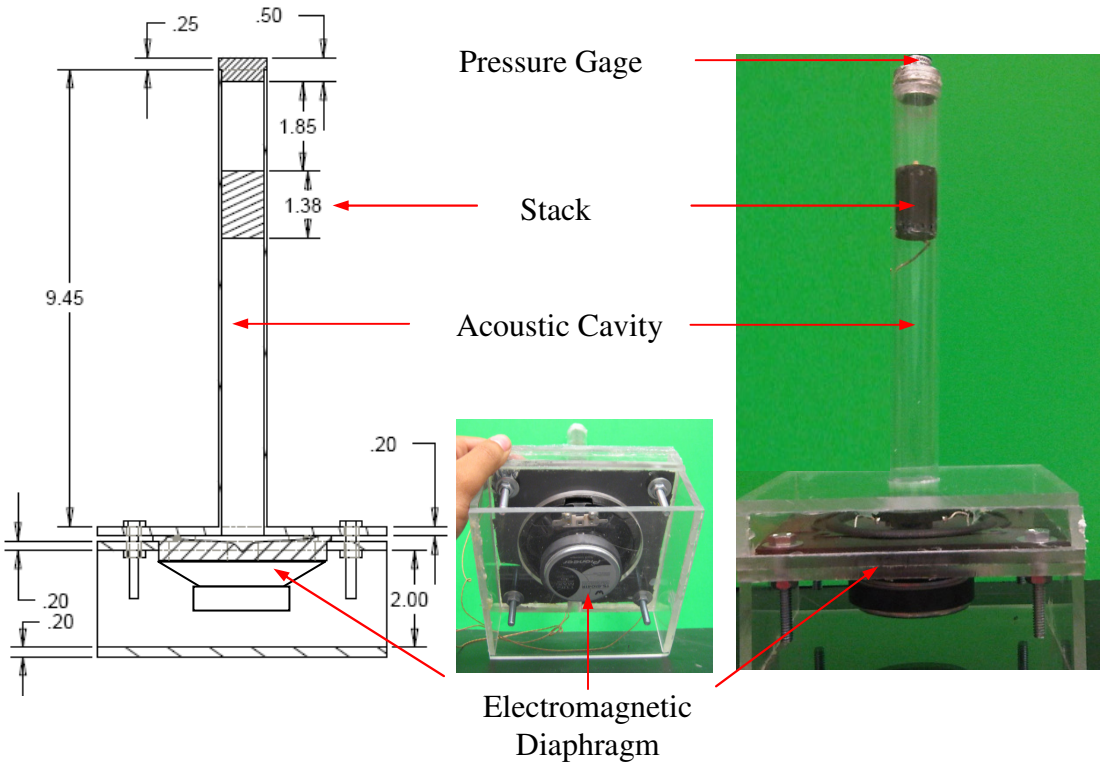

(a) – schematic drawing (b) - photograph

Figure 4.23: Dimensions of the electromagnetic driven thermoacoustic refrigerator

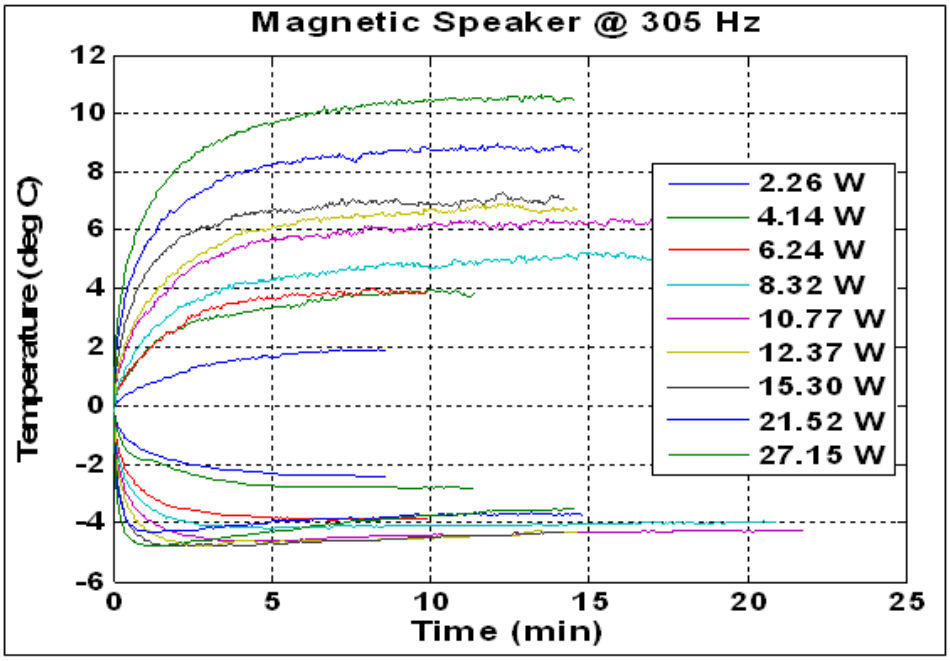

Figure 4.24: Response of Electromagnetic Driven TAR at Various Power Levels

The steady state temperature difference for the piezoelectric and the electromagnetic-driven refrigerators are plotted against the input power as shown in Figure 4.25. The comparison is carried out when the electromagnetic speaker is driven at its resonant frequency of 305Hz and at the resonant frequency of the piezoelectric speaker, *i.e.* at 395Hz. The figure suggests that, for the same input power, the piezoelectric driver produces almost twice as much temperature difference than its electromagnetically driven counterpart.

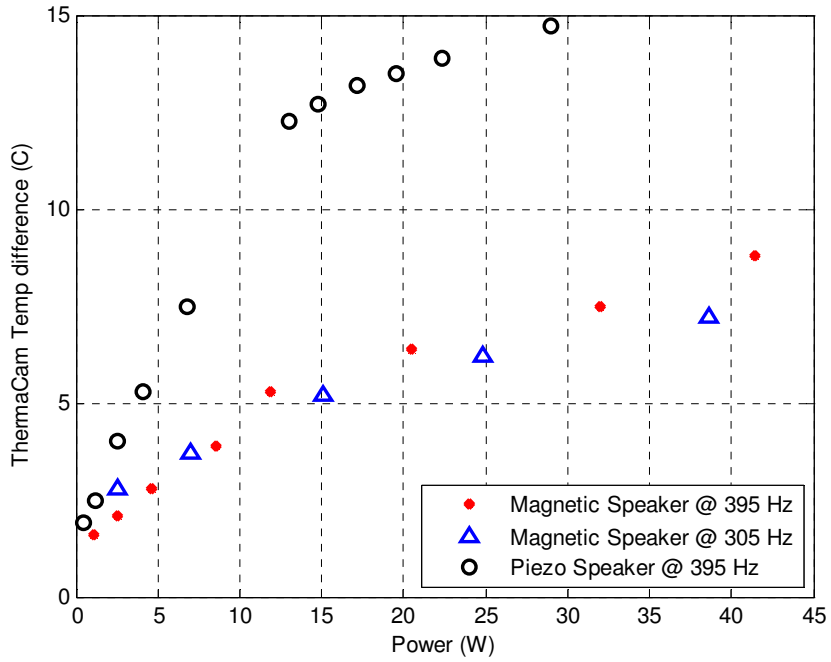

Figure 4.25: Steady State Temperature Difference versus Input Power

4.3.5 Alternate Piezoelectric Refrigerator Heat Exchanger Configurations

Experiments were also performed in which the areas above and below the stack where the heat transfer takes place were altered. The results of these

experiments are shown in Figure 4.26. The magenta line plots the temperature history for the original configuration. The light blue line shows the effect of adding a bigger aluminum plug in the end which has more surface area and thus better heat conduction. The blue line then shows what happens when the acrylic tube above the stack (on the hot end) is cut off and replaced with a copper pipe. The green line shows what happens when a fan is added which blows across the copper. Insulation is then added to the bottom side of the refrigerator which is shown by the red line. Finally, all of the changes are run together to produce the gold line.

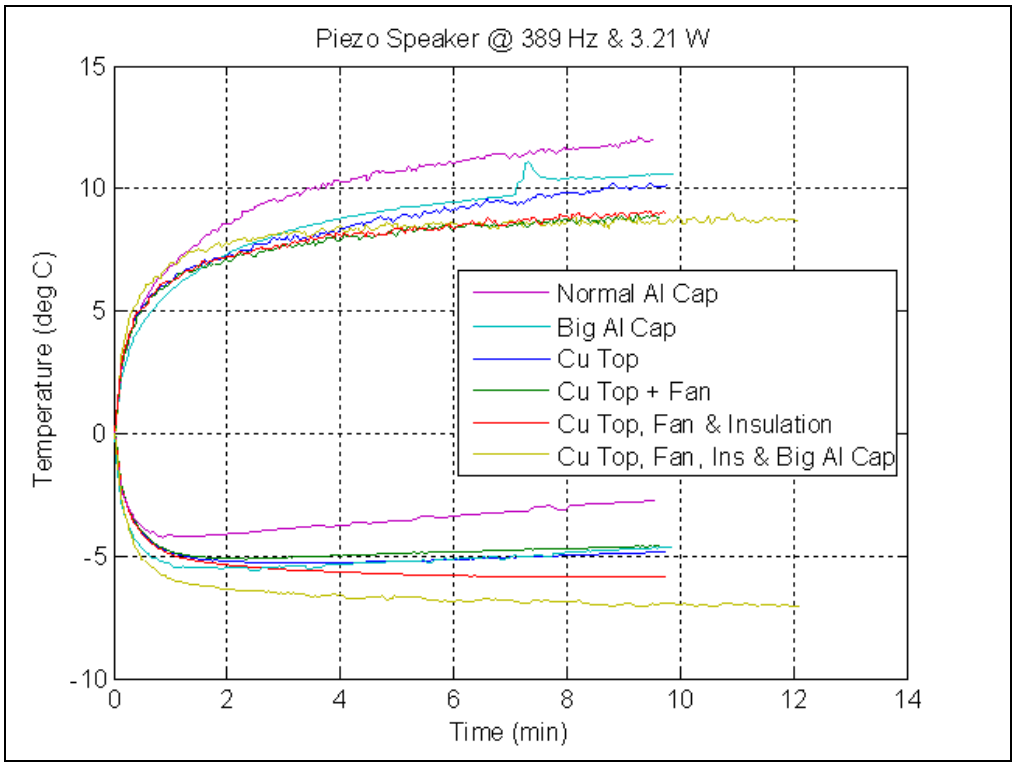

Figure 4.26: Piezoelectrically-driven refrigerator under various heat exchanger configurations

In Figure 4.26, it is shown that the changes to the heat exchangers do not significantly alter the final steady state temperature difference inside the refrigerator. This is expected as the temperature difference is more dependent on the stack

geometry than the heat exchanger geometry. However, altering the heat exchangers does alter the where that temperature difference happens to be. Both the hot and cold sides get successively cooler as the changes detailed take place.

4.3.6 Temperature Distribution inside the Thermoacoustic Refrigerator

Table 4.1 summarizes the effect of input power on the steady-state temperature attained by the piezoelectrically-driven refrigerator when it is excited at its resonant frequency of 395Hz.

INPUT POWER (WATTS)	TEMPERATURE DISTRIBUTION	INFRARED CAMERA		THERMOCOUPLES	
		Cold Temp. (SP01-Deg. C)	Hot Temp. (SP02-Deg. C)	Cold Temp. (Deg. C)	Hot Temp. (Deg. C)
5.512	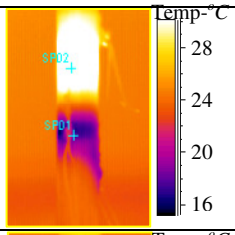	20.5	29.1	17.3	29.7
4.095	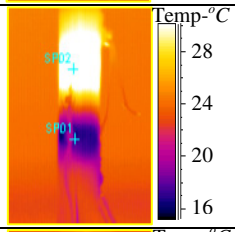	20.2	28.1	17.4	28.5
2.965	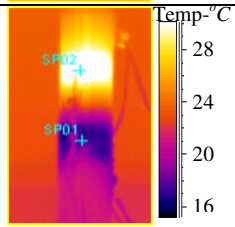	20.3	26.2	17.7	25.6
1.624	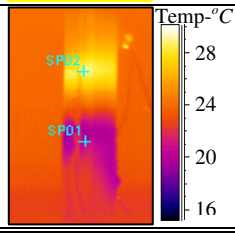	21.4	24.8	19.2	24.3

Table 4.1: Effect of input power on steady-state temperatures inside piezoelectrically-driven refrigerator

A comparison between the temperatures measured by the thermocouples and the infrared camera system reveals a good agreement within ± 1 degree *C* as shown in Figure 4.27.

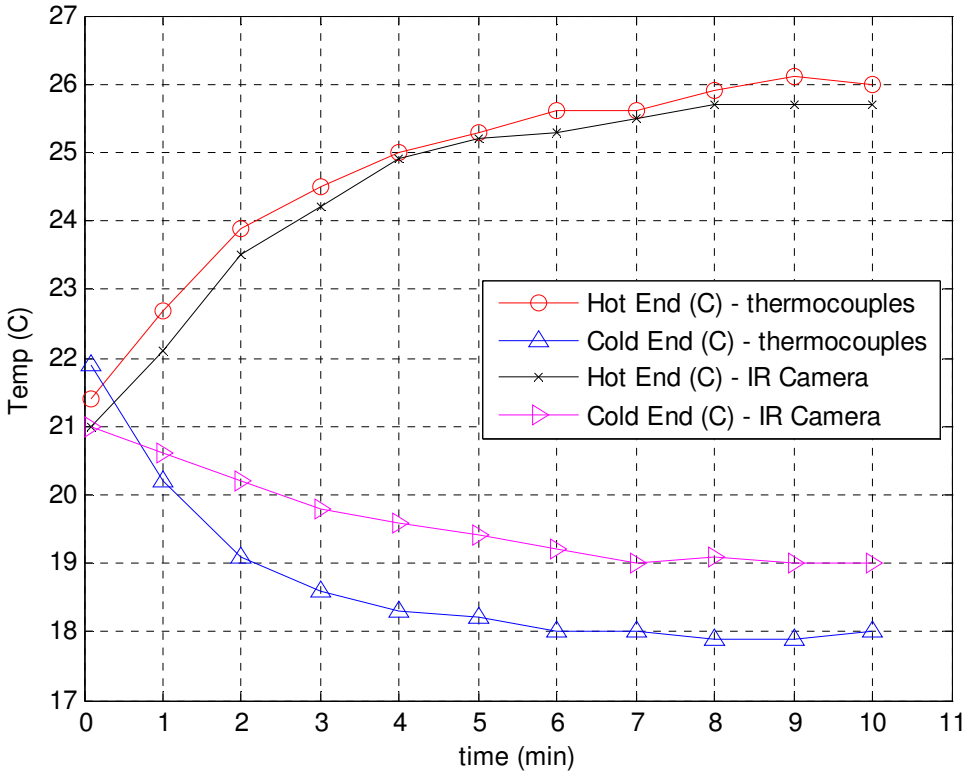

Figure 4.27: Comparison between the temperatures measured by the thermocouples and the infrared camera system for a piezoelectrically driven refrigerator operating at 395Hz with input power of 2.965W

4.3.7 Flow Distribution inside the Thermoacoustic Refrigerator

The velocity distribution inside the piezoelectrically-driven thermoacoustic refrigerator is measured using the 3-D stereoscopic imaging Particle Image Velocimetry (PIV) system from LaVision, Inc. (Ypsilanti, MI) shown in Figure 4.28. The system uses two cameras to image illuminated flow particles, injected inside the harvester, from different angles. The combination of both camera projections allows the reconstruction of the "real" particle displacement inside the measurement area and the evaluation of all three velocity components.

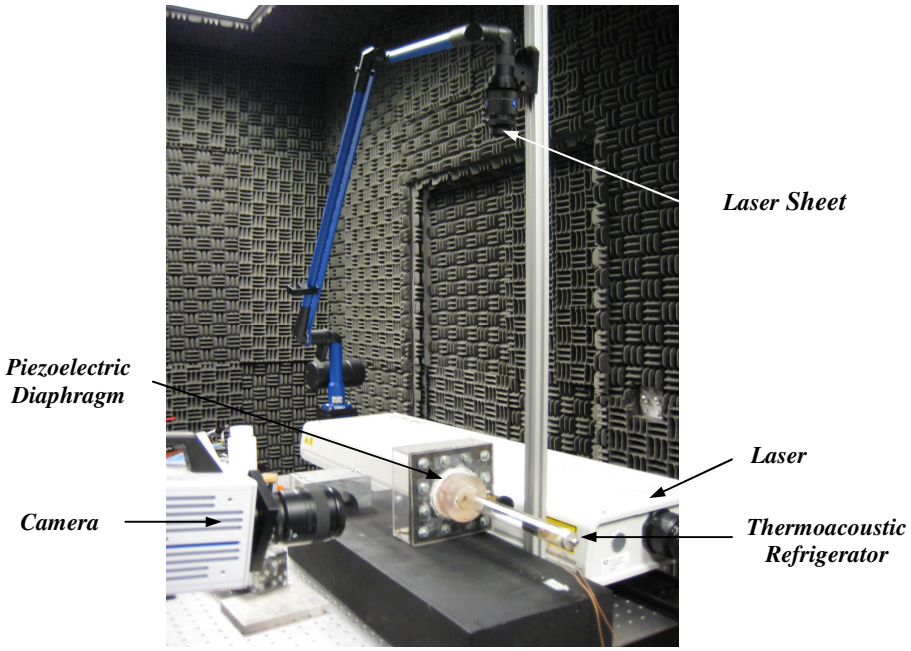

Figure 4.28: Measurement of the velocity distribution inside the piezoelectrically-driven thermoacoustic refrigerator using 3-D stereo Particle Image Velocimetry (PIV)

Figure 4.29 shows the velocity field at the beginning of the period τ of acoustic wave oscillations indicating near zero flow velocities. Figure 4.30 displays the velocity fields for different instants of acoustic wave oscillation cycle indicating forward, zero, backward, and zero flow fields at time $t = 0.25\ \tau$, $0.5\ \tau$, $0.75\ \tau$, and τ respectively.

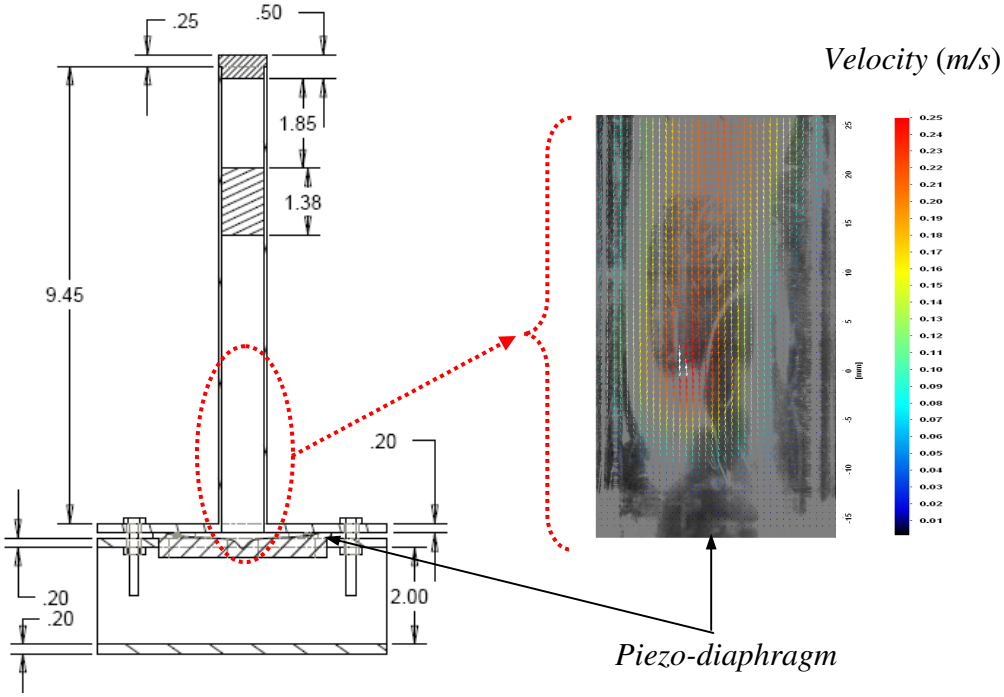

Figure 4.29: Velocity field at $t = 0\ \tau$

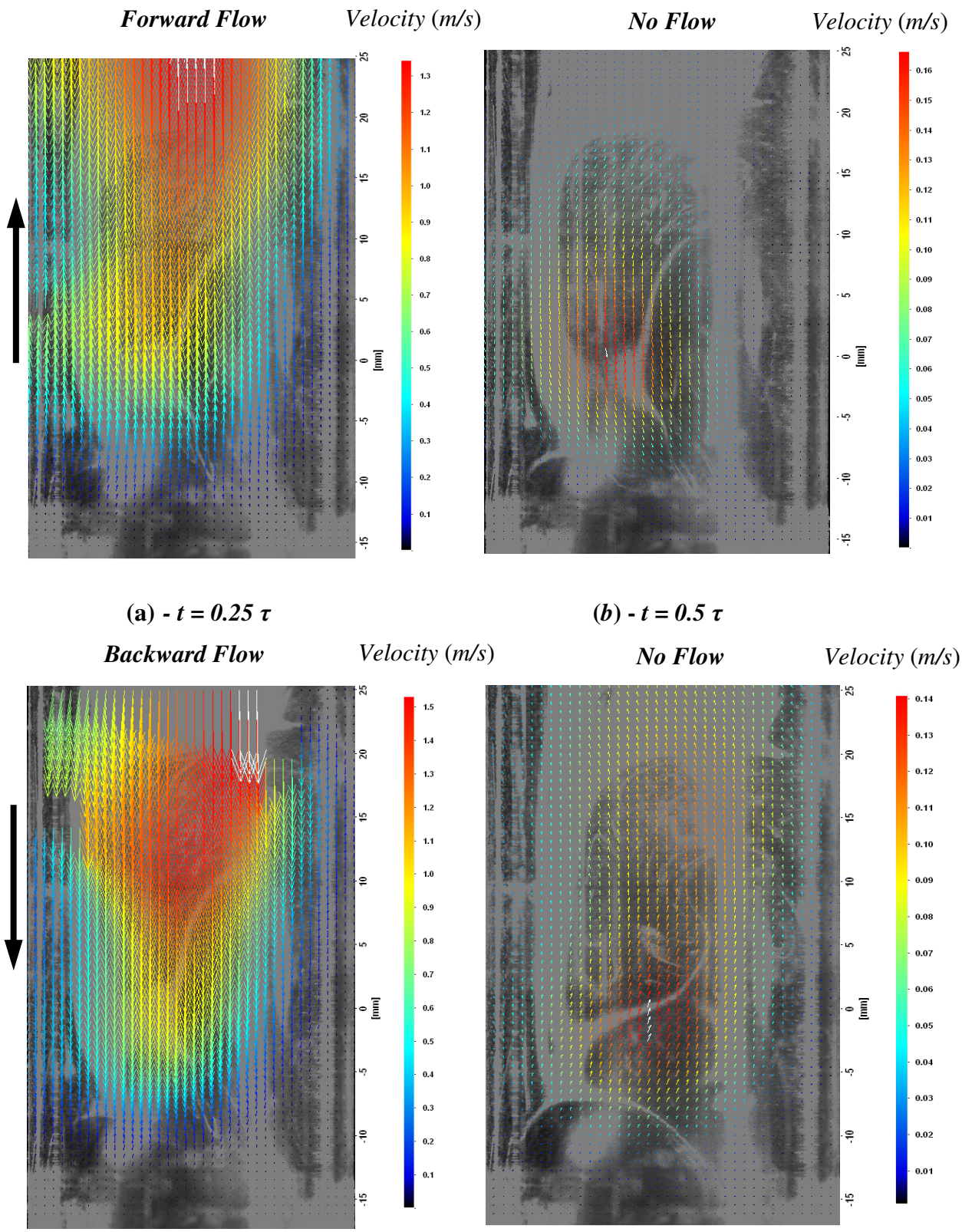

(a) - $t = 0.25\ \tau$ **(b) - $t = 0.5\ \tau$**

(c) - $t = 0.75\ \tau$ **(d) - $t = \tau$**

Figure 4.30: Velocity field at different instants of acoustic wave oscillation cycle

The detailed distributions of the flow fields are given in Tables 4-2 through 4-6 for the different time instants of the oscillation cycle.

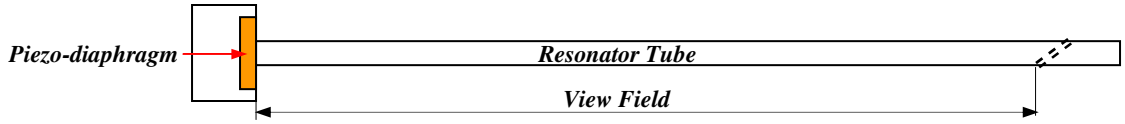

y-direction (cm)		x-direction (cm)																
		-17.3664	-14.5607	-11.7549	-8.94921	-6.14347	-3.33773	-0.53199	2.27376	5.0795	7.88524	10.691	13.4967	16.3025	19.1082	21.9139	24.7197	
		0	0.28057	0.56115	0.841719	1.122293	1.402867	1.683441	1.964016	2.24459	2.525164	2.80574	3.08631	3.36689	3.64746	3.92803	4.20861	
21.7299	1.77299	0	0	0	0	0	0	0	0	0	0	0	0	0	0	0	0	Outside Tube
18.9242	1.49242	0	0	0	0	0	0	0	0	0	0	0	0	0	0	0	0	
16.1184	1.21184	-0.0267149	-0.0256772	-0.023084	-0.0193317	-0.0142727	-0.0084258	-0.0024299	0.0024369	0.0046231	0.0024205	-0.0047388	-0.0140986	-0.0231412	-0.0291805	-0.0336536	-0.0352298	
13.3127	0.93127	-0.0302056	-0.0285713	-0.0248372	-0.0199333	-0.0141468	-0.0081378	-0.0027663	0.0002673	-0.0010306	-0.0081712	-0.02067	-0.0339483	-0.0439687	-0.0477987	-0.0487241	-0.0481865	
10.507	0.6507	-0.0379747	-0.0351059	-0.0290079	-0.0217091	-0.0144876	-0.0085576	-0.0054756	-0.0076206	-0.0169228	-0.0332774	-0.0534586	-0.0702684	-0.0780849	-0.074899	-0.0673754	-0.0622936	
7.70122	0.370122	-0.0496366	-0.0454294	-0.0367359	-0.0267438	-0.0181352	-0.013283	-0.0148637	-0.025095	-0.0437184	-0.0666908	-0.0874883	-0.0982993	-0.0948295	-0.0783159	-0.0588752	-0.0481511	
4.89548	0.089548	-0.0661977	-0.0609853	-0.0502708	-0.0381204	-0.0287057	-0.0259231	-0.0333103	-0.0513123	-0.07526	-0.0961885	-0.105798	-0.0993503	-0.0776069	-0.0465029	-0.0175349	-0.00314859	Centerline
2.08974	-0.191026	-0.0877443	-0.0823912	-0.0712682	-0.0585411	-0.0492389	-0.0482268	-0.0589261	-0.0789444	-0.0995135	-0.108895	-0.100176	-0.0735012	-0.0353339	0.0052255	0.0375285	0.0523537	
-0.715998	-0.4715998	-0.105579	-0.100995	-0.0913286	-0.0800426	-0.0718414	-0.0711558	-0.0801906	-0.0945095	-0.104366	-0.0993323	-0.0759934	-0.038127	0.0051021	0.0446442	0.0725287	0.0844797	
-3.52174	-0.752174	-0.10732	-0.104431	-0.0982211	-0.0906601	-0.084724	-0.0829918	-0.0861353	-0.0899523	-0.0875418	-0.0728017	-0.0454697	-0.0097176	0.0269015	0.0579507	0.0782935	0.0866246	
-6.32748	-1.032748	-0.0843506	-0.0831151	-0.0804979	-0.0771663	-0.0741406	-0.07185	-0.0698747	-0.0657737	-0.056799	-0.0411797	-0.0200147	0.0042181	0.0275329	0.0466047	0.0586597	0.06347	
-9.13322	-1.313322	-0.0510551	-0.0510665	-0.0512458	-5.14E-02	-0.0510656	-0.0491631	-0.0448735	-0.0376541	-0.0278904	-0.0163508	-0.0040657	0.0083802	0.0200475	0.0297644	0.0361749	0.0387862	
-11.939	-1.5939	-0.0305358	-0.0309319	-0.032056	-0.0335472	-0.0344713	-0.0332497	-0.0290038	-0.0219552	-0.0135898	-5.40E-03	0.0018466	0.0083565	0.0143501	0.019485	0.0230373	0.0245083	
-14.7447	-1.87447	0	0	0	0	0	0	0	0	0	0	0	0	0	0	0	0	Outside Tube
-17.5504	-2.15504	0	0	0	0	0	0	0	0	0	0	0	0	0	0	0	0	
-20.3562	-2.43562	0	0	0	0	0	0	0	0	0	0	0	0	0	0	0	0	
-23.1619	-2.71619	0	0	0	0	0	0	0	0	0	0	0	0	0	0	0	0	
		-5.032E-07	-4.725E-07	-4.087E-07	-3.357E-07	-2.824E-07	-2.765E-07	-3.379E-07	-4.527E-07	-5.706E-07	-6.244E-07	-5.744E-07	-4.215E-07	-2.026E-07	2.996E-08	2.152E-07	3.00211E-07	
		-3.085E-06	-2.951E-06	-2.668E-06	-2.338E-06	-2.099E-06	-2.079E-06	-2.343E-06	-2.761E-06	-3.049E-06	-2.902E-06	-2.22E-06	-1.114E-06	1.491E-07	1.304E-06	2.119E-06	2.4681E-06	
		-5.791E-06	-5.635E-06	-5.3E-06	-4.892E-06	-4.571E-06	-4.478E-06	-4.648E-06	-4.854E-06	-4.723E-06	-3.928E-06	-2.453E-06	-5.243E-07	1.452E-06	3.127E-06	4.224E-06	4.67396E-06	
		-6.638E-06	-6.541E-06	-6.335E-06	-6.073E-06	-5.835E-06	-5.654E-06	-5.499E-06	-5.176E-06	-4.47E-06	-3.241E-06	-1.575E-06	3.32E-07	2.167E-06	3.668E-06	4.616E-06	4.99493E-06	
		-5.281E-06	-5.282E-06	-5.301E-06	-5.317E-06	-5.282E-06	-5.085E-06	-4.642E-06	-3.895E-06	-2.885E-06	-1.691E-06	-4.205E-07	8.668E-07	2.074E-06	3.079E-06	3.742E-06	4.01199E-06	
		-3.914E-06	-3.965E-06	-4.109E-06	-4.3E-06	-4.419E-06	-4.262E-06	-3.718E-06	-2.814E-06	-1.742E-06	-6.92E-07	2.367E-07	1.071E-06	1.839E-06	2.498E-06	2.953E-06	3.14152E-06	
		-8.342E-08	-7.685E-08	-6.335E-08	-4.804E-08	-3.617E-08	-3.267E-08	-4.197E-08	-6.466E-08	-9.484E-08	-1.212E-07	-1.333E-07	-1.252E-07	-9.779E-08	-5.86E-08	-2.21E-08	-3.96755E-09	
		-1.006E-06	-9.207E-07	-7.445E-07	-5.42E-07	-3.675E-07	-2.692E-07	-3.012E-07	-5.086E-07	-8.86E-07	-1.352E-06	-1.773E-06	-1.992E-06	-1.922E-06	-1.587E-06	-1.193E-06	-9.75876E-07	
		-1.709E-06	-1.58E-06	-1.306E-06	-9.771E-07	-6.521E-07	-3.852E-07	-2.464E-07	-3.43E-07	-7.617E-07	-1.498E-06	-2.406E-06	-3.163E-06	-3.515E-06	-3.371E-06	-3.032E-06	-2.80377E-06	
		-2.107E-06	-1.993E-06	-1.732E-06	-1.39E-06	-9.867E-07	-5.676E-07	-1.929E-07	1.865E-08	-7.188E-08	-5.699E-07	-1.442E-06	-2.368E-06	-3.067E-06	-3.334E-06	-3.398E-06	-3.36093E-06	
		-2.524E-06	-2.426E-06	-2.181E-06	-1.827E-06	-1.349E-06	-7.961E-07	-2.296E-07	2.303E-07	4.368E-07	2.287E-07	-4.478E-07	-1.332E-06	-2.187E-06	-2.757E-06	-3.18E-06	-3.32882E-06	
Volume Velocity (m/s)		-3.264E-05	-3.184E-05	-3.015E-05	-2.804E-05	-2.588E-05	-2.389E-05	-2.22E-05	-2.062E-05	-1.882E-05	-1.639E-05	-1.321E-05	-8.77E-06	-3.31E-06	2.597E-06	7.044E-06	9.11735E-06	

Table 4.2: Flow field at $t = 0\ \tau$

y-direction (cm)		x-direction (cm)																
		-17.3664	-14.5607	-11.7549	-8.94921	-6.14347	-3.33773	-0.53199	2.27376	5.0795	7.88524	10.691	13.4967	16.3025	19.1082	21.9139	24.7197	
		4.25	4.53057	4.81115	5.091719	5.372293	5.652867	5.933441	6.214016	6.49459	6.775164	7.05574	7.33631	7.61689	7.89746	8.17803	8.45861	
21.7299	1.77299	0	0	0	0	0	0	0	0	0	0	0	0	0	0	0	0	Outside Tube
18.9242	1.49242	0	0	0	0	0	0	0	0	0	0	0	0	0	0	0	0	
16.1184	1.21184	-1.14769	-1.14519	-1.14015	-1.1343	-1.12878	-1.12262	-1.11578	-1.11358	-1.12189	-1.14312	-1.16824	-1.19277	-1.21274	-1.24747	-1.26688	-1.27241	
13.3127	0.93127	-1.14638	-1.14371	-1.1383	-1.13206	-1.12627	-1.12039	-1.11475	-1.11447	-1.125	-1.14853	-1.17645	-1.20324	-1.22518	-1.24747	-1.26688	-1.27241	
10.507	0.6507	-1.1458	-1.14267	-1.13633	-1.1291	-1.1228	-1.11805	-1.11608	-1.12138	-1.13747	-1.16485	-1.19498	-1.22144	-1.23837	-1.24795	-1.25039	-1.25095	
7.70122	0.370122	-1.1501	-1.14643	-1.13891	-1.13045	-1.12383	-1.12152	-1.12577	-1.13903	-1.16066	-1.18747	-1.21156	-1.22701	-1.22883	-1.21946	-1.20526	-1.19732	
4.89548	0.089548	-1.1527	-1.15033	-1.14477	-1.13725	-1.13144	-1.1316	-1.14051	-1.15706	-1.17601	-1.19154	-1.19756	-1.19225	-1.17444	-1.14983	-1.12595	-1.11441	Centerline
2.08974	-0.191026	-1.11026	-1.11124	-1.11228	-1.11061	-1.10973	-1.11288	-1.1219	-1.13113	-1.13371	-1.12611	-1.1079	-1.0835	-1.05485	-1.02906	-1.00925	-1.00127	
-0.715998	-0.4715998	-0.969429	-0.975604	-0.987884	-0.99747	-1.00608	-1.01201	-1.01515	-1.00682	-0.984007	-0.950135	-0.912098	-0.879829	-0.855435	-0.844463	-0.841171	-0.842488	
-3.52174	-0.752174	-0.705248	-0.713191	-0.732502	-0.753139	-0.774521	-0.786402	-0.78564	-0.76337	-0.722872	-0.674688	-0.63173	-0.606282	-0.59788	-0.606881	-0.620571	-0.629937	
-6.32748	-1.032748	-0.392366	-0.398612	-0.417617	-0.442897	-0.472123	-0.489112	-0.488225	-0.463322	-0.422536	-0.378603	-0.344544	-0.330564	-0.334606	-0.353731	-0.374225	-0.386024	
-9.13322	-1.313322	-0.13186	-0.133091	-0.144522	-1.67E-01	-0.198946	-0.220721	-0.225015	-0.208839	-0.181291	-0.153073	-0.133774	-0.129757	-0.138516	-0.155824	-0.172241	-0.18087	
-11.939	-1.5939	-0.0182761	-0.0170358	-0.0237735	-0.0435144	-0.0737081	-0.096405	-0.103319	-0.0932643	-0.0749998	-5.70E-02	-0.0457709	-0.0450005	-0.0527427	-0.0655543	-0.0773063	-0.0832631	
-14.7447	-1.87447	0	0	0	0	0	0	0	0	0	0	0	0	0	0	0	0	Outside Tube
-17.5504	-2.15504	0	0	0	0	0	0	0	0	0	0	0	0	0	0	0	0	
-20.3562	-2.43562	0	0	0	0	0	0	0	0	0	0	0	0	0	0	0	0	
-23.1619	-2.71619	0	0	0	0	0	0	0	0	0	0	0	0	0	0	0	0	
		-6.367E-06	-6.372E-06	-6.378E-06	-6.369E-06	-6.364E-06	-6.382E-06	-6.433E-06	-6.486E-06	-6.501E-06	-6.457E-06	-6.353E-06	-6.213E-06	-6.049E-06	-5.901E-06	-5.787E-06	-5.74157E-06	
		-2.832E-05	-2.85E-05	-2.886E-05	-2.914E-05	-2.939E-05	-2.957E-05	-2.966E-05	-2.941E-05	-2.875E-05	-2.776E-05	-2.665E-05	-2.57E-05	-2.499E-05	-2.467E-05	-2.458E-05	-2.46135E-05	
		-3.805E-05	-3.848E-05	-3.952E-05	-4.064E-05	-4.179E-05	-4.243E-05	-4.239E-05	-4.119E-05	-3.9E-05	-3.64E-05	-3.409E-05	-3.271E-05	-3.226E-05	-3.275E-05	-3.348E-05	-3.39892E-05	
		-3.088E-05	-3.137E-05	-3.287E-05	-3.485E-05	-3.715E-05	-3.849E-05	-3.842E-05	-3.646E-05	-3.325E-05	-2.98E-05	-2.711E-05	-2.601E-05	-2.633E-05	-2.784E-05	-2.945E-05	-3.03791E-05	
		-1.364E-05	-1.377E-05	-1.495E-05	-1.731E-05	-2.058E-05	-2.283E-05	-2.328E-05	-2.16E-05	-1.875E-05	-1.583E-05	-1.384E-05	-1.342E-05	-1.433E-05	-1.612E-05	-1.782E-05	-1.8709E-05	
		-2.343E-06	-2.184E-06	-3.047E-06	-5.578E-06	-9.448E-06	-1.236E-05	-1.324E-05	-1.195E-05	-9.614E-06	-7.307E-06	-5.867E-06	-5.768E-06	-6.761E-06	-8.403E-06	-9.909E-06	-1.06728E-05	
		-1.453E-06	-1.45E-06	-1.443E-06	-1.433E-06	-1.426E-06	-1.426E-06	-1.437E-06	-1.458E-06	-1.482E-06	-1.501E-06	-1.509E-06	-1.502E-06	-1.48E-06	-1.449E-06	-1.419E-06	-1.40427E-06	
		-2.331E-05	-2.323E-05	-2.308E-05	-2.291E-05	-2.278E-05	-2.273E-05	-2.282E-05	-2.308E-05	-2.352E-05	-2.407E-05	-2.455E-05	-2.487E-05	-2.49E-05	-2.471E-05	-2.443E-05	-2.4266E-05	
		-5.157E-05	-5.143E-05	-5.114E-05	-5.082E-05	-5.054E-05	-5.032E-05	-5.023E-05	-5.047E-05	-5.12E-05	-5.243E-05	-5.378E-05	-5.498E-05	-5.574E-05	-5.617E-05	-5.628E-05	-5.63039E-05	
		-7.996E-05	-7.977E-05	-7.939E-05	-7.896E-05	-7.856E-05	-7.815E-05	-7.775E-05	-7.773E-05	-7.847E-05	-8.011E-05	-8.206E-05	-8.392E-05	-8.545E-05	-8.701E-05	-8.836E-05	-8.87485E-05	
		-0.0001084	-0.0001082	-0.0001077	-0.0001072	-0.0001067	-0.0001061	-0.0001054	-0.0001052	-0.000106	-0.000108	-0.0001104	-0.0001127	-0.0001146	-0.0001179	-0.0001197	-0.000120228	
Volume Velocity (m/s)		-0.0003843	-0.0003848	-0.0003884	-0.0003952	-0.0004047	-0.0004108	-0.0004111	-0.0004051	-0.0003965	-0.0003897	-0.0003862	-0.0003878	-0.0003929	-0.0004029	-0.0004112	-0.000415056	

Table 4.3: Flow field at $t = 0.25\ \tau$

y-direction (cm)		x-direction (cm)																
		-17.3664	-14.5607	-11.7549	-8.94921	-6.14347	-3.33773	-0.53199	2.27376	5.0795	7.88524	10.691	13.4967	16.3025	19.1082	21.9139	24.7197	
		4.25	4.53057	4.81115	5.091719	5.372293	5.652867	5.933441	6.214016	6.49459	6.775164	7.05574	7.33631	7.61689	7.89746	8.17803	8.45861	
21.7299	1.77299	0	0	0	0	0	0	0	0	0	0	0	0	0	0	0	0	Outside Tube
18.9242	1.49242	0	0	0	0	0	0	0	0	0	0	0	0	0	0	0	0	
16.1184	1.21184	2.31072	2.30496	2.2913	2.2712	2.24724	2.22158	2.19587	2.171	2.14609	2.11818	2.08049	2.02784	1.9619	1.89854	1.80655	1.76181	
13.3127	0.93127	2.31106	2.30548	2.29214	2.27231	2.24848	2.2227	2.19615	2.16889	2.13934	2.10482	2.06035	2.0033	1.93682	1.87116	1.80655	1.76181	
10.507	0.6507	2.31007	2.30487	2.2923	2.27328	2.25001	2.22384	2.19472	2.1612	2.12149	2.07477	2.02022	1.95952	1.89757	1.84041	1.79636	1.77596	
7.70122	0.370122	2.30004	2.2963	2.28635	2.26878	2.24412	2.21178	2.1719	2.12391	2.07087	2.01682	1.96552	1.91874	1.87849	1.8471	1.82732	1.8193	
4.89548	0.089548	2.24714	2.24634	2.24144	2.22524	2.19482	2.14657	2.08389	2.01194	1.94589	1.89836	1.875	1.86914	1.86975	1.87052	1.86997	1.86962	Centerline
2.08974	-0.191026	2.09254	2.09764	2.102	2.08739	2.04418	1.96636	1.86531	1.75922	1.68189	1.65644	1.68482	1.74249	1.79669	1.83018	1.84246	1.845	
-0.715998	-0.4715998	1.77082	1.78204	1.79544	1.7825	1.72696	1.62324	1.48973	1.3582	1.2764	1.27622	1.35289	1.46583	1.563	1.61926	1.63729	1.63958	
-3.52174	-0.752174	1.29912	1.31512	1.33532	1.32604	1.26629	1.15394	1.01001	0.874614	0.79812	0.813991	0.911348	1.04341	1.15406	1.2168	1.23733	1.23975	
-6.32748	-1.032748	0.776793	0.791867	0.810932	0.80565	0.757169	0.667093	0.551868	0.44653	0.388787	0.40502	0.483912	0.588604	0.6762	0.726284	0.744114	0.74672	
-9.13322	-1.313322	3.67E-01	3.79E-01	3.94E-01	3.93E-01	0.361378	0.303647	0.229834	0.164205	0.128323	0.137308	0.182531	0.241944	0.292798	0.323388	0.337277	0.340582	
-11.939	-1.5939	0.182001	0.190576	2.01E-01	0.201746	0.181529	0.144773	0.0979854	0.057302	0.0344506	3.79E-02	0.0618525	0.0938273	0.122384	0.140875	0.151231	0.154395	
-14.7447	-1.87447	0	0	0	0	0	0	0	0	0	0	0	0	0	0	0	0	Outside Tube
-17.5504	-2.15504	0	0	0	0	0	0	0	0	0	0	0	0	0	0	0	0	
-20.3562	-2.43562	0	0	0	0	0	0	0	0	0	0	0	0	0	0	0	0	
-23.1619	-2.71619	0	0	0	0	0	0	0	0	0	0	0	0	0	0	0	0	
		1.2E-05	1.203E-05	1.205E-05	1.197E-05	1.172E-05	1.128E-05	1.07E-05	1.009E-05	9.644E-06	9.499E-06	9.661E-06	9.992E-06	1.03E-05	1.049E-05	1.057E-05	1.05798E-05	
		5.174E-05	5.206E-05	5.245E-05	5.208E-05	5.045E-05	4.742E-05	4.352E-05	3.968E-05	3.729E-05	3.729E-05	3.953E-05	4.282E-05	4.566E-05	4.731E-05	4.783E-05	4.79008E-05	
		7.01E-05	7.096E-05	7.205E-05	7.155E-05	6.832E-05	6.226E-05	5.45E-05	4.719E-05	4.306E-05	4.392E-05	4.917E-05	5.63E-05	6.227E-05	6.565E-05	6.676E-05	6.68925E-05	
		6.113E-05	6.232E-05	6.382E-05	6.34E-05	5.959E-05	5.25E-05	4.343E-05	3.514E-05	3.06E-05	3.187E-05	3.808E-05	4.632E-05	5.322E-05	5.716E-05	5.856E-05	5.8765E-05	
		3.799E-05	3.92E-05	4.075E-05	4.062E-05	3.738E-05	3.141E-05	2.377E-05	1.699E-05	1.327E-05	1.42E-05	1.888E-05	2.503E-05	3.029E-05	3.345E-05	3.489E-05	3.52294E-05	
		2.333E-05	2.443E-05	2.583E-05	2.586E-05	2.327E-05	1.856E-05	1.256E-05	7.345E-06	4.416E-06	4.862E-06	7.928E-06	1.203E-05	1.569E-05	1.806E-05	1.939E-05	1.97906E-05	
		2.832E-06	2.831E-06	2.824E-06	2.804E-06	2.766E-06	2.705E-06	2.626E-06	2.535E-06	2.452E-06	2.392E-06	2.363E-06	2.355E-06	2.356E-06	2.357E-06	2.356E-06	2.35592E-06	
		4.661E-05	4.654E-05	4.634E-05	4.598E-05	4.548E-05	4.483E-05	4.402E-05	4.305E-05	4.197E-05	4.087E-05	3.984E-05	3.889E-05	3.807E-05	3.744E-05	3.703E-05	3.68716E-05	
		0.000104	0.0001037	0.0001032	0.0001023	0.0001013	0.0001001	9.878E-05	9.727E-05	9.549E-05	9.338E-05	9.093E-05	8.82E-05	8.541E-05	8.283E-05	8.085E-05	7.9934E-05	
		0.0001612	0.0001608	0.0001599	0.0001585	0.0001568	0.000155	0.0001532	0.0001513	0.0001492	0.0001468	0.0001437	0.0001397	0.0001351	0.0001305	0.000126	0.000122883	
		0.0002183	0.0002178	0.0002165	0.0002146	0.0002123	0.0002099	0.0002075	0.0002051	0.0002028	0.0002001	0.0001966	0.0001916	0.0001854	0.0001794	0.0001707	0.000166471	
Volume Velocity (m/s)		0.0007892	0.0007927	0.0007957	0.0007897	0.0007694	0.000736	0.0006946	0.0006557	0.0006302	0.0006282	0.0006367	0.0006533	0.0006637	0.0006646	0.0006549	0.000647674	

Table 4.4: Flow field at $t = 0.5\ \tau$

y-direction (cm)		x-direction (cm)																
		-17.3664	-14.5607	-11.7549	-8.94921	-6.14347	-3.33773	-0.53199	2.27376	5.0795	7.88524	10.691	13.4967	16.3025	19.1082	21.9139	24.7197	
		4.25	4.53057	4.81115	5.091719	5.372293	5.652867	5.933441	6.214016	6.49459	6.775164	7.05574	7.33631	7.61689	7.89746	8.17803	8.45861	
21.7299	1.77299	0	0	0	0	0	0	0	0	0	0	0	0	0	0	0	0	Outside Tube
18.9242	1.49242	0	0	0	0	0	0	0	0	0	0	0	0	0	0	0	0	
16.1184	1.21184	2.0849	2.20004	2.21E+00	2.22872	2.24836	2.26219	2.26866	2.26693	2.26004	2.25577	1.99887	1.53274	0.646891	0.534577	0.349006	0.250962	
13.3127	0.93127	2.0849	2.16097	2.18641	2.21054	2.23157	2.2453	2.25128	2.25134	2.24416	2.21281	1.99887	1.53274	0.857269	0.600257	0.376576	0.265123	
10.507	0.6507	2.0849	2.10054	2.13561	2.1672	2.19506	2.19898	2.20771	2.21194	2.2058	2.16057	1.99887	1.53274	1.09992	0.730306	0.435285	0.295902	
7.70122	0.370122	2.01103	2.01303	2.0228	2.05	2.09339	2.11443	2.1232	2.12627	2.11904	2.07463	1.92876	1.65065	1.26039	0.837276	0.493173	0.32891	
4.89548	0.089548	1.88907	1.87455	1.83771	1.88704	1.93664	1.9738	1.96916	1.95498	1.93568	1.90499	1.81117	1.60202	1.2633	0.851547	0.499263	0.32756	Centerline
2.08974	-0.191026	1.5	1.533	1.60042	1.67868	1.73504	1.74348	1.7059	1.65294	1.60227	1.55885	1.55503	1.36571	1.06206	0.703445	0.413997	0.268504	
-0.715998	-0.4715998	1.02351	1.11011	1.25676	1.36157	1.42213	1.41147	1.33952	1.246	1.16005	1.08424	1.00889	0.9	0.644915	0.451128	0.269397	0.171894	
-3.52174	-0.752174	0.72002	0.766972	0.863059	0.962072	1.01459	0.991488	0.905933	0.795575	0.693244	0.594403	0.452363	0.330541	0.225203	0.19773	0.122271	0.077442	
-6.32748	-1.032748	4.14E-01	0.439973	0.4967	0.55807	0.589686	0.565942	0.497845	0.41051	0.329421	0.248888	0.177685	0.114065	0.0796246	0.0530896	0.0362742	0.0228961	
-9.13322	-1.313322	1.83E-01	1.94E-01	2.17E-01	2.42E-01	0.250816	0.231883	0.192575	0.145905	0.103656	0.0656866	0.0362203	0.0152611	0.0053715	0.00155	0.000639	0.000229865	
-11.939	-1.5939	8.20E-02	0.0858717	9.35E-02	0.100463	0.0975443	0.0829855	0.0620421	0.0413464	0.0245218	9.99E-03	0.0005507	-0.004885	-0.005572	-0.0047939	-0.0033474	-0.00267622	
-14.7447	-1.87447	0	0	0	0	0	0	0	0	0	0	0	0	0	0	0	0	Outside Tube
-17.5504	-2.15504	0	0	0	0	0	0	0	0	0	0	0	0	0	0	0	0	
-20.3562	-2.43562	0	0	0	0	0	0	0	0	0	0	0	0	0	0	0	0	
-23.1619	-2.71619	0	0	0	0	0	0	0	0	0	0	0	0	0	0	0	0	
		8.601E-06	8.791E-06	9.177E-06	9.626E-06	9.949E-06	9.998E-06	9.782E-06	9.478E-06	9.188E-06	8.939E-06	8.917E-06	7.831E-06	6.09E-06	4.034E-06	2.374E-06	1.53968E-06	
		2.99E-05	3.243E-05	3.672E-05	3.978E-05	4.155E-05	4.124E-05	3.913E-05	3.64E-05	3.389E-05	3.168E-05	2.948E-05	2.629E-05	1.884E-05	1.318E-05	7.871E-06	5.02193E-06	
		3.885E-05	4.138E-05	4.657E-05	5.191E-05	5.474E-05	5.35E-05	4.888E-05	4.293E-05	3.74E-05	3.207E-05	2.441E-05	1.783E-05	1.215E-05	1.067E-05	6.597E-06	4.178E-06	
		3.261E-05	3.462E-05	3.909E-05	4.392E-05	4.641E-05	4.454E-05	3.918E-05	3.231E-05	2.592E-05	1.959E-05	1.398E-05	8.977E-06	6.266E-06	4.178E-06	2.855E-06	1.80187E-06	
		1.891E-05	2.003E-05	2.248E-05	2.508E-05	2.594E-05	2.399E-05	1.992E-05	1.509E-05	1.072E-05	6.795E-06	3.747E-06	1.579E-06	5.556E-07	1.603E-07	6.609E-08	2.37769E-08	
		1.051E-05	1.101E-05	1.199E-05	1.288E-05	1.25E-05	1.064E-05	7.953E-06	5.3E-06	3.143E-06	1.28E-06	7.059E-08	-6.262E-07	-7.142E-07	-6.145E-07	-4.291E-07	-3.43043E-07	
		2.38E-06	2.362E-06	2.316E-06	2.378E-06	2.44E-06	2.487E-06	2.481E-06	2.463E-06	2.439E-06	2.4E-06	2.282E-06	2.019E-06	1.592E-06	1.073E-06	6.291E-07	4.127E-07	
		4.076E-05	4.08E-05	4.1E-05	4.155E-05	4.243E-05	4.285E-05	4.303E-05	4.309E-05	4.295E-05	4.205E-05	3.909E-05	3.345E-05	2.554E-05	1.697E-05	9.995E-06	6.666E-06	
		9.384E-05	9.454E-05	9.612E-05	9.754E-05	9.88E-05	9.897E-05	9.937E-05	9.956E-05	9.928E-05	9.724E-05	8.997E-05	6.899E-05	4.951E-05	3.287E-05	1.959E-05	1.33182E-05	
		0.0001454	0.0001507	0.0001525	0.0001542	0.0001556	0.0001566	0.000157	0.000157	0.0001565	0.0001543	0.0001394	0.0001069	5.979E-05	4.187E-05	2.627E-05	1.84919E-05	
		0.000197	0.0002079	0.0002088	0.0002106	0.0002124	0.0002138	0.0002144	0.0002142	0.0002135	0.0002131	0.0001889	0.0001448	6.112E-05	5.051E-05	3.298E-05	2.37131E-05	
Volume Velocity (m/s)		0.0006188	0.0006446	0.0006668	0.0006894	0.0007029	0.0006986	0.0006811	0.0006578	0.000635	0.0006095	0.0005402	0.0004181	0.0002407	0.0001749	0.0001088	7.48247E-05	

Table 4.5: Flow field at $t = 0.75\ \tau$

y-direction (cm)		x-direction (cm)																
		-17.3664	-14.5607	-11.7549	-8.94921	-6.14347	-3.33773	-0.53199	2.27376	5.0795	7.88524	10.691	13.4967	16.3025	19.1082	21.9139	24.7197	
		4.25	4.53057	4.81115	5.091719	5.372293	5.652867	5.933441	6.214016	6.49459	6.775164	7.05574	7.33631	7.61689	7.89746	8.17803	8.45861	
21.7299	1.77299	0	0	0	0	0	0	0	0	0	0	0	0	0	0	0	0	Outside Tube
18.9242	1.49242	0	0	0	0	0	0	0	0	0	0	0	0	0	0	0	0	
16.1184	1.21184	-1.83332	-1.80739	-1.80E+00	-1.78888	-1.75048	-1.63544	-1.39683	-1.05023	-0.673041	-0.364985	-0.169024	-0.0754145	-0.0351625	-0.0174608	-0.0068469	-0.00300045	
13.3127	0.93127	-1.83332	-1.8179	-1.81049	-1.79773	-1.75855	-1.64645	-1.42047	-1.09379	-0.734933	-0.435494	-0.236619	-0.130917	-0.0734198	-0.0381184	-0.0147127	-0.00541683	
10.507	0.6507	-1.83332	-1.83037	-1.8252	-1.81301	-1.77427	-1.67276	-1.47753	-1.19618	-0.879521	-0.601666	-0.398733	-0.266168	-0.168548	-0.0913949	-0.0371643	-0.0146173	
7.70122	0.370122	-1.83819	-1.83633	-1.83209	-1.81809	-1.78259	-1.69926	-1.5452	-1.3207	-1.05975	-0.817	-0.621862	-0.465898	-0.323562	-0.190654	-0.091356	-0.0472801	
4.89548	0.089548	-1.84025	-1.83854	-1.80732	-1.77857	-1.74128	-1.68387	-1.56863	-1.39473	-1.19017	-0.992148	-0.824057	-0.666785	-0.500527	-0.323075	-0.178328	-0.109864	Centerline
2.08974	-0.191026	-1.84025	-1.83854	-1.80732	-1.58326	-1.59703	-1.56426	-1.47249	-1.32959	-1.16303	-1.03519	-0.901378	-0.776605	-0.641288	-0.45921	-0.287243	-0.198745	
-0.715998	-0.4715998	-0.99522	-1.01746	-1.14678	-1.25632	-1.31855	-1.29618	-1.21447	-1.08853	-0.942879	-0.825263	-0.75	-0.715499	-0.662229	-0.524914	-0.35911	-0.265648	
-3.52174	-0.752174	-0.840984	-0.851691	-0.876351	-0.913793	-0.931274	-0.910729	-0.838041	-0.730412	-0.608411	-0.486781	-0.466547	-0.507303	-0.552207	-0.479215	-0.351747	-0.27229	
-6.32748	-1.032748	-5.44E-01	-0.537149	-0.528785	-0.53018	-0.529451	-0.509582	-0.456141	-0.379832	-0.295582	-0.241884	-0.247753	-0.306006	-0.352332	-0.330624	-0.254819	-0.202779	
-9.13322	-1.313322	-2.55E-01	-2.44E-01	-2.27E-01	-2.21E-01	-0.22001	-0.210758	-0.181649	-0.140158	-0.0990593	-0.0773012	-0.0905309	-0.131453	-0.168414	-0.168203	-0.135559	-1.11E-01	
-11.939	-1.5939	-1.16E-01	-0.105315	-8.96E-02	-0.0838914	-0.0855622	-0.0831554	-0.0680998	-0.0459192	-0.0253082	-1.63E-02	-0.0265651	-0.052481	-0.0772387	-0.082504	-0.0687027	-0.0570858	
-14.7447	-1.87447	0	0	0	0	0	0	0	0	0	0	0	0	0	0	0	0	Outside Tube
-17.5504	-2.15504	0	0	0	0	0	0	0	0	0	0	0	0	0	0	0	0	
-20.3562	-2.43562	0	0	0	0	0	0	0	0	0	0	0	0	0	0	0	0	
-23.1619	-2.71619	0	0	0	0	0	0	0	0	0	0	0	0	0	0	0	0	
		-1.055E-05	-1.054E-05	-1.036E-05	-9.079E-06	-9.158E-06	-8.97E-06	-8.444E-06	-7.624E-06	-6.669E-06	-5.936E-06	-5.169E-06	-4.453E-06	-3.677E-06	-2.633E-06	-1.647E-06	-1.13966E-06	
		-2.908E-05	-2.973E-05	-3.35E-05	-3.67E-05	-3.852E-05	-3.787E-05	-3.548E-05	-3.18E-05	-2.755E-05	-2.411E-05	-2.191E-05	-2.09E-05	-1.935E-05	-1.534E-05	-1.049E-05	-7.76098E-06	
		-4.538E-05	-4.595E-05	-4.728E-05	-4.931E-05	-5.025E-05	-4.914E-05	-4.522E-05	-3.941E-05	-3.283E-05	-2.626E-05	-2.517E-05	-2.737E-05	-2.98E-05	-2.586E-05	-1.898E-05	-1.46918E-05	
		-4.285E-05	-4.227E-05	-4.161E-05	-4.172E-05	-4.167E-05	-4.01E-05	-3.59E-05	-2.989E-05	-2.326E-05	-1.904E-05	-1.95E-05	-2.408E-05	-2.773E-05	-2.602E-05	-2.005E-05	-1.59582E-05	
		-2.639E-05	-2.52E-05	-2.348E-05	-2.286E-05	-2.276E-05	-2.18E-05	-1.879E-05	-1.45E-05	-1.025E-05	-7.996E-06	-9.364E-06	-1.36E-05	-1.742E-05	-1.74E-05	-1.402E-05	-1.14507E-05	
		-1.492E-05	-1.35E-05	-1.148E-05	-1.075E-05	-1.097E-05	-1.066E-05	-8.729E-06	-5.886E-06	-3.244E-06	-2.087E-06	-3.405E-06	-6.727E-06	-9.901E-06	-1.058E-05	-8.806E-06	-7.31736E-06	
		-2.319E-06	-2.317E-06	-2.277E-06	-2.241E-06	-2.194E-06	-2.122E-06	-1.977E-06	-1.758E-06	-1.5E-06	-1.25E-06	-1.038E-06	-8.402E-07	-6.307E-07	-4.071E-07	-2.247E-07	-1.3844E-07	
		-3.725E-05	-3.722E-05	-3.713E-05	-3.685E-05	-3.613E-05	-3.444E-05	-3.132E-05	-2.677E-05	-2.148E-05	-1.656E-05	-1.26E-05	-9.442E-06	-6.558E-06	-3.864E-06	-1.852E-06	-9.58223E-07	
		-8.252E-05	-8.238E-05	-8.215E-05	-8.16E-05	-7.986E-05	-7.529E-05	-6.65E-05	-5.384E-05	-3.959E-05	-2.708E-05	-1.795E-05	-1.198E-05	-7.586E-06	-4.114E-06	-1.673E-06	-6.57908E-07	
		-0.0001279	-0.0001268	-0.0001263	-0.0001254	-0.0001227	-0.0001148	-9.908E-05	-7.629E-05	-5.126E-05	-3.038E-05	-1.65E-05	-9.131E-06	-5.121E-06	-2.659E-06	-1.026E-06	-3.77815E-07	
		-0.0001732	-0.0001708	-0.0001703	-0.000169	-0.0001654	-0.0001545	-0.000132	-9.923E-05	-6.359E-05	-3.449E-05	-1.597E-05	-7.126E-06	-3.322E-06	-1.65E-06	-6.47E-07	-2.83509E-07	
Volume Velocity (m/s)		-0.0005924	-0.0005867	-0.0005858	-0.0005855	-0.0005796	-0.0005498	-0.0004834	-0.000387	-0.0002812	-0.0001952	-0.0001486	-0.0001357	-0.0001311	-0.0001105	-7.942E-05	-6.07346E-05	

Table 4.6: Flow field at $t = \tau$

The data displayed in Tables 4-2 through 4-6 are used to compute the volume velocity of the acoustic wave as it flows through the resonator tube at different instants of time. This is achieved by integrating the flow velocities over the cross sectional area of the resonator tube. The obtained results are used to validate the mathematical model of the piezoelectrically-driven thermoacoustic refrigerator as will be discussed in Chapter 5.

4.3.8 Noise Radiation by the Thermoacoustic Refrigerator

In this section, the noise radiated by the piezoelectrically-driven thermoacoustic refrigerator is determined at different levels of input electrical power using a sound level meter as shown in Figure 4.31. The sound level meter used is manufactured by Radio Shack and has the specifications listed in Table 4.7. It is placed at a distance of 1 meter from the centerline of the resonator tube according to international standards ISO-3744 and 3745.

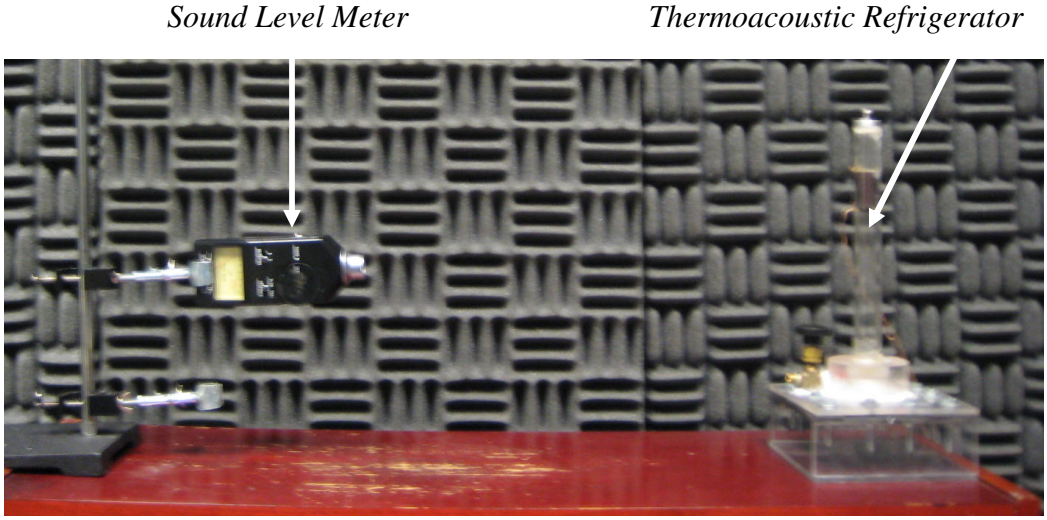

Figure 4.31: Measurement of the sound pressure level of the noise radiated by the piezoelectrically-driven thermoacoustic refrigerator

- Microphone type: Electret Condenser
- Range: 50 - 126 dB
- Accuracy: ± 2 dB @ 114 dB
- Reference 0 dB = 0.0002 MicroBar
- Weighting: A and C
- Signal output: 1 Volt (peak-peak min.)
- Impedance: 10 kOhms (min. load)
- Distortion: Less than 2% at 1 kHz.
- Power: 9 Volts battery
- Size (approx): (H x W x D): 6" x 2" x 2" - 159 x 64 x 44 mm
- Weight: 5.8 oz - 165 grams

Table 4.7: Specifications of Radio Shack sound level meter

Figure 4.32 summarizes the effect of the input power on the octave band analysis of the sound pressure level (*SPL*) of the piezoelectrically-driven thermoacoustic refrigerator when it is operating at its resonant frequency of 395Hz. The obtained results indicate that the peak SPL is obtained always at the resonant frequency and ranges between 77.75dB at input power of 0.427 W and 90 dB when the input power becomes 6.8 dB. Note that all the *SPL* are carried out using the C weighting filter of the sound level meter in order to simulate the *SPL* heard by the human ear.

Figure 4.33 displays the effect of the input power on the maximum *SPL* of the piezoelectrically-driven thermoacoustic refrigerator at 395Hz.

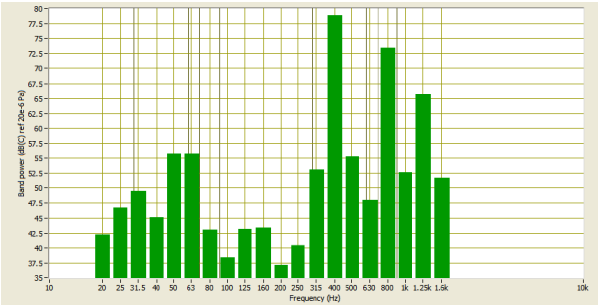

(a) – 0.427 W

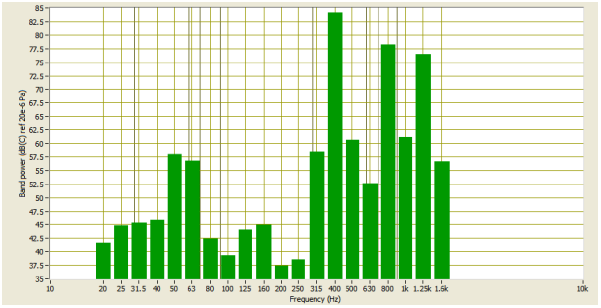

(b) – 1.173 W

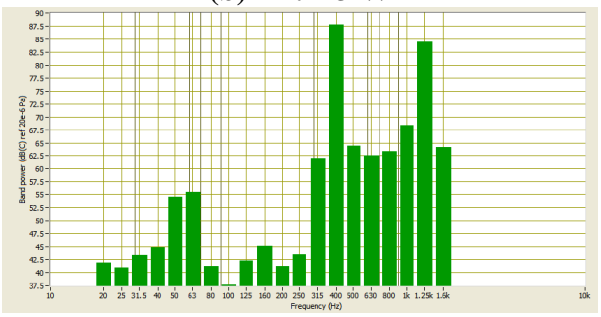

(c) – 2.52 W

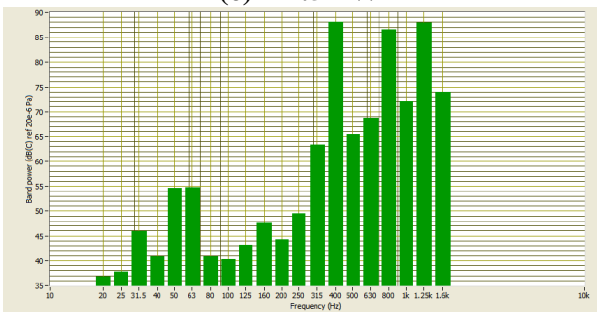

(d) – 4.14 W

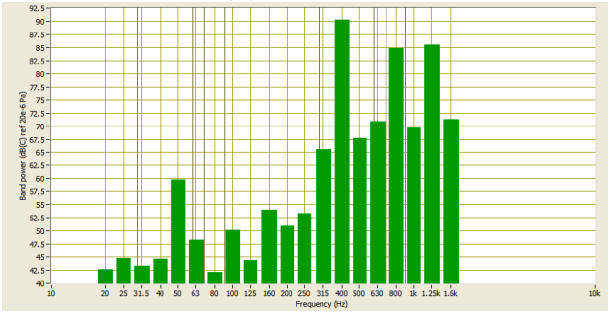

(e) – 6.8 W

Figure 4.32: Effect of input power on the sound pressure level spectrum of the piezoelectrically-driven thermoacoustic refrigerator when operating at frequency of 395Hz

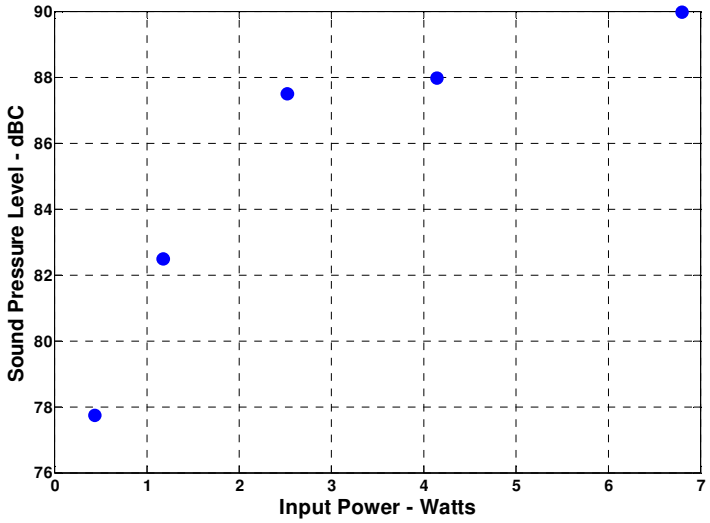

Figure 4.33: Effect of input power on the maximum sound pressure level of the piezoelectrically-driven thermoacoustic refrigerator

4.4 Summary

This chapter has presented the design, construction, and performance evaluation of a piezelectrically driven thermoacoustic refrigerator. The details of the design and the construction process are outlined along with a detailed description of the different components. Finally, it discusses the experimental performance of this piezoelectrically-driven thermoacoustic refrigerator as compared with the classical electromagnetically driven thermoacoustic refrigerators. The obtained experimental results are used to validate a predictive model of the piezoelectrically-driven thermoacoustic refrigerator in the fifth chapter.

Chapter 5: Modeling

The piezoelectrically-driven thermoacoustic refrigerator was modeled using the thermoacoustics modeling software DELTAEC. This chapter first gives an overview of the software and how it is used. It then goes on to detail how the driver was modeled within the software before concluding with a comparison between the experimental results given in the previous section and the results predicted by the model.

5.1 Modeling in DELTAEC

DeltaEC numerically integrates the momentum, continuity, and energy equations derived in chapter 2. It solves these equations in one dimension across sections referred to as segments. Models are made by stringing multiple segments together to have the numerical integration carried out across the created network of segments.

The solver assumes that all oscillating variables have a time dependence of $\mathrm{Re}\left(e^{i\omega t}\right)$. This assumption on the time dependence transforms the temporal part of the governing equations from differential equations in time to algebraic equations of time. This leaves the governing equations as spatial differential equations which are much easier to solve than the starting partial differential equations.

5.1.1 Segments

Thermoacoustic devices are broken up such that continuous regions with similar physical properties become segments. For instance, a long area with a constant cross section becomes a duct segment. An area where there is a constant

tapering of the cross section becomes a cone segment. The stack segment is used to model stacks in thermoacoustic devices, while another type of segment is used to model electromagnetic speakers. Each of these segments assumes one dimensional flow throughout, though flows can be split or combined at the ends of segments much in the way segments of pipes can be, as is discussed in the following section.

5.1.2 Models

Models are built from a combination of segments strung together. As an example, consider a simple thermoacoustic refrigerator comprised of an electromagnetic loud speaker, resonator, heat exchangers, configured as seen in Figure 5.1.

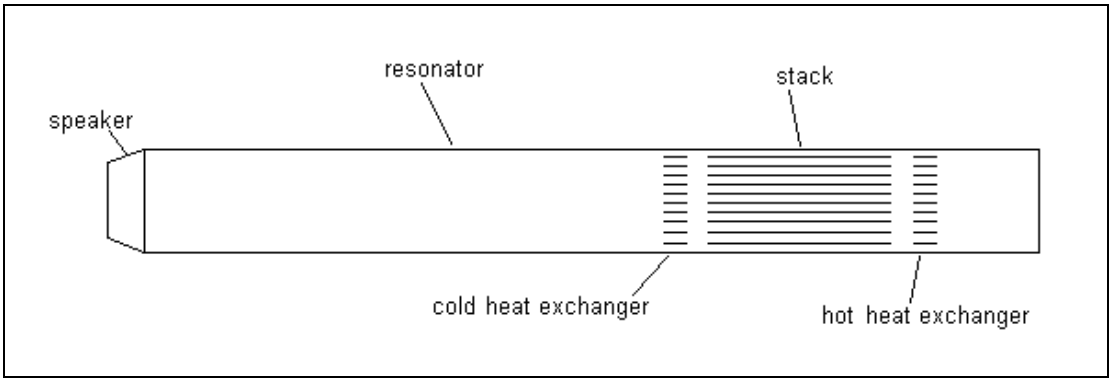

Figure 5.1: Example Thermoacoustic Refrigerator

This refrigerator would be broken into 6 segments with a 7^{th} terminating segment at the end when modeled in DeltaEC. The segments are fairly self evident. The first segment would be the speaker followed by a duct segment representing the resonator up until the cold heat exchanger begins. Segments for the cold heat exchanger, the stack, and the hot heat exchanger would follow and then a second duct

segment would be used to represent the portion of the resonator beyond the hot heat exchanger. At the end, a segment called a *hard end* in DeltaEC is used to create a zero displacement boundary condition at the end of the previous segment. A sketch of this setup is seen in Figure 5.2.

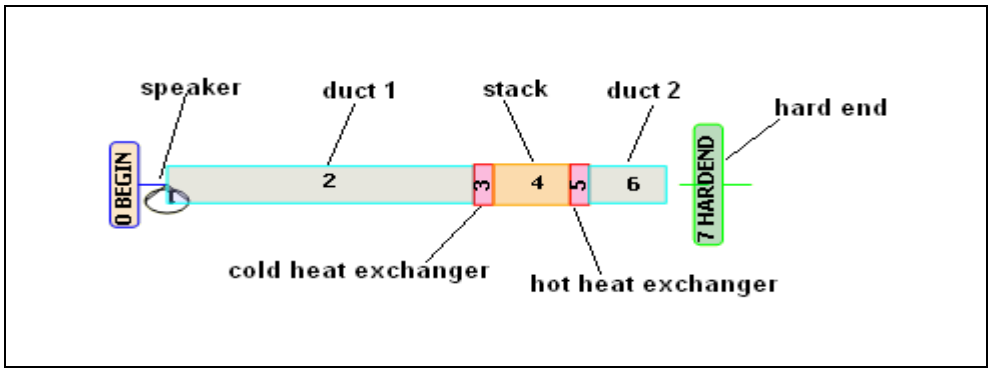

Figure 5.2: DeltaEC model of the refrigerator shown in Figure 5.1

More complicated thermoacoustic devices can easily be modeled as well. Take for instance, the first thermoacoustic refrigerator built by Hofler [21]. This refrigerator is pictured in Figure 5.3.

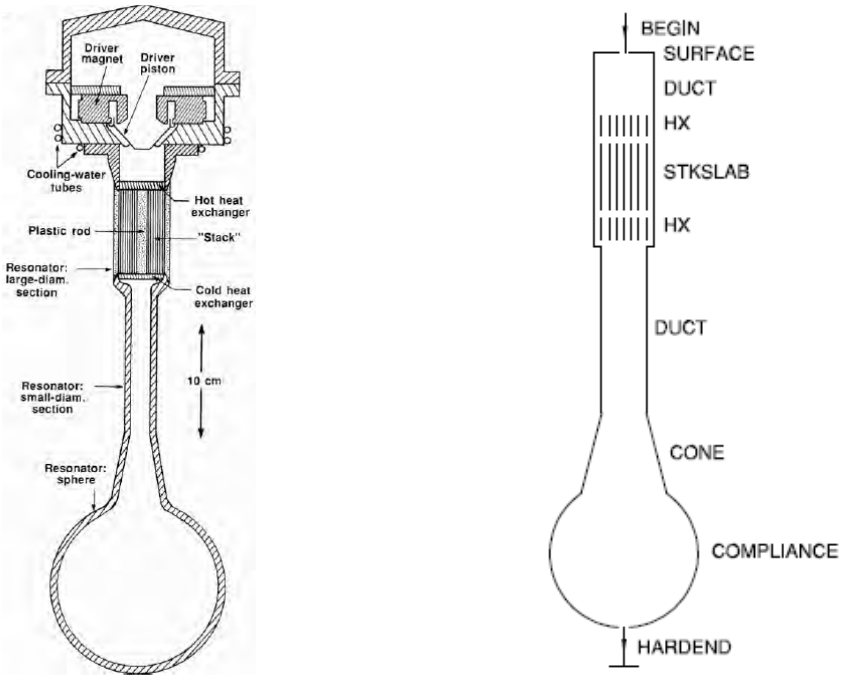

Figure 5.3: Hofler's thermoacoustic refrigerator is shown left and the DeltaEC model of it is pictured on the right. Both taken from [88]

The model shown on the right is comprised of 10 segments which are labeled in the picture. Note that the speaker is not included in this model. This is because this model which was built by the staff at Los Alamos National Laboratory chooses to skip the speaker segment which would convert voltage and current into pressure and volumetric flow rate, and rather input the pressure and volumetric flow rate to the refrigerator directly.

DeltaEC contains a user interface which is shown in Figure 5.4. Note that the user interface is displaying the model of Hofler's thermoacoustic refrigerator which goes along with the DeltaEC user's guide. This user interface has all of the segments of a model strung together. Each segment has a number of variables within it which

describe the physical characteristics of the segment. These variables are input by the user.

The BEGIN segment is the first segment in every model within DeltaEC. This segment defines the high level parameters of the model. As seen in Figure 5.4, the mean pressure, driving frequency, and starting temperature are put in as seen in lines 3 – 5 respectively. Lines 6 – 9 contain the magnitude of the oscillating pressure amplitude, the phase of the oscillating pressure amplitude, the amplitude of the volumetric flow, and the phase of the volumetric flow respectively. Finally, line 11 contains the selection of a gas type to use with this model.

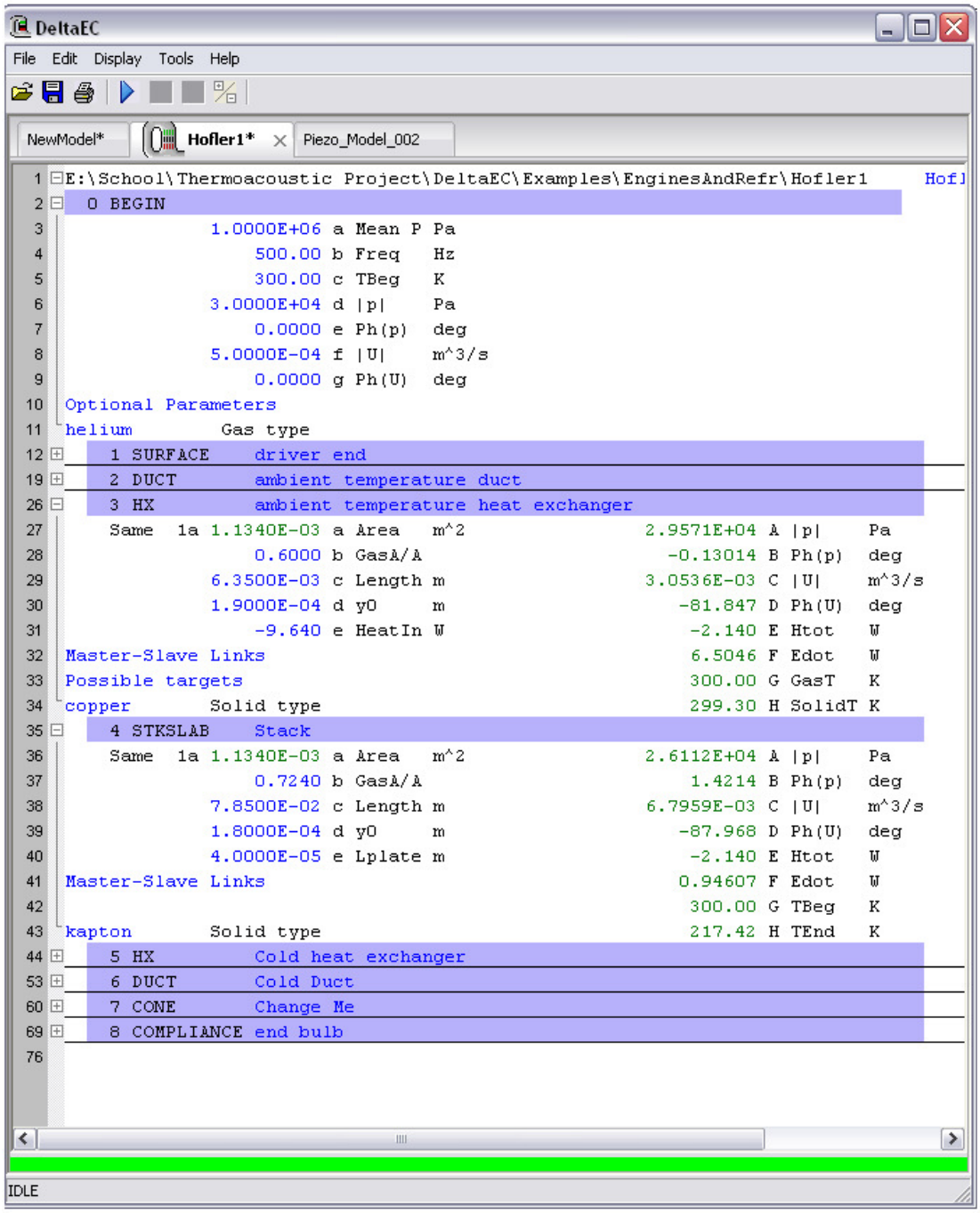

Figure 5.4: DeltaEC User Interface showing various segments from Hofler's refrigerator modeled

The ambient temperature heat exchanger segment is also shown in Figure 5.4.

DeltaEC assumes that the heat exchanger geometry within a heat exchanger segment

is a parallel stack of plates. This segment contains two columns, one on the left under the column of entries from the BEGIN segment, and another one on the right which the BEGIN segment does not have. The column on the left is a column of user inputs while the column on the right is a column of solutions at the beginning of the segment.

As seen in the left column, the cross sectional area is defined in line 27. Line 28 defines the ratio of gas occupied cross section to the total cross section. The heat exchanger length and spacing between parallel plates are defined in lines 29 and 30. Finally, the material out of which the heat exchanger is made is defined in line 34. Note that the segment on the stack is also shown in figure 5.4 but is not discussed as it is very similar to the heat exchanger segment.

When the model is solved within DeltaEC, solutions for many of the variables are plotted. For Hofler's refrigerator, the real and imaginary parts of the pressure are shown in Figure 5.5. Note that the real part of the pressure is plotted in 10kilo-Pa which makes its amplitude 10,000 times higher than that shown on the vertical axis, while the imaginary part of the pressure is plotted in kilo-Pa which makes its amplitude 1,000 times larger than that which is shown on the vertical axis.

Figure 5.6 shows the mean temperature which plotted along the refrigerator in degree Kelvin. This figure shows the predicted temperature drop across the stack due to the thermoacoustic effect. Note that the BEGIN segment of the model is represented by the left side of the graph, while the HARDEND side of the model is seen on the right.

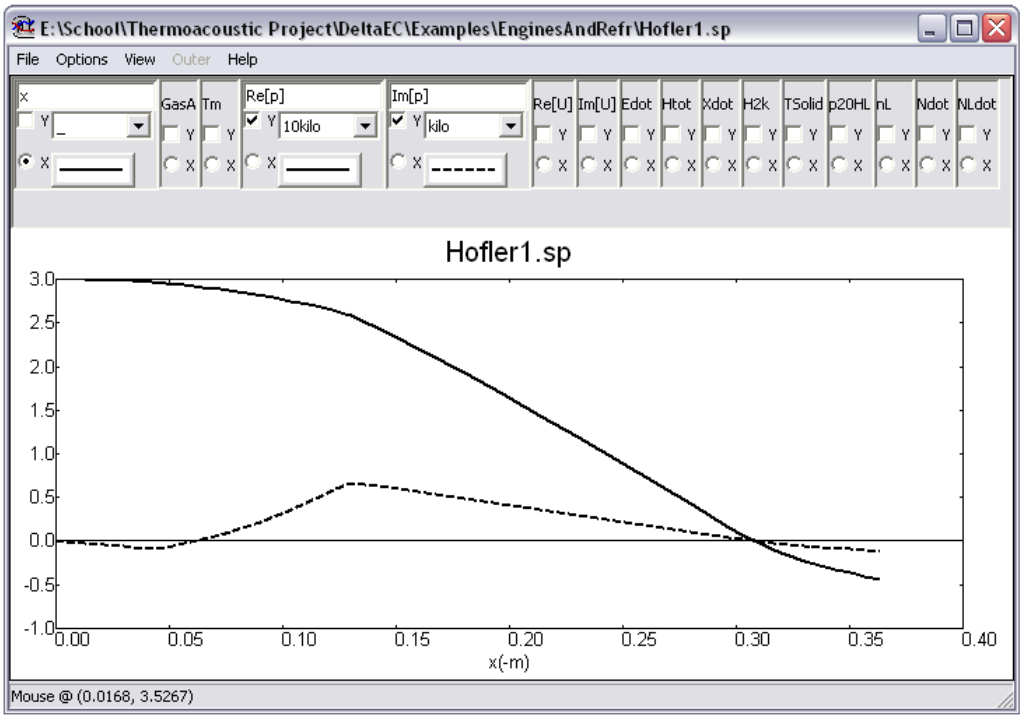

Figure 5.5: DeltaEC results for the real and imaginary pressure in the Hofler refrigerator

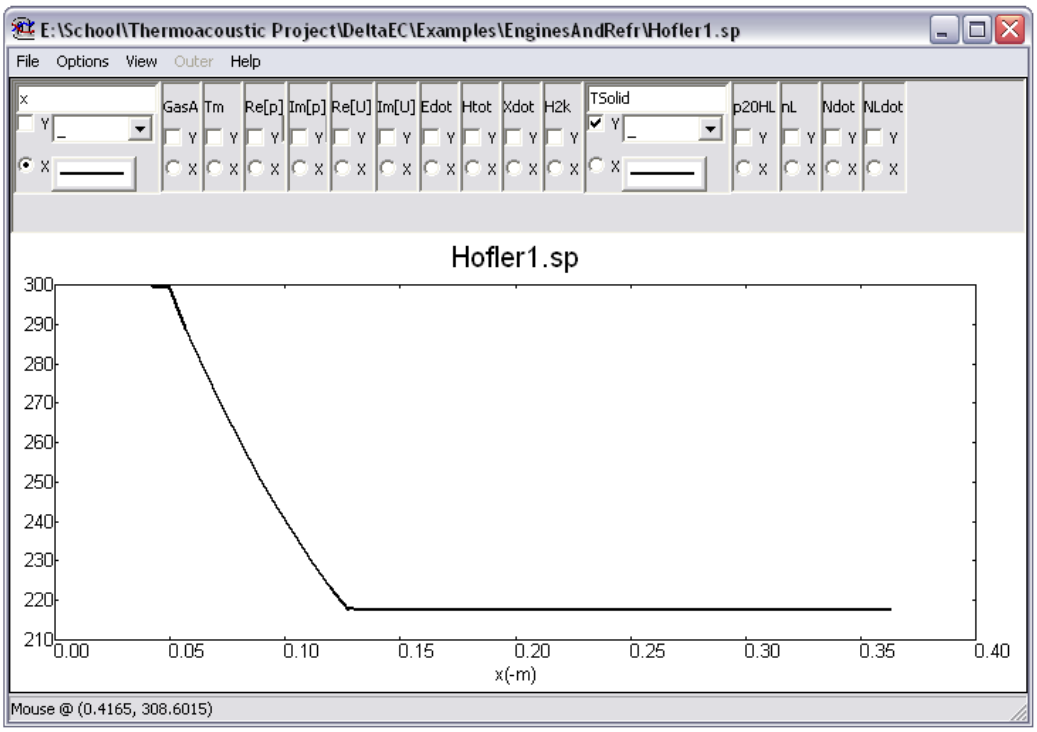

Figure 5.6: DeltaEC results for the temperature throughout the Hofler refrigerator

5.2 Modeling for the Piezoelectrically-driven Thermoacoustic Refrigerator

This chapter details the DeltaEC modeling of the piezoelectrically-driven thermoacoustic refrigerator described in chapter 4. The first section details the process by which the complicated speaker was converted to a simple DeltaEC segment. The DeltaEC segments are then described individually before the model as a whole is discussed.

5.2.1 Speaker Modeling

The speaker was modeled in DeltaEC by using a segment called VEDUCER. VEDUCER models the coupled relationship between the electrical and mechanical parts of the transducer.

$$\begin{Bmatrix} V_s \\ P \end{Bmatrix} = \begin{bmatrix} Z_e & T_{s1} \\ T_{s2} & Z_m \end{bmatrix} \begin{Bmatrix} I \\ Q \end{Bmatrix} \tag{5.1}$$

In equation (5-1), the two effort variables on the left are V_s which is the voltage and P which is the pressure. The flow variables are I which is the current, and Q which is the volumetric flow rate. The remaining four variables correlate the effort variables to the flow variables. Because both the effort and flow variables are complex numbers, the four correlation variables are also complex numbers. These variables are the electric impedance *Ze,* the cross correlation variables T_{s1} and T_{s2}, and the mechanical impedance *Zm*.

The electrical impedance was found by taking a sample of the PZ-94 Harsh Environment Speaker and removing the piezoelectric disk. The piezoelectric disk was then clamped between two surfaces that were not electrically conductive. The

two electrodes were connected to an impedance analyzer which gave the real and imaginary parts of the electrical impedance.

The cross correlation terms are assumed to follow the relationship $T_{s1} = -T_{s2}$. T_{s1} was found by running the speaker at a known voltage, measuring the output volumetric flow rate, and then using the relationship $V_s = T_{s1}Q$ to determine the real and imaginary parts of T_{s1}. Note that T_{s1} is frequency dependent and so the experiment was done at the operating frequency of the refrigerator and must be found again if a different operating frequency is to be used.

The experimental setup for finding T_{s1} is pictured in figure 5.7 below. The speaker was run at 1 Vrms at 395 Hz. A scanning Laser Doppler Vibrometer (LDV) was used to scan over the surface of the speaker, determining the volumetric velocity at each scanned point. The resolution over the speaker diaphragm was 2966 points. The average velocity of these points was multiplied by the area of the diaphragm to calculate the volumetric flow rate. The phase was also recorded by the scanning LDV.

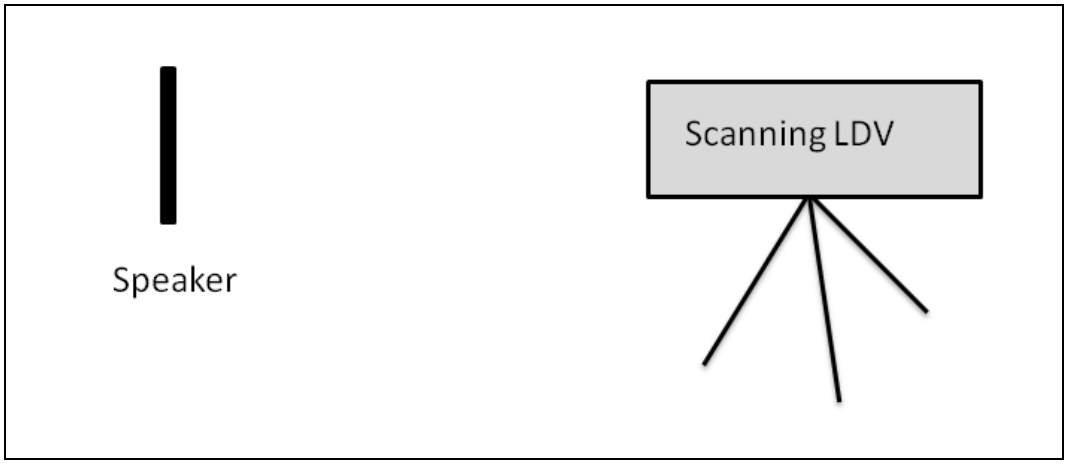

Figure 5.7: Experimental setup for finding cross correlation variables

The mechanical impedance was found by applying a dynamic force to the back of the speaker and measuring the volumetric flow rate on the front end using the scanning LDV to scan the speaker face as before. The mechanical impedance was then found by first dividing the force by the area of the piezo-diaphragm to obtain an equivalent pressure. Once the equivalent pressure and volumetric flow rate were known, the mechanical impedance was readily found using equation (5.1). The experimental setup is pictured in Figure 5.8.

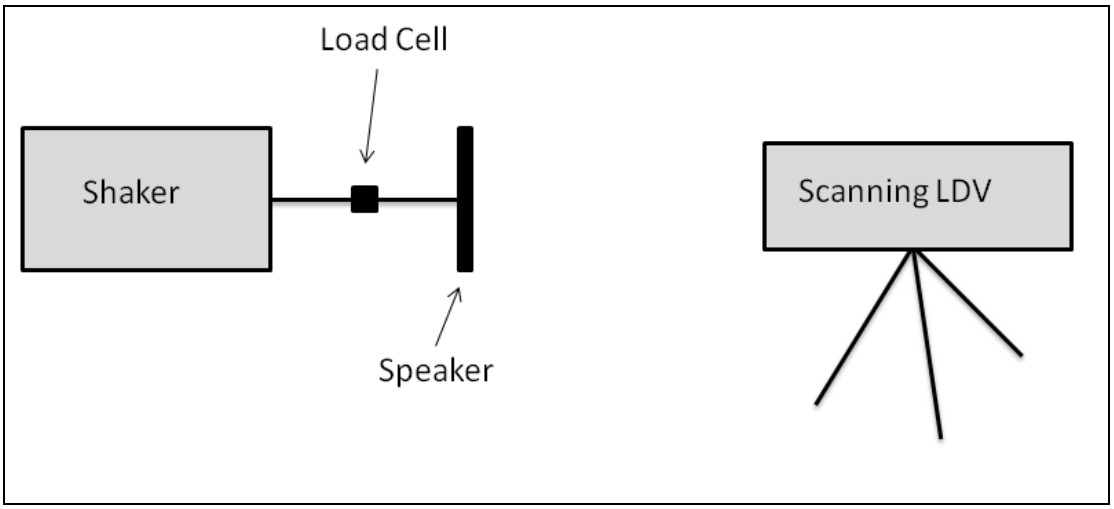

Figure 5.8: Experimental setup for measuring the mechanical impedance

In this setup, the shaker is attached to a steel rod and set to shake a 395 Hz. The steel rod is attached to a dynamic load cell which is in turn attached to another steel rod which is glued to the back of the piezo-diaphragm on the speaker. The load cell measures the dynamic force which is put into the piezo speaker diaphragm. The scanning LDV once again measures the volumetric flow rate on the front end, and the mechanical impedance is then found as described in the previous paragraph.

5.2.2 DelteEC Model

The thermoacoustic refrigerator described in chapter 4 was modeled using 8 segments in DeltaEC. The first segment is the BEGIN segment which contains some high level parameters for the experiment. This segment is shown in Figure 5.9.

```
2   0 BEGIN
3              1.0000E+05 a Mean P Pa
4                  395.00 b Freq   Hz
5                  300.00 c TBeg   K
6                  0.0000 d |p|    Pa
7                  0.0000 e Ph(p)  deg
8   Gues        -5.4232E-04 f |U|    m^3/s
9   Gues        -3.3214E+04 g Ph(U)  deg
10  Optional Parameters
11  air           Gas type
```

Figure 5.9: Segment 0 modeling high level parameters for the thermoacoustic refrigerator

Line 3 (Indicated by the column on the far left) contains the mean pressure for the thermoacoustic refrigerator, which is atmospheric pressure. Line 4 indicates the driving frequency of the experiment which is 395 Hz. Line 5 indicates the starting temperature throughout the refrigerator which is 300 degrees K.

Lines 6 and 7 represent the magnitude and phase of the pressure input to the back of the speaker diaphragm. Since the speaker is electrically driven only, these parameters are left zero. Lines 8 and 9 contain are the magnitude and phase of the volumetric flow rate at the back of the speaker. Because the volumetric flow rate is dependent on the effort variables, these parameters are labeled as guesses and are part of the solution in DeltaEC. Also shown in Figure 5.9 is that the gas type was selected to be air.

The segment for the piezoelectric speaker comes along next in the thermoacoustic refrigerator model. This segment is shown in Figure 5.10.

```
12  1 VEDUCER     Change Me
13                14.640 a Re(Ze) ohms                111.79 A |p|     Pa
14               -372.71 b Im(Ze) ohms                152.44 B Ph(p)   deg
15                8023.0 c Re(T1) V-s/m^3          5.4235E-04 C |U|     m^3/s
16           5.5470E+04 d Im(T1) V-s/m^3                86.398 D Ph(U)   deg
17               -8023.0 e Re(T2) Pa/A                -0.30074 E Htot    W
18          -5.5470E+04 f Im(T2) Pa/A              1.2308E-02 F Edot    W
19           1.3570E+06 g Re(Zm) Pa-s/m^3             -0.30074 G WorkIn  W
20          -2.6640E+06 h Im(Zm) Pa-s/m^3               38.000 H Volts   V
21                38.000 i |V|     V                2.7717E-02 I Amps    A
22                0.0000 j Ph(V)   deg                 -124.83 J Ph(Ze)  deg
23                                                     111.79 K |Px|    Pa
24                                                     152.44 L Ph(Px)  deg
```

Figure 5.10: Segment model of the piezoelectric speaker

Lines 13 through 20 contain the real and imaginary parts of the electrical impedance, cross correlation constants, and mechanical impedance respectively. These numbers were found in section 5.2.1. Lines 21 and 22 contain the input voltage is the same as that put into the thermoacoustic refrigerator during operation.

Figure 5.11 below shows the first duct segment which is next in the series. This segment models the part of the resonator between the speaker and the stack. Line 26 is the cross sectional area of this tube while lines 27 and 28 are the perimeter of the cross section and length of the tube respectively.

```
25  2 DUCT        Cold Duct
26            3.8795E-04 a Area   m^2                514.38 A |p|     Pa
27                0.1190 b Perim  m                   -2.949 B Ph(p)   deg
28                0.1778 c Length m                2.4798E-04 C |U|     m^3/s
29  Master-Slave Links                                78.731 D Ph(U)   deg
30  Optional Parameters                             -0.30074 E Htot    W
31  ideal         Solid type                        9.2290E-03 F Edot    W
```

Figure 5.11: Segment modeling the region between the speaker and the stack

The next segment is the cold heat exchanger pictured in Figure 5.12. Though the refrigerator did not have a built in cold heat exchanger built in, heat did conduct through the walls of the resonator and so a heat exchanger was added to the DeltaEC model to capture this added heat. The length of this heat exchanger was trimmed down to 1 mm in order to minimize its effect on everything except the heat added to the system.

```
32    3 HX          Cold Heat Exchanger
33              3.8795E-04 a Area    m^2              517.26 A |p|     Pa
34                  0.7000 b GasA/A                   -3.1603 B Ph(p)   deg
35              1.0000E-03 c Length  m              2.4506E-04 C |U|     m^3/s
36              1.9000E-04 d y0      m                 78.722 D Ph(U)   deg
37                  0.2986 e HeatIn  W            -2.1441E-03 E Htot    W
38  Master-Slave Links                             8.9498E-03 F Edot    W
39  Possible targets                                   300.00 G GasT    K
40  copper        Solid type                           301.47 H SolidT  K
```

Figure 5.12: Segment modeling the heat input to the cold side of the refrigerator from the outside

The heat load for the cold heat exchanger was estimated by using the difference between the temperature read by the cold heat exchanger and the ambient temperature as the driving temperature, and calculating an approximate thermal resistance for the resonator using its geometry and thermal conductivity. The temperature difference is then divided by this thermal resistance to find the heat flux which is entered in line 37 above.

The stack was modeled as shown in Figure 5.13. In line 43, the ratio of gas to solid in the cross section is computed by measuring the thickness and length of the film, as well as taking into account the number of fishing line strands in the cross section. Line 44 gives the length of the stack, line 45 the spacing between layers of the stack, and line 46 the thickness of the film which the stack is constructed out of.

```
41   4 STKSLAB     Stack
42              3.8795E-04 a Area    m^2                623.15 A |p|     Pa
43                  0.5517 b GasA/A                     -10.46 B Ph(p)   deg
44              3.5000E-02 c Length m                1.5786E-04 C |U|     m^3/s
45              1.7500E-04 d y0      m                   78.977 D Ph(U)   deg
46              1.0000E-04 e Lplate m               -2.1441E-03 E Htot    W
47 Master-Slave Links                                4.8344E-04 F Edot    W
48                                                       300.00 G TBeg    K
49 kapton       Solid type                               317.84 H TEnd    K
```

Figure 5.13: The segment modeling the stack

The next segment in the model is the hot heat exchanger. The hot heat exchanger was modeled in the same way the cold heat exchanger was. The segment is seen in Figure 5.14. The hot duct was modeled in the same way as the cold duct and is shown in Figure 5.15.

```
50   5 HX          Hot Heat Exchanger
51              3.8795E-04 a Area    m^2                625.01 A |p|     Pa
52                  0.7000 b GasA/A                     -10.55 B Ph(p)   deg
53              1.0000E-03 c Length m                1.5431E-04 C |U|     m^3/s
54              1.9000E-04 d y0      m                   79.142 D Ph(U)   deg
55                 -0.9953 e HeatIn W                  -0.99744 E Htot    W
56 Master-Slave Links                                2.5972E-04 F Edot    W
57 Possible targets                                      317.84 G GasT    K
58 copper       Solid type                               310.10 H SolidT  K
```

Figure 5.14: The segment modeling the hot heat exchanger

```
59   6 DUCT        Hot Duct
60              3.8795E-04 a Area    m^2                644.24 A |p|     Pa
61              6.9400E-02 b Perim   m                  -10.577 B Ph(p)   deg
62              3.5000E-02 c Length m                3.5229E-17 C |U|     m^3/s
63 Master-Slave Links                                    174.56 D Ph(U)   deg
64 Optional Parameters                               -0.99744 E Htot    W
65 ideal        Solid type                          -1.1302E-14 F Edot    W
```

Figure 5.15: The segment modeling the hot duct

The final segment is titled the HARDEND. This segment is a wall at the end of the hot duct segment which terminates the refrigerator. It is shown in Figure 5.16 below. This segment contains two variables which are the reciprocals of the real and imaginary parts of the acoustic impedance. These are set to zero indicating that there is infinite acoustic impedance at this point.

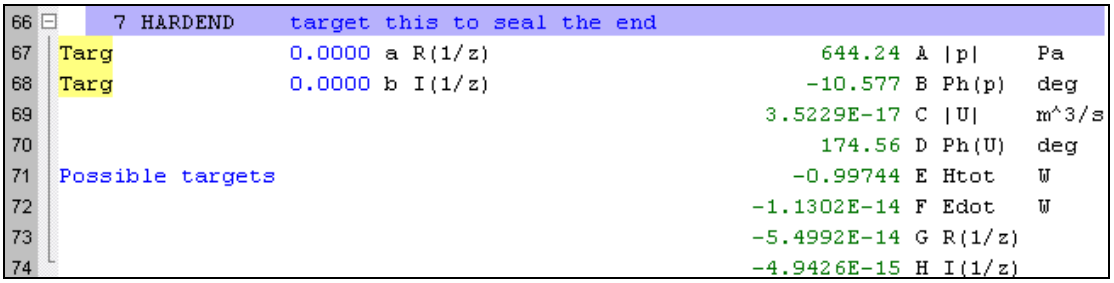

Figure 5.16: The segment modeling the termination of the refrigerator

A schematic of this refrigerator generated in DeltaEC showing all the segments and how they are linked is seen in Figure 5.17. Note that the numbers in the schematic match the number found in the title line of each of the segments above.

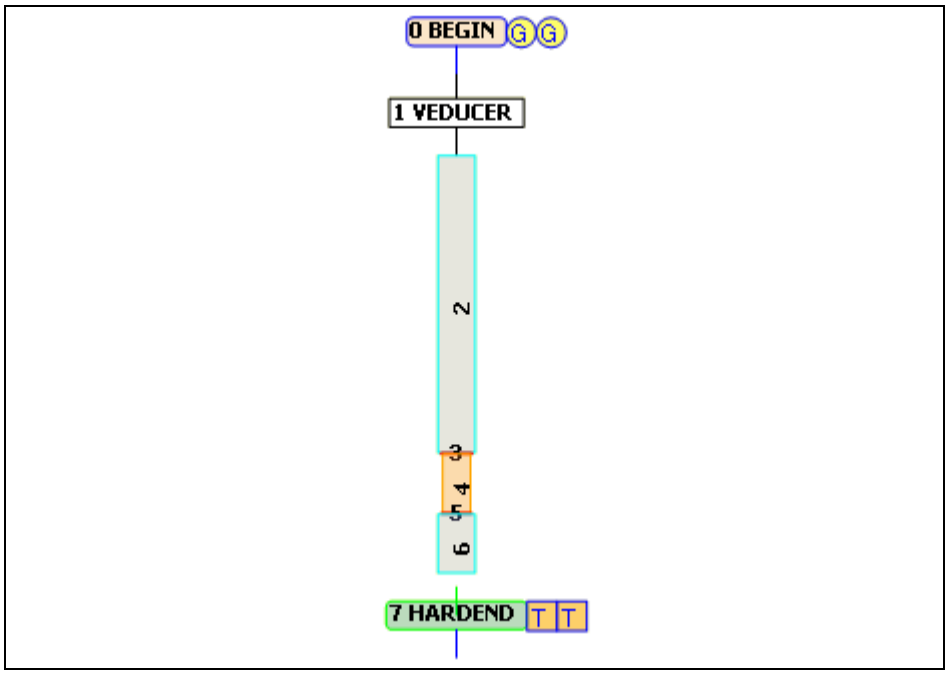

Figure 5.17: DeltaEC Schematic of the piezoelectrically-driven thermoacoustic refrigerator

5.3 DeltaEC Model Results

The DeltaEC results for the temperature are shown in Figure 5.18. As seen in this figure, a temperature difference of approximately 18 degrees K is predicted across the stack. This agrees well with the experimental results as seen in Figure 4.17 which predict about a 20 degree K temperature difference. The real and imaginary parts of the pressure are also plotted in Figure 5.19.

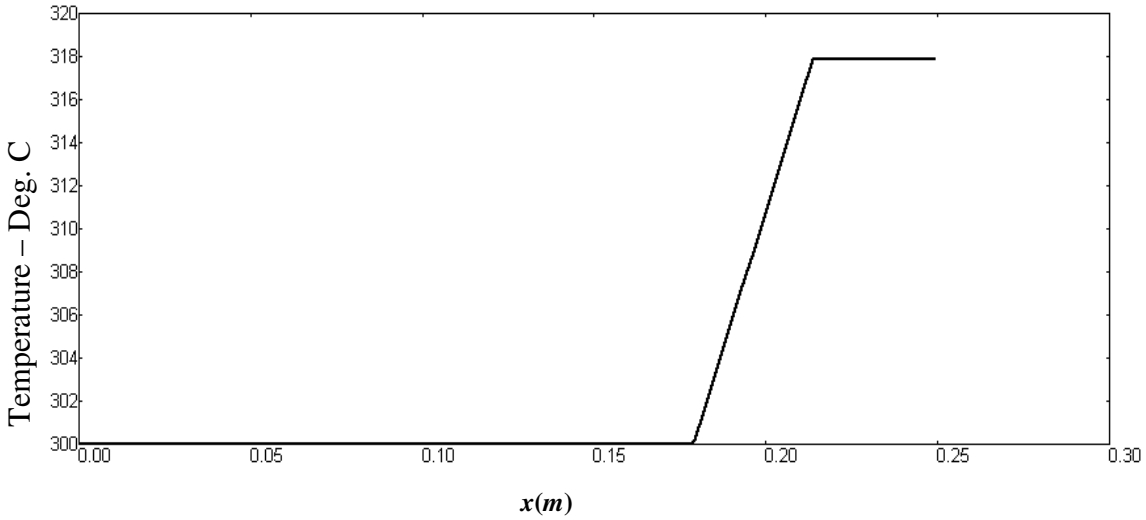

Figure 5.18: Temperature as a function of distance down the refrigerator

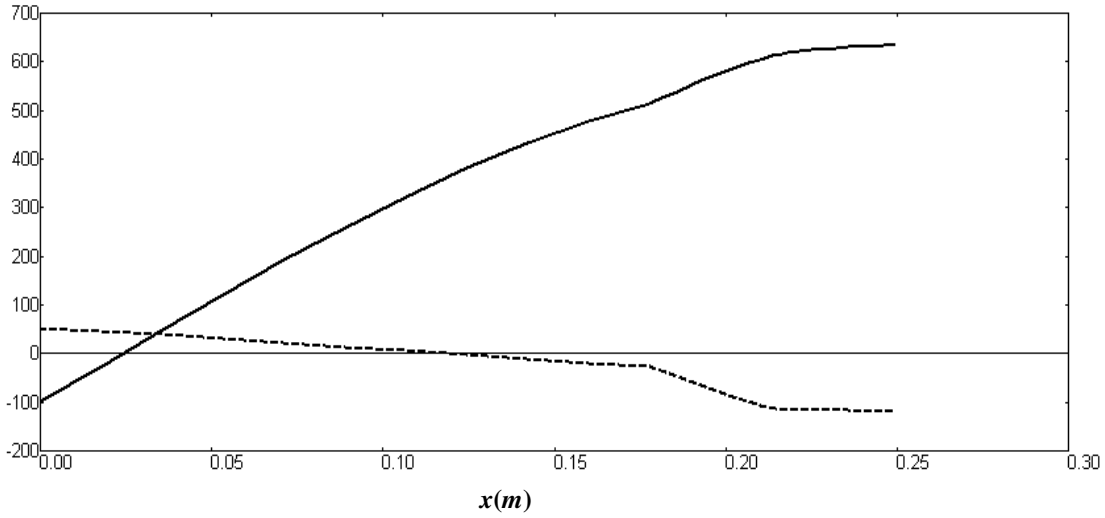

Figure 5.19: Real (Solid line) and imaginary (Dotted line) parts of the pressure in the refrigerator

More detailed comparisons between the experimental results presented in Chapter 4 and the theoretical predictions of DeltaEC are presented in what follows.

a. Temperature Differences:

Figure 5.20 shows comparisons between the experimental temperature difference and the corresponding predictions of DeltaEC for different input power levels. The displayed results are obtained when the piezoelectrically-driven thermoacoustic refrigerator is excited at its resonant frequency of 395Hz. It can be seen that there is a close agreement between theory and experiments.

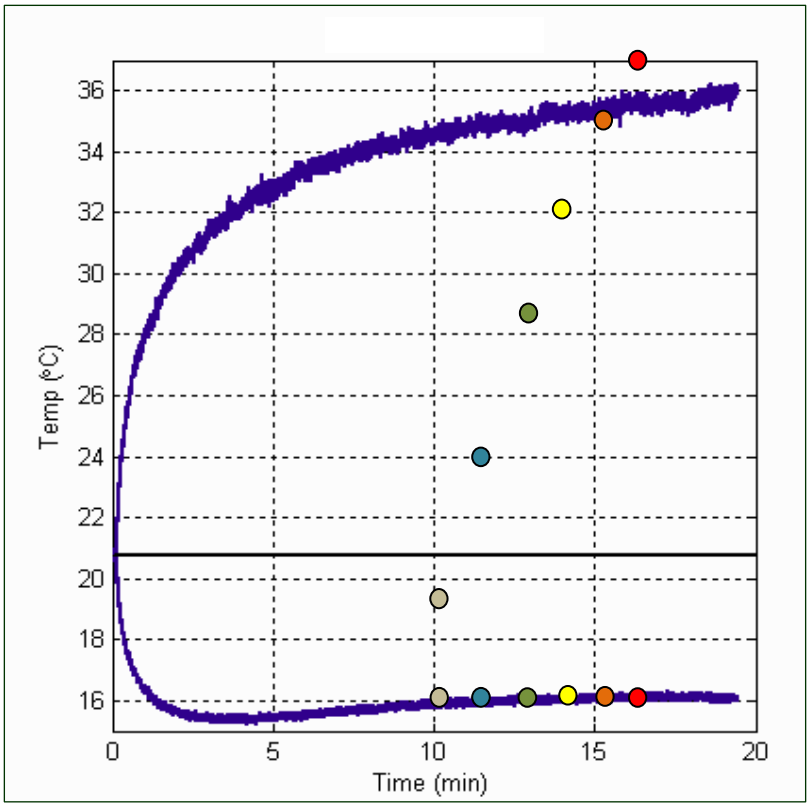

SYMBOL	METHOD
	Experimental output - 38 V, 0.2 A, Power =7.6 W
	DeltaEC – 38 V, 0.2 A → Power ≈ 7.6 W
	DeltaEC – 36 V, 0.189 A → Power ≈ 6.804 W
	DeltaEC – 34 V, 0.179 A → Power ≈ 6.1 W
	DeltaEC – 32 V, 0.168 A → Power ≈ 5.376 W
	DeltaEC – 30 V, 0.158 A → Power ≈ 4.74 W
	DeltaEC – 28 V, 0.147 A → Power ≈ 4.12 W

Figure 5.20: Comparisons between the experimental temperature difference and the predictions of DeltaEC for different input power levels when the thermoacoustic refrigerator is operating at 395Hz

Figure 5.21 shows similar comparisons when the piezoelectrically-driven thermoacoustic refrigerator is operating at an off-resonance frequency of 380Hz. In the figure, the lines denote the experimental results and the triangles denote the predictions of the DeltaEC model. The figure suggests a close agreements between the experiment results and the theoretical predictions with errors not exceeding ± 2 degrees C.

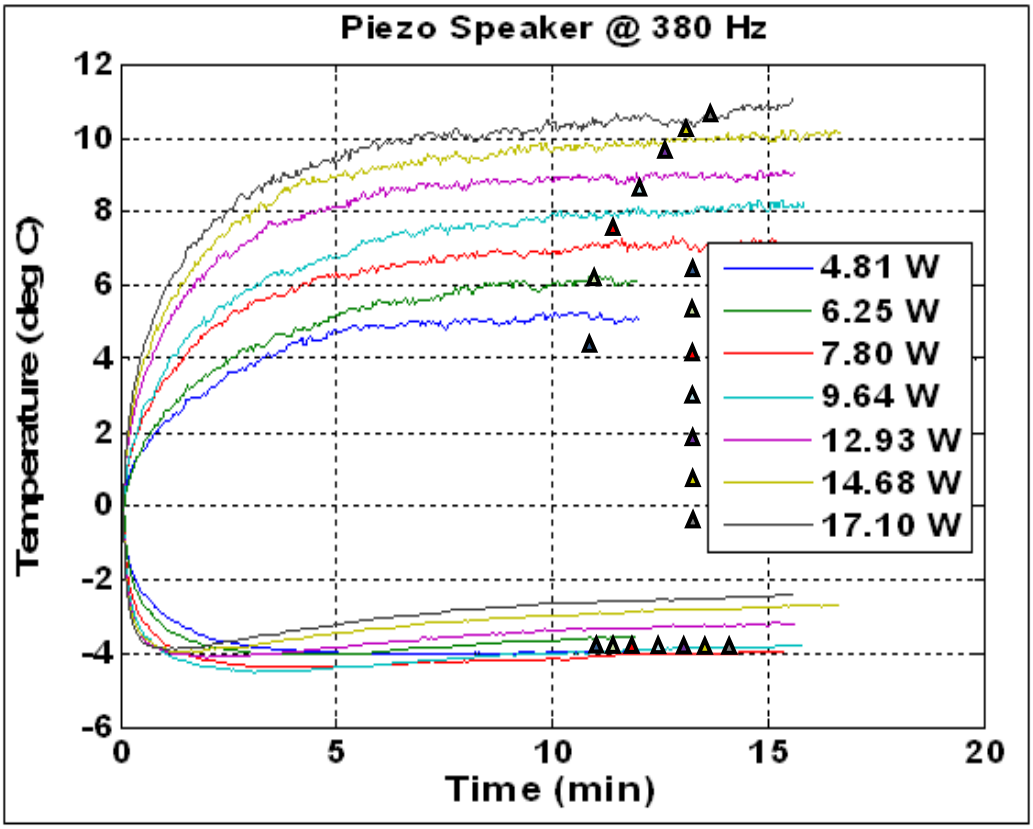

Figure 5.21: Comparisons between the experimental temperature difference and the predictions of DeltaEC for different input power levels when the thermoacoustic refrigerator is operating at 380Hz

Figure 5.22 summarizes the comparison between theoretical and the steady-state experimental temperature differences at excitation frequency of 380 Hz.

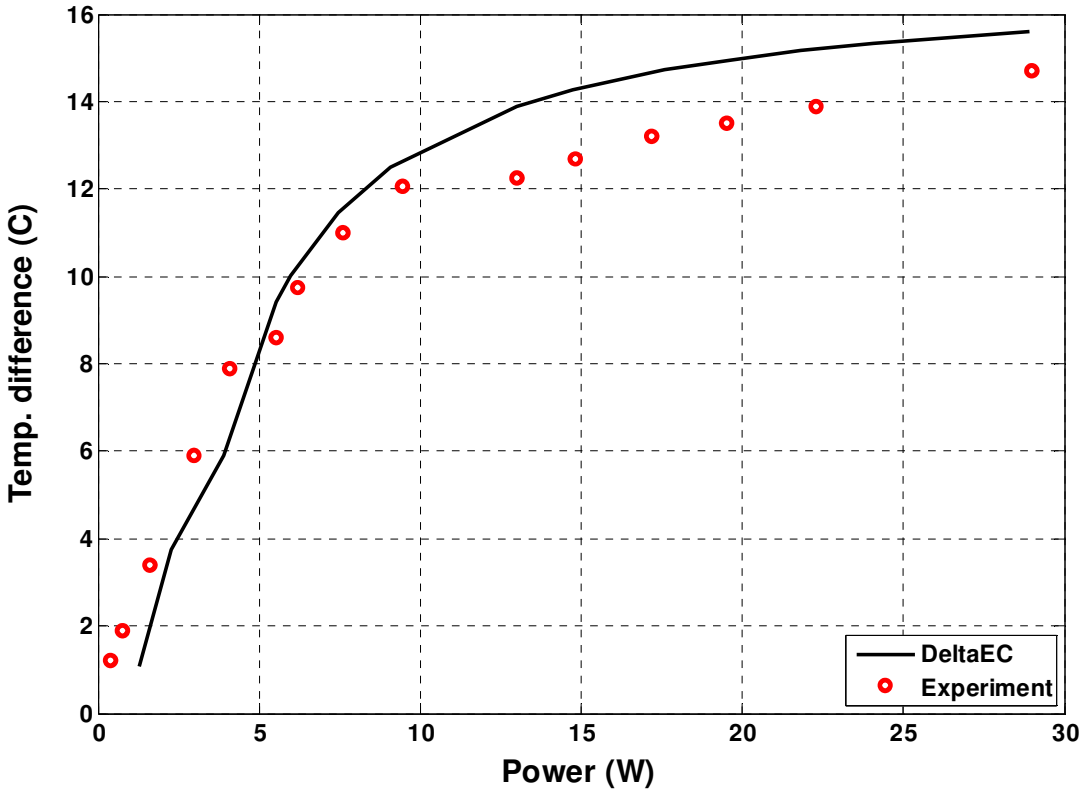

Figure 5.22: Summary of comparisons between the theoretical and the steady-state experimental temperature differences at excitation frequency of 380 Hz

b. Flow velocities

Figure 5.23 shows comparisons between the theoretical predictions of the volume velocities by DeltaEC and the corresponding experimental results as measured by using the Particle Image Velocimetry (PIV) at excitation frequency of 395 Hz.

The displayed results indicate close agreement between theory and experiments.

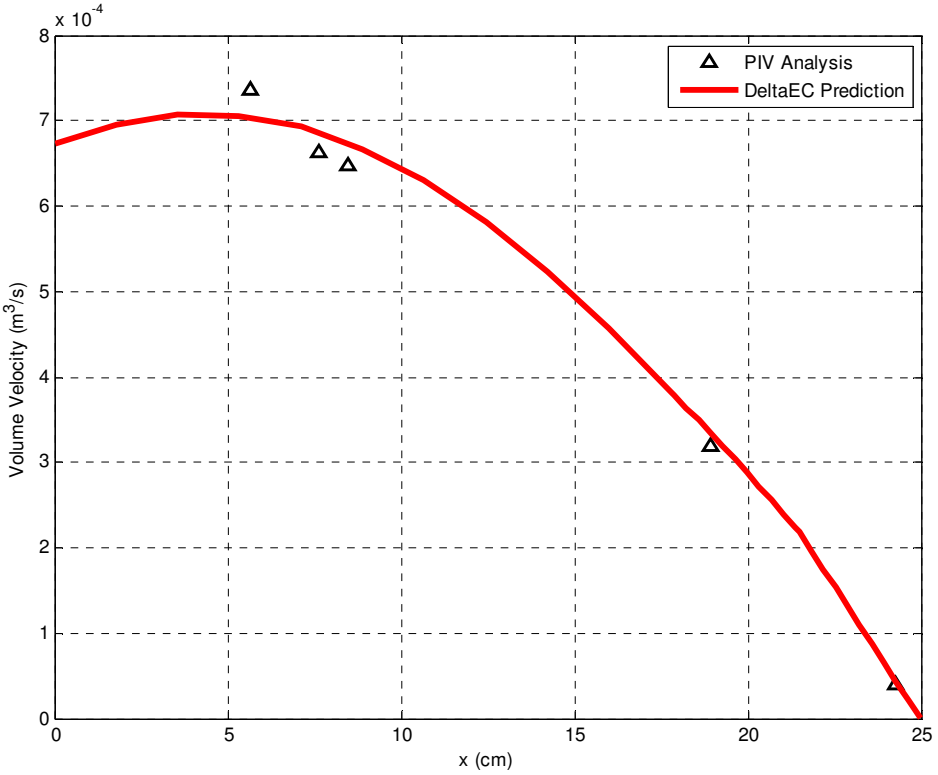

Figure 5.23: Comparison between the theoretical and the experimental volume velocities at excitation frequency of 395 Hz

5.4 Summary

This chapter has presented a detailed modeling of the piezoelectrically-driven refrigerator using DeltaEC software package. Comparisons between the predictions of the DeltaEC package and the obtained experimental results are also presented. Close agreements between theory and experiments are observed.

Chapter 6: Conclusions

Thermoacoustic refrigerators can be driven using piezoelectric drivers. However, significant displacement is hard to obtain with piezoelectric drivers. Any piezoelectrically-driven thermoacoustic refrigerator will have to have some complicated driver setup like the one used in this thesis, or be designed to operate at high frequencies which require small dimensions.

At lower frequencies, piezoelectric drivers are not going to be able to compete with electromagnetic drivers due to their limited displacements, and would likely only by a good solution in cases where the magnetic fields that electromagnetic drivers bring along with them are not acceptable. For the high frequency case, as the dimensions get smaller, the cost and difficulty of manufacturing go up. As the cost and difficulty of manufacturing go up, so does the importance of modeling such as that done for this thesis.

The piezoelectrically-driven thermoacoustic refrigerator built and modeled here was sized large enough so that the dimensions would not be hard to work with while still small enough so that the piezoelectric driver would still be able to deliver significant acoustic power. The length scales are on the order of inches with the exception of the stack which has dimensions on the order of tenths of an inch. The driving frequency of the refrigerator is 395 Hz. The piezoelectrically-driven thermoacoustic refrigerator is shown to successfully produce a steady state temperature difference of 18 degrees C across the stack.

The refrigerator is then modeled using DeltaEC [88], a software produced by *Los Alamos National Laboratory* which can be used to model thermoacoustic devices.

The modeled results are seen to agree well with the experimental results. However, the model was not developed independently of the experimental results because the numbers for the heat transfer into the cold side of the refrigerator and out of the hot side of the refrigerator were obtained from measurement of the refrigerator in operation.

As noted in the literature, heat transfer under the oscillatory flow of thermoacoustic refrigerators is something that is not well understood [80]. This creates a major limitation on the amount of modeling that can be done before a design is made, especially with the modeling approach used in this thesis which is very sensitive correctly predicting the heat transferred at the hot and cold heat exchangers.

This leads to the conclusion that piezoelectrically-driven thermoacoustic refrigerator models are limited by the same hang up that every other thermoacoustic refrigerator model is limited by, namely that heat transfer with oscillatory flow is not well understood and does not have good models. Until good models for heat transfer under oscillating flow are developed, the potential for piezoelectrically-driven thermoacoustic refrigerators will likely remain limited because the cost of constructing small enough refrigerators will be too high.

Bibliography

[1] N. Rott, *Thermoacoustics*, Advances in Applied Mechanics, 20:135-175, 1980

[2] J. Wheatley, T. Hofler, G. W. Swift, and A. Migliori, *Understanding some simple phenomena in thermoacoustics with applications to acoustical heat engines*, Am. J. Phys. 53 (2), February 1985

[3] M. E. H. Tijani, *Loudspeaker-driven thermo-acoustic refrigeration*, Ph.D. Thesis at Technische Universiteit Eindhoven, 2001

[4] B. Higgins, *Nicholson's Journal* **I**, 130 (1802)

[5] P. L. Rijke, *Notiz uber eine neue Art, die in einer an beiden enden offenen Rohre enthaltene Luft in Schwingungen zu versetzen,* Ann. Phys. (Leipzig) [2] **107**,339 (1859)

[6] K. T. Feldman, Jr., *Review of the literature on Rijke thermoacoustic phenomena*, J. Sound Vib. 7, **83** (1968)

[7] J.W. Strutt (Lord Rayleigh), *The Theory of Sound*, 2nd ed., Vol. II (Dover 1945), §322g-j

[8] C. Sondhauss, *Ueber die Schallschwingungen der Luft in erhitzten Glas-Rohren und in gedeckten Pfeifen von ungleicher Weite,* Ann. Phys. (Leipzig) [2] **79**, 1 (1850)

[9] K. W. Taconis and J. J. M. Beenakker, *Measurements concerning the vapor-liquid equilibrium of solutions of ^{3}He in ^{4}He below 2.19K,* Physica **15**, 733 (1949)

[10] N. Rott, *Damped and thermally driven acoustic oscillations in wide and narrow tubes,* Z. Angew. Math. Phys. **20**, 230 (1969)

[11] N. Rott, *Thermally driven acoustic oscillations, part II: Stability limit for helium,* Z. Angew. Math. Phys. **24**, 54 (1973)

[12] N. Rott, *Thermally driven acoustic oscillations, part III: Second-order heat flux,*Z. Angew. Math. Phys. **26**, 43 (1975)

[13] N. Rott and G. Zouzoulas, *Thermally driven acoustic oscillations, part IV: Tubes with variable cross-section,* Z. Angew. Math. Phys. **27**, 197 (1976)

[14] N. Rott, *The influence of heat conduction on acoustic streaming*, Z. Angew. Math. Phys. **25**, 417 (1974)

[15] W.E. Gifford and R. C. Longsworth, *Surface heat pumping,* Adv. Cryog. Eng. **11**, 171 (1966)

[16] P. Merkli and H. Thomann, *Thermoacoustic effects in a resonant tube,* J. Fluid Mech. **70**, 161 (1975)

[17] G. W. Swift, *Thermoacoustics: A unifying perspective for some engines and refrigerators,* American Institute for Physics Press, New York, 2002

[18] G. W. Swift, *Thermoacoustic Engines,* J. Acoust. Soc. Am. **84** (4), 1145 (1988)

[19] J. C. Wheatley, T. Hofler, G. W. Swift and A. Migliori, *Experiments with an Intrinsically Irreversible Acoustic Heat Engine,* Physical Review Letters **50** (7), 499 (1983)

[20] J. C. Wheatley, T. Hofler, G.W. Swift, and A. Milgliori, *An intrinsically irreversible thermoacoustic heat engine,* J. Acoust. Soc. Am. **74**, 153 (1983)

[21] T. J. Hofler, *Thermoacoustic refrigerator design and performance,* Ph.D. dissertation, Physics Department, University of California at San Diego, (1986)

[22] J. C. Wheatley, G. W. Swift, and A. Migliori, *The natural heat engines,* Los Alamos Science **14**, 2 (Fall 1986)
[23] S. L. Garrett, J. A. Adeff, and T. J. Hofler, *Thermoacoustic refrigerator for space applications,*J. Thermophysics and Heat Transfer (AIAA) **7**(4), 595 (1993)
[24] J. A. Adeff and T. J. Hofler, *Design and construction of a solar-powered, thermoacoustically driven, thermoacoustic refrigerator,* J. Acoust. Soc. Am **107** (6), L37 (2000)
[25] D. J. McKelvey and S. C. Ballister, *Shipboard electronic thermoacoustic cooler,* Masters of Science in Engineering Acoustics and Master of Science in Applied Physics, June 1995. DTIC Report No. AD A300-514
[26] The Pennsylvania State Univesity, Graduate Program in Acoustics, thermoacoustics http://www.acs.psu.edu/thermoacoustics/refrigeration
[27] M. E. H. Tijani, J. C. H. Zeegers and A. T. A. M. de Waele, *Construction and performance of a thermoacoustic refrigerator,* Cryogenics **42**, 59 (2002)
[28] D. A. Russel and P. Weibull, *Tabletop thermoacoustic refrigerator for demonstrations,* Am. J. Phys. **70** (12), 1231 (2002)
[29] Ben & Jerry's Homemade Ice Cream, http://www.Benjerry.com
[30] S. Direk, *Design of a mini thermo-acoustic refrigerator,* Masters Thesis, Naval Postgraduate School (2001)
[31] M. A. Saad, *Thermodynamics: Principles and Practice,* Prentice-Hall, Inc. 95 (1997)
[32] K. Wark, *Thermodynamics,* McGraw-Hill, Inc., New York, NY (1983)
[33] Reference 32, equation (2-5)
[34] Reference 17, equation (2.3)
[35] Reference 32, equation (2-8)
[36] Reference 17, equation (2.15)
[37] Reference 17, equation (2.16)
[38] Reference 17, variant of (2.8)
[39] Reference 17, equation (2.19)
[40] Reference 17, equation (2.23)
[41] Reference 17, equation (2.28)
[42] Reference 17, equation (2.29)
[43] Reference 17, equation (2.33)
[44] B. R. Munson, D. F. Young, T. H. Okiishi, *Fundamentals of Fluid Mechanics Fifth Edition,*Wiley, (2006)
[45] Reference 44, equation (11.1)
[46] Reference 44, equation (11.14)
[47] Reference 44, equation (11.15)
[48] Reference 17, equation (2.92)
[49] Reference 17, equation (1.1)
[50] Reference 17, equation (1.2)
[51] Reference 17, equation (1.3)
[52] Reference 17, equation (4.69)
[53] Reference 17, equation (4.66)
[54] Reference 17, equation (4.67)

[55] Reference 17, pages 88-89
[56] Reference 17, equation (4.52)
[57] Reference 17, equation (4.53)
[58] Reference 17, equation (4.54)
[59] Reference 17, equation (5.19)
[60] Reference 17, equation (5.22)
[61] Reference 17, equation (5.20)
[62] Reference 17, equation (5.21)
[63] Reference 17, equation (5.24)
[64] Reference 17, equation (2.93)
[65] Reference 17, equation (5.25)
[66] Reference 17, equation (5.26)
[67] M. E. H. Tijani, J. C. H. Zeegers, and A. T. A. M. de Waele, *Design of thermoacoustic refrigerators,* Cryogenics **42**, 49-57 (2002)
[68] M. E. H. Tijani, J. C. H. Zeegers, and A. T. A. M. de Waele, *Construction and performance of a thermoacoustic refrigerator,* Cryogenics **43**, 49-66 (2002)
[69] M. Wetzel and C. Herman, *Design optimization of thermoacoustic refrigerators,* Intl J. Refrig, **20**, 3-21 (1997)
[70] R. S. Reid and G. W. Swift, *Experiments with a flow-through thermoacoustic refrigerator,* J. Acoust. Soc. Am. **108** (6), 2835-2842 (2000)
[71] R. S. Waikeland, *Use of electrdynamic drivers in thermoacoustic refrigerators,* J. Acoust. Soc. Am. **107**, 827-832, (2000)
[72] M. E. H. Tijani, J. C. H. Zeegers, and A. T. A. M. de Waele, *A gas-spring system for optimizing loudspeakers in thermoacoustic refrigerators,* Journal of Applied Physics **92**, 4 (2002)
[73] Y. Li, B. L. Minner, G. T. C. Chiu, L. Mongeau, and J. E. Braun, *Adaptive tuning of an electrodynaically driven thermoacoustic cooler,* J. Acoust. Soc. Am. **111** (3), 1251-1258 (2002)
[74] Y. Li, M. A. Rotea, G. T. C. Chiu, L. G. Mongeau, an I. S. Paek, *Extremum seeking control of tunable thermoacoustic cooler,* Proceeding of the 2004 American Control Conference, Boston, MA June 30 – July 2 (2004)
[75] D. L. Gardner and G. W. Swift, *Use of intertance in orifice pulse tube refrigerators,* Cryogenics **37**, 117-121 (1997)
[76] T. J. Hofler, *Thermoacoustic refrigerator design and performance,* Ph.D. dissertation, Physics Department, University of California at San Diego (1986)
[77] M. E. H. Tijani, J. C. H. Zeegers, and A. T. A. M. de Waele, *The optimal stack spacing for thermoacoustic refrigeration,* J. Acoust. Soc. Am. **112** (1) July (2002)
[78] D. A. Russel and P. Weibull, *Tabletop thermoacoustic refrigerator for demonstrations,* Am. J. Phys. **70** (12), December (2002)
[79] P. Blanc-Benon, E. Besnoin, and O. Knio, *Experimental and computational visulization of the flow field in a thermoacoustic stack,* Comptes Rendus Mecanique **331**, 17-24 (2003)
[80] I. Paek, J. E. Braun, and L. Mongeau, *Characterizing heat transfer coefficients for heat exchangers in thermoacoustic coolers,* J. Acoust. Soc. Am. **118,** 2271-2280 (2005)

[81] E. C. Nsofor, S. Celik, and X. Wang, *Experimental study of the heat transfer at the heat exchanger of the thermoacoustic refrigerating system,* Applied Thermal Engineering **27,** 2435-2442 (2007)
[82] J. R. Belcher, W. V. Slaton, R Raset, H. E. Bass, and J. Lightfoot, *Working gases in thermoacoustic engines,* J. Acoust. Soc. Am. **105** (5), May (1999)
[83] M. E. H. Tijani, J. C. H. Zeegers, and A. T. A. M. de Waele, *Prandtl number and thermoacoustic refrigerators,* J. Acoust. Soc. Am. **112** (1), July (2002)
[84] F. W. Giacobbe, *Estimation of Prandtl numbers in binary gas mixtures of helium and other noble gases,* J. Acoust. Soc. Am **96** (6), December (1994)
[85] A. Worlikar, O. M. Knio, and R. Klein, *Numerical Simulation of a Thermoacoustic Refrigerator*, ESAIM Proceedings, Vol 1, 363-375, 1996
[86] A. Worlikar, O. M. Knio, and R. Klein, *Numerical Simulation of a Thermoacoustic Refrigerator II: Stratified Flow around the Stack,* J. Comput. Phys., **144**, 299-324, (1998)
[87] D. Marx and P. Blanc-Benon, *Numerical Simulation of Stack-Heat Exchangers Coupling in a Thermoacoustic Refrigerator,* AIAA J., **42**, 1338-1347, (2004)
[88] W. Ward, J. Clark, and G. Swift, *Design Environment for Low-amplitude Thermoacoustic Energy Conversion (DELTAEC),* Los Alamos National Laboratory: http://www.lanl.gov/thermoacoustics/DeltaEC.html
[89] M. E. Poese and S. L. Garrett, *Performance measurements on a thermoacoustic refrigerator driven at high amplitudes,* J. Acoust. Soc. Am. **107**, 2480-2486 (2000)
[90] R. S. Reid, W. C. Ward, and G. W. Swift, *Cyclic Thermodynamics with Open Flow,* Phys. Rev. Lett., **80**, 4617-4620, (1998)
[91] R. A. Hiller and G. W. Swift, *Condensation in a steady-flow thermoacoustic refrigerator,* J. Acoust. Soc. Am., **108**, 1521-1527, (2000)
[92] G. W. Swift, D. L. Gardner, and S. Backhaus, *Acoustic recovery of lost power in pulse tube refrigerators,* J. Acoust. Soc. Am., **105**, 711-724, (1998)
[93] R. S. Reid and G. W. Swift, *Experiments with a flow-through thermoacoustic refrigerator,* J. Acoust. Soc. Am., **108**, 2835-2842, (2000)
[94] ISL Products website, *PZ-94 Harsh Environment Speaker,* http://www.islproducts.com/prod/piezos/PZ-94.htm
[95] The Engineering Toolbox, *Air Properties* http://www.engineeringtoolbox.com/air-properties-d_156.html